

DTIC FILE COPY

2

SACLANTCEN MEMORANDUM
serial no.: SM-203

SACLANT UNDERSEA
RESEARCH CENTRE
MEMORANDUM

AD-A200 582



Deconvolution by homomorphic
and Wiener filtering

P. Nicolas

September 1988

DTIC
SELECTED
NOV 23 1988
S E

DISTRIBUTION STATEMENT A
Approved for public release
Distribution unlimited

SACLANT Undersea Research Centre provides the Supreme Allied Commander Atlantic (SACLANT) with scientific and technical assistance in accordance with the terms of its NATO charter, which entered into force on 1 January 1983. Without prejudice to this main task—namely, the policy direction of SACLANT—the Centre also renders scientific and technical assistance to the individual NATO nations.

88 1122 054

This document is released to a NATO Government at the direction of SACLANT Undersea Research Centre subject to the following conditions:

- The recipient NATO Government agrees to use its best endeavours to ensure that the information herein disclosed, whether or not it bears a security classification, is not dealt with in any manner (a) contrary to the intent of the provisions of the Charter of the Centre, or (b) prejudicial to the rights of the owner thereof to obtain patent, copyright, or other like statutory protection therefor.
- If the technical information was originally released to the Centre by a NATO Government subject to restrictions clearly marked on this document the recipient NATO Government agrees to use its best endeavours to abide by the terms of the restrictions so imposed by the releasing Government.

Page count for SM-203
(excluding covers)

Pages	Total
i-vi	6
1-65	65
ⓐ1-ⓐ62	62
	<hr/>
	133

SACLANT Undersea Research Centre
Viale San Bartolomeo 400
19026 San Bartolomeo (SP), Italy

tel: 0187 540 111
telex: 271148 SACENT I

NORTH ATLANTIC TREATY ORGANIZATION

Deconvolution by
homomorphic and
Wiener filtering

P. Nicolas

The content of this document pertains
to work performed under Project 02 of
the SACLANTCEN Programme of Work.
The document has been approved for
release by The Director, SACLANTCEN.

Issued by:
Systems Research Division



J. Marchment
Division Chief

DTIC
ELECTE
NOV 23 1988
S **D**
E

**Deconvolution by homomorphic and
Wiener filtering**

P. Nicolas

Executive Summary: The demand for more sensitive perception of submarine signals buried within ocean noise requires statistical methods of analysis. A statistical sonar theory is concerned with the development of probability models for signals, interferences, and underwater experiment conditions, and, based on these models, the development of methods for the detection, identification, and classification of submarines.

Studies dealing with propagation in shallow water generally model the received signal as a convolution between a transmitted pulse (or wavelet) and the medium response. In this final report of one such study the principal aim is to extract more information on the medium - such as backscattering effects and multipath structure from a signal received on a point receiver or an array at a lower signal-to-noise ratio - than has been achieved previously. This clearly could have a direct impact on future sonar systems.

The principal advantage of the so-called method is that it does not require the usual assumption of minimum phase signals (or that all signals have a well behaved phase structure) and is therefore capable of coping with more realistic propagation conditions where, in general, the various signal arrivals have a complex mixed-phase structure.

The performance of the method is demonstrated using both simulated and real at-sea data. With the simulated data, deconvolution of the wavelet can be achieved down to a signal-to-noise ratio of -5 dB, while the multipaths are well separated at a signal-to-noise ratio of 5 dB. Using an explosive source and a vertical array receiver at sea one can separate the very close reflected and refracted paths near the surface in the order of 1 or 2 ms.



Accession For	
NTIS GRA&I	<input checked="" type="checkbox"/>
DTIC TAB	<input checked="" type="checkbox"/>
Unannounced	<input type="checkbox"/>
Justification	<input checked="" type="checkbox"/>
By _____	
Distribution/	
Availability Codes	
Dist	Avail and/or Special
A-1	

SACLANTCEN SM-20:

- iv -

:ntentionally blank page

**Deconvolution by homomorphic and
Wiener filtering**

P. Nicolas

Abstract: This study is concerned with deconvolution methods applied to underwater propagation in shallow water, whereby the received signal is modelled as the convolution between the transmitted pulse and the medium impulse response. The aim of the method is to extract information on backscattering, travel time delays, boundary reflection and refraction from the received signal on a point receiver or an array for both seismic and active sonar data. Since experimental data are generally mixed phase, due in part to the multiple reflections (bottom and surface), the conventional linear filtering which assumes the minimum phase property, loses in efficacy. In order to handle this mixed phase characteristic of the data, we proceed in two steps. We first apply a homomorphic filter (complex cepstrum) to deconvolve the wavelet. Then we deconvolve the medium impulse response by means of Wiener filter. The efficacy of the method is shown on both simulated and real data for explosive and active sonar data.

Keywords: active sonar ◦ backscattering ◦ bottom reflection ◦ boundary reflection ◦ complex cepstrum ◦ deconvolution ◦ homomorphic filtering ◦ linear filtering ◦ low frequency ◦ propagation ◦ receiver ◦ refraction ◦ seismic data ◦ shallow water ◦ surface reflection ◦ towed array ◦ travel time delay ◦ wavelet ◦ Wiener filtering

Contents

1. Introduction	1
2. Definition of the wavelet	2
3. Homomorphic deconvolution	5
3.1. Homomorphic systems	5
3.2. Complex cepstrum	6
4. Deconvolution of the medium response by Wiener filtering	20
4.1. Assumptions about the signals	20
4.2. Derivation of the Wiener filter	21
5. Combination of homomorphic deconvolution and Wiener filtering	27
5.1. Factorization of the mixed phase signals	27
5.2. Procedure to deconvolve the wavelet and the medium response	28
6. Results	29
6.1. Results obtained by simulation	29
6.2. Results obtained with experimental data	34
7. Conclusions	37
 References	 39
 Appendix A - Minimum-phase signals and their properties	 41
Appendix B - An example derivation of the complex cepstrum	47
Appendix C - Estimation of the rank of the correlation matrix R_{ss}	62

1. Introduction

In many fields of physics, such as geophysics, seismics and sonar, we are faced with problems of deconvolution. The observed signal received from a sensor in these fields is often considered to be formed by the convolution of the transmitted signal with the propagation medium impulse response. The goal of deconvolution filtering is to recover the medium impulse response from the recorded signal. Different methods have evolved according to the type of *a priori* information included in the signal modelling. If the transmitted signal is known exactly, Wiener filtering is conventionally applied under the assumption of minimum-phase signals¹ [1-3]. If the source signal is not known exactly (which is the case for an explosive) but can be modelled by a parametric transfer function, linear prediction methods can be used with success [4-6]. However these methods require the minimum phase condition. In real life the received signal is generally mixed-phase which is the case for seismic data. When considering this real constraint, another approach is non-linear filtering based on the generalized superposition principle proposed by Oppenheim and called homomorphic deconvolution [7]. This is based on the separation of the so-called wavelet and the medium impulse response in the cepstral domain [8,9]. Here we present a method which combines linear and non-linear filtering [10]. The aim of this method is to extract information on backscattering, travel-time delays, and boundary reflection and refraction from the received signal at a point receiver or an array--for both seismic and active sonar data. Since no assumption of minimum phase is made, we first apply a homomorphic technique (complex cepstrum) in order to deconvolve the wavelet.² The deconvolved wavelet is then taken as the known signal, and we estimate the boundary reflections and travel time-delays by means of Wiener filtering.

The report is structured as follows: first, we define the wavelet and the modelling of the medium behaviour; second, we advance the concept of homomorphic deconvolution and its mathematical formulation; third, we apply Wiener filtering to the recovery of boundary reflection and propagation time-delays; fourth we propose an improvement of the deconvolution method based on a combination of homomorphic deconvolution and Wiener filtering; and fifth the application to seismic and active sonar experiments is illustrated. We present results obtained on both simulated and field-recorded marine seismic data and active sonar data. We point out how the method can be used successfully in active sonar to analyse backscattering statistics. The important notion of minimum-phase signals, phase unwrapping and mathematical investigation of the complex cepstrum through models are expanded in appendices.

¹ The term 'minimum-phase signal' is defined in Appendix A.

² The term wavelet was introduced by among other people, Tribolet [11], and is defined and explained in the first part of the present report.

2. Definition of the wavelet

This section is devoted to the definition of the wavelet. It will be shown later that the wavelet contains information on the probability characteristics of reverberation and propagation conditions. The study of the statistical features of reverberation presents two points of specific interest: one is the properties of reverberation as sonar interference; the other is reverberation as a phenomenon which helps us to estimate the properties of the water medium and its boundaries. Reverberation can be classified into three types: volume reverberation, reverberation from a layer; and reverberation from a boundary. A propagation signal can originate from an explosion or can be a controlled pulse transmitted from a point source and received on an array of hydrophones (here a vertical array). As it propagates through the medium it follows three paths: the direct path; the surface reflected path; and the bottom-layer reflected path. Figure 1 represents the case of a source and an array closer to the surface as opposed than in Fig. 2, which shows a source and an array closer to the bottom. These figures present a simplified propagation model and do not take into account the ghosts and multiple arrivals; in a more realistic model these can be removed by adaptive linear filtering [12].

The backscatterings at the sea surface and at the layer boundary are defined respectively by the impulse response functions $h_s(t)$ and $h_l(t)$. The medium propagation is defined by the impulse response $h_m(t)$. These three impulse responses are random processes. In the first case (Fig. 1), the received signal is dominated by the direct arrival and the surface-reflected arrival. The layer-bottom reflected arrival comes much later and is therefore not included. Assuming that the medium and the surface boundary act as linear filters, the signal $y_1(t)$ —composed of the direct and surface-reflected paths—is given in the time interval $[0, T]$ by

$$y_1(t) = h_m(t) * x(t) + h_m(t) * h_s(t) * \delta(t - \tau_s) * x(t), \quad (1)$$

where $x(t)$ is the transmitted signal and τ_s the propagation time-delay along the surface path. In the second case (Fig. 2) and under the same assumption, the signal $y_2(t)$ —composed of the direct and bottom-layer reflected arrivals—is given, in the time interval $[0, T]$, by

$$y_2(t) = h_m(t) * x(t) + h_m(t) * h_l(t) * \delta(t - \tau_l) * x(t), \quad (2)$$

where τ_l is the propagation time-delay along the bottom-layer path.

Because the impulse responses $h_m(t)$, $h_l(t)$ and $h_s(t)$ are random processes, $y_1(t)$ and $y_2(t)$ defined on $[0, T]$ are to be considered as particular realizations of random

signals. By taking the fourier transform of both sides of (1) and (2), we have

$$Y_1(f) = H_m(f)X(f) + H_m(f)H_s(f)X(f)e^{-j2\pi f\tau_s}, \quad (3)$$

$$Y_2(f) = H_m(f)X(f) + H_m(f)H_i(f)X(f)e^{-j2\pi f\tau_i}, \quad (4)$$

where $Y_1(f)$ and $Y_2(f)$ are particular realizations of the spectrum of the signals $y_1(t)$ and $y_2(t)$ respectively. Both of the equations (3) and (4) can be factored in two ways

$$Y_1(f) = H_m(f)X(f) \left[1 + H_s(f)e^{-j2\pi f\tau_s} \right] \quad (5a)$$

$$= H_m(f)H_s(f)X(f)e^{-j2\pi f\tau_s} \left[1 + \frac{1}{H_s(f)}e^{j2\pi f\tau_s} \right], \quad (5b)$$

$$Y_2(f) = H_m(f)X(f) \left[1 + H_i(f)e^{-j2\pi f\tau_i} \right] \quad (6a)$$

$$= H_m(f)H_i(f)X(f)e^{-j2\pi f\tau_i} \left[1 + \frac{1}{H_i(f)}e^{j2\pi f\tau_i} \right]. \quad (6b)$$

By definition, the wavelet is given, with respect to the factored expression by

$$W_1(f) = \begin{cases} H_m(f)X(f) & \text{(first factored expression)} \\ H_m(f)H_s(f)X(f) & \text{(second factored expression)}, \end{cases}$$

$$W_2(f) = \begin{cases} H_m(f)X(f) & \text{(first factored expression)} \\ H_m(f)H_i(f)X(f) & \text{(second factored expression)}. \end{cases}$$

Depending on the factored expression, the wavelet contains information on only medium propagation or on both medium propagation and boundary backscattering. In order to separate the wavelet from the other components, we can take the complex logarithm of $Y_1(f)$ and $Y_2(f)$. If the surface impulse response is minimum phase (definition and details on minimum-phase signals are given in Appendix A), the modulus of $H_s(f)$ is less than unity and one uses the first factored expression.

$$\begin{aligned} \log Y_1(f) &= \log H_m(f)X(f) \left[1 + H_s(f)e^{-j2\pi f\tau_s} \right] \\ &= \log W_1(f) + H_s(f)e^{-j2\pi f\tau_s} - \frac{1}{2}H_s(f)^2e^{-j4\pi f\tau_s}. \end{aligned}$$

If the surface impulse response is not minimum phase, the module of $H_s(f)$ is greater than unity and the second factored expression is used:

$$\begin{aligned} \log Y_1(f) &= \log H_m(f) \log H_s(f)X(f)e^{-j2\pi f\tau_s} \left[1 + \frac{1}{H_s(f)}e^{j2\pi f\tau_s} \right] \\ &= \log W_2(f) + \frac{1}{H_s(f)}e^{j2\pi f\tau_s} - \frac{1}{2H_s(f)^2}e^{j4\pi f\tau_s} - e^{j2\pi f\tau_s}. \end{aligned}$$

We can do the same for the bottom-layer reflected path. Then, by using an appropriate filter and suppressing the linear phase component when the impulse response is not minimum phase, we can extract the wavelet from the received signal. In fact, instead of filtering the signal in the frequency domain, we filter the inverse fourier transform of the complex logarithm, which is the complex cepstrum by definition (see Sect. 3).

In brief, the wavelet is an artificial transmitted signal in the sense that it represents the transmitted signal modified by the propagation and backscattering characteristics. Depending on the boundary properties, the wavelet carries more information or less information (minimum or not minimum phase property). By extracting the impulse response functions $h_m(t)$, $h_s(t)$ and $h_l(t)$, we improve the modelling of medium propagation and backscattering statistics which can be compared to existing theoretical models.

3. Homomorphic deconvolution

3.1. HOMOMORPHIC SYSTEMS

In reverberation we are faced with the problem of filtering signals that have been combined by convolution. It would be advantageous to transform these non-linear systems into linear systems by applying the appropriate filtering. This leads to systems which obey the 'generalized principle of superposition'. Given two inputs let us assume that they are related together by a rule \circ . If s is a scalar let $:$ be a rule to combine s with any of the two inputs. Similarly, we denote \circ the rule to combine the outputs together and \bullet a rule to combine a scalar with an output. If H is the system transformation, we state:

$$H[x_1(t) \circ x_2(t)] = H[x_1(t)] \circ H[x_2(t)],$$

$$H[s : x_1(t)] = s \bullet H[x_1(t)].$$

The systems that verify the two preceding equations are said to obey a 'generalized principle of superposition' [9]. It can be shown that if the system inputs constitute a vector space with the operations \circ and $:$ corresponding to vector addition and scalar multiplication and the system outputs constitute a vector space with the operation \circ and \bullet corresponding to vector addition and scalar multiplication, then all systems of this kind can be represented as a cascade of three systems referred as the 'canonical representation of homomorphic systems', shown in Fig. 3.

The first system D_\circ has the following property:

$$D_\circ[x_1(t) \circ x_2(t)] = D_\circ[x_1(t)] + D_\circ[x_2(t)] = \hat{x}_1(t) + \hat{x}_2(t),$$

$$D_\circ[s : x_1(t)] = s D_\circ[x_1(t)] = s \hat{x}_1(t).$$

The effect of the system D_\circ is to transform the signals $x_1(t)$ and $x_2(t)$ according to the rule \circ into a conventional linear combination of corresponding signals $D_\circ[x_1(t)]$ and $D_\circ[x_2(t)]$. The system L is a linear system:

$$L[\hat{x}_1(t) + \hat{x}_2(t)] = L[\hat{x}_1(t)] + L[\hat{x}_2(t)] = \hat{y}_1(t) + \hat{y}_2(t),$$

$$L[s \hat{x}_1(t)] = s L[\hat{x}_1(t)] = s \hat{y}_1(t).$$

The system D_\circ^{-1} transforms from addition to the rule \circ :

$$D_\circ^{-1}[\hat{y}_1(t) + \hat{y}_2(t)] = D_\circ^{-1}[\hat{y}_1(t)] \circ D_\circ^{-1}[\hat{y}_2(t)] = y_1(t) \circ y_2(t),$$

$$D_\circ^{-1}[s \hat{y}_1(t)] = s \bullet D_\circ^{-1}[\hat{y}_1(t)] = s \bullet y_1(t).$$

All the homomorphic systems with the same input and the same output differ only in the linear part. Consequently, by choosing the transformations D_o and D_e we are left with a linear problem.

We are going to apply these results to convolved inputs signals. The rule \diamond becomes the convolution $*$. We choose the output rule \circ to be equal to the input rule and therefore \circ is also equal to the convolution $*$. The canonical representation of an homomorphic deconvolution system is shown in Fig. 4.

3.2. COMPLEX CEPSTRUM

■ 3.2.1. Mathematical representation of the system D_e and definition of the complex cepstrum

The system D_e is defined by the property that the z-transform (or the fourier transform on the unit circle) of its output is equal to the complex logarithm of the z-transform (or the fourier transform on the unit circle) of its input:

$$\begin{aligned}\tilde{x}(n) &= D_e[x(n)], \\ \tilde{X}(z) &= \log X(z),\end{aligned}$$

where $x(n)$ is the nth sample of $x(t)$. According to this definition, the characteristic system D_e of the homomorphic deconvolution is as shown in Fig. 5.

The output of the system D_e , denoted $\tilde{x}(n)$, is called the complex cepstrum of the input signal $x(n)$. This terminology is used by analogy to the power cepstrum defined by Bogert, Healy and Tukey. Specifically, the cepstrum of a signal was defined as the power spectrum of the logarithm of the power spectrum.

Remark These quantities are not too far from each other, because the power cepstrum is proportional to the even part of the complex cepstrum.

■ 3.2.2. Definition of the complex logarithm

In this section the complex logarithm chosen as the homomorphic system D_e is defined. One first sets the definition of the logarithm and then considers more particularly the phase unwrapping problem. Its prevalent role and the critical points of the different phase unwrapping methods are pointed out. To finish, some examples of phase unwrapping are given.

■ 3.2.2a. Definition

Let be $x(n)$ a real sequence and $X(z)$ its z-transform, one wants to define the

logarithm of $X(z)$. The complex logarithm is a 'multi-valued function' and therefore one must choose a determination for which the logarithm is a continuous function. Usually one takes the 'principal value determination' defined by

$$\log X(z) = \log |X(z)| + j \text{Arg}[X(z)],$$

where $\text{Arg}[X(z)] \in (-\pi, +\pi)$.

All the other determinations are obtained by adding a multiple of 2π to $\text{Arg}[X(z)]$. In our case the sequence $x(n)$ is a convolution of two sequences, $x_1(n)$ and $x_2(n)$:

$$\log X(z) = \log X_1(z) + \log X_2(z).$$

The principal value of the logarithm of the product of complex sequences is not always the sum of the principal value of each of the signals. This is in contradiction with the unicity of the homomorphic system D_* , and means that the complex logarithm cannot be defined from the principal determination alone. Besides given properties of the sequences $x(n)$ one needs another definition of the complex logarithm.

The complex logarithm will be defined from its derivative. If one assumes a single-value differentiable complex logarithm (principal value) and the analyticity of $X(z)$ one can derive the phase as follows:

$$\frac{d}{dz} \hat{X}(z) = \frac{d}{dz} [\log X(z)] = \frac{d}{dz} [\log |X(z)| + j \arg[X(z)]] = \frac{1}{X(z)} \frac{dX(z)}{dz}.$$

The evaluation of the complex logarithm on the unit circle $z = e^{j\omega}$ is performed in the following manner:

$$\frac{d}{dz} \hat{X}(z) = \frac{1}{jz} \frac{d\hat{X}(e^{j\omega})}{d\omega} = \frac{1}{X(e^{j\omega})} \frac{dX(e^{j\omega})}{d\omega} \frac{1}{jz},$$

so

$$\frac{d\hat{X}(e^{j\omega})}{d\omega} = \frac{1}{X(e^{j\omega})} \frac{dX(e^{j\omega})}{d\omega}.$$

Given $\hat{X}(e^{j\omega}) = \hat{X}_R(e^{j\omega}) + j\hat{X}_I(e^{j\omega})$, we have

$$\frac{d\hat{X}(e^{j\omega})}{d\omega} = \frac{d\hat{X}_R(e^{j\omega})}{d\omega} + j \frac{d\hat{X}_I(e^{j\omega})}{d\omega},$$

$$\hat{X}'(e^{j\omega}) = \hat{X}'_R(e^{j\omega}) + j\hat{X}'_I(e^{j\omega}),$$

where the prime indicates the differentiation with respect to ω .

Hence,

$$\begin{aligned} \frac{X'(e^{j\omega})}{X(e^{j\omega})} &= \frac{[X'_R(e^{j\omega}) + jX'_I(e^{j\omega})][X_R(e^{j\omega}) - jX_I(e^{j\omega})]}{|X(e^{j\omega})|^2}, \\ &= \frac{1}{|X(e^{j\omega})|^2} \left[[X'_R(e^{j\omega})X_R(e^{j\omega}) + X'_I(e^{j\omega})X_I(e^{j\omega})] \right. \\ &\quad \left. + j[X'_I(e^{j\omega})X_R(e^{j\omega}) - X'_R(e^{j\omega})X_I(e^{j\omega})] \right]. \end{aligned}$$

Since

$$\hat{X}'(e^{j\omega}) = \frac{X'(e^{j\omega})}{X(e^{j\omega})} = \frac{d}{d\omega} \log |X(e^{j\omega})| + j \frac{d}{d\omega} \arg[X(e^{j\omega})],$$

we have

$$\frac{d}{d\omega} \arg[X(e^{j\omega})] = \frac{X'_I(e^{j\omega})X_R(e^{j\omega}) - X'_R(e^{j\omega})X_I(e^{j\omega})}{|X(e^{j\omega})|^2}.$$

Property of the phase derivative: The phase derivative is an even function of ω since $z(t)$ is a real function.

Proof:

$$X(e^{j\omega}) = \int_{-\infty}^{+\infty} z(t)e^{-j\omega t} dt = X_R(e^{j\omega}) + jX_I(e^{j\omega})$$

$$\begin{aligned} X(e^{-j\omega}) &= \int_{-\infty}^{+\infty} z(t)e^{j\omega t} dt = \overline{X_R(e^{j\omega}) + jX_I(e^{j\omega})} \\ &= X_R(e^{j\omega}) - jX_I(e^{j\omega}) \end{aligned}$$

$$X(e^{-j\omega}) = X_R(e^{-j\omega}) + jX_I(e^{-j\omega}),$$

and hence,

$$\begin{aligned} X_R(e^{-j\omega}) &= X_R(e^{j\omega}), & X_I(e^{-j\omega}) &= -X_I(e^{j\omega}), \\ X'_R(e^{-j\omega}) &= -X'_R(e^{j\omega}), & X'_I(e^{-j\omega}) &= X'_I(e^{j\omega}), \end{aligned}$$

and

$$\frac{d}{d\omega} \arg[X(e^{j\omega})] = \frac{d}{d\omega} \arg[X(e^{-j\omega})].$$

Assumption: both $X(z)$ and $\hat{X}(z)$ are analytic in a region included the unit circle $X(z)$ and $\hat{X}(z)$ have no singularities on the unit circle. Consequently the functions $X_I(e^{j\omega})$, $X_R(e^{j\omega})$, $X'_I(e^{j\omega})$ and $X'_R(e^{j\omega})$ are analytic and the phase derivative is analytic in the convergence domain of $X(z)$ and $\hat{X}(z)$. Let us recall the following theorem:

Theorem: Let Ω be a continuum of the complex plane and f a continuous function on Ω . The necessary and sufficient condition for the function f to have a primitive is that the integral

$$\int_C f(z) dz$$

is null for any contour C included in Ω . Under this condition all the primitives $F(z)$ are obtained by the formula

$$F(z) = \int_{z_0}^z f(u) du + K,$$

where z_0 is a point of Ω and K an arbitrary complex constant. $\int_{z_0}^z f(u) du$ is the integral of f on any path of Ω , starting from the point z_0 and joining the point z .

As $d/dz X(z)$ is analytic in the convergence domain of $X(z)$ and $\hat{X}(z)$, we have according to the Cauchy theorem,

$$\int_C \frac{d}{dz} \arg[X(z)] dz = 0$$

on any contour C included in the convergence domain. According to previous results the phase is defined without any ambiguity on the unit circle to within an integration constant:

$$\arg[X(e^{j\omega})] = \int_0^\omega \frac{d}{d\omega} \arg[X(e^{j\omega})] d\omega + K.$$

The constant K is evaluated in the following way: the complex logarithm must fulfill the requirement, given two sequences $x_1(n)$ and $x_2(n)$,

$$\log X_1(e^{j\omega})X_2(e^{j\omega}) = \log X_1(e^{j\omega}) + \log X_2(e^{j\omega})$$

which is equivalent to

$$\begin{aligned} \log |X_1(e^{j\omega})X_2(e^{j\omega})| + j \arg[X_1(e^{j\omega})X_2(e^{j\omega})] \\ = \log |X_1(e^{j\omega})| + j \arg[X_1(e^{j\omega})] + \log |X_2(e^{j\omega})| + j \arg[X_2(e^{j\omega})]. \end{aligned}$$

One must have $\arg[X_1(e^{j\omega})X_2(e^{j\omega})] = \arg[X_1(e^{j\omega})] + \arg[X_2(e^{j\omega})]$, or

$$\begin{aligned} \int_0^\omega \frac{d}{d\omega} \arg[X_1(e^{j\omega})X_2(e^{j\omega})] d\omega + K_{12} &= \int_0^\omega \frac{d}{d\omega} \arg[X_1(e^{j\omega})] d\omega + K_1 \\ &+ \int_0^\omega \arg[X_2(e^{j\omega})] d\omega + K_2. \end{aligned}$$

To have this equality verified for any sequences $x_1(n)$ and $x_2(n)$, the constants K_1 , K_2 and K_{12} must vanish. To have the constant $K = 0$ means $\arg[X(e^{j\omega})]_{\omega=0} = 0$; but $X(e^{j\omega})|_{\omega=0} = \sum_{n=-\infty}^{+\infty} x(n)$, and so $\arg[\sum_{n=-\infty}^{+\infty} x(n)] = 0$.

■ 3.2.2b. *Properties of the phase $\arg\{X(e^{j\omega})\}$ and requirements for the signal $x(n)$*

The determination of the constant K leads to a specific property for the sequence $x(n)$: the dc component (polarity) must be positive.

And the phase has the following properties:

- (1) $\arg\{X(e^{j\omega})\}$ is an odd function of ω such that

$$\begin{aligned}\arg\{X(e^{-j\omega})\} &= \int_0^{-\omega} \frac{d}{d\omega} \arg\{X(e^{-j\omega})\} d\omega \\ &= \int_0^{-\omega} \frac{d}{d\omega} \arg\{X(e^{j\omega})\} d\omega \\ &= -\arg\{X(e^{j\omega})\},\end{aligned}$$

- (2) $\arg\{X(e^{j\omega})\}$ is a continuous function of ω ,

- (3) $\arg\{X(e^{j\omega})|_{\omega=\pi}\} = \int_0^{\pi} \frac{d}{d\omega} \arg\{X(e^{j\omega})\} d\omega = 0$ because $\arg\{X(e^{j\omega})\}$ is periodic in ω with a period 2π and is an odd function of ω .

Since the phase derivative is an even function of ω , we have

$$\begin{aligned}\int_{-\pi}^0 \frac{d}{d\omega} \arg\{X(e^{j\omega})\} d\omega &= -\int_{\pi}^0 \frac{d}{d\omega} \arg\{X(e^{-j\omega})\} d\omega \\ &= \int_0^{\pi} \frac{d}{d\omega} \arg\{X(e^{j\omega})\} d\omega.\end{aligned}$$

And so,

$$\frac{1}{2\pi} \int_{-\pi}^{\pi} \frac{d}{d\omega} \arg X(e^{j\omega}) d\omega = \frac{1}{\pi} \int_0^{\pi} \frac{d}{d\omega} \arg X(e^{j\omega}) d\omega,$$

and the previous requirement, for $\omega = \pi$, leads to a second property of the sequence $x(n)$: $x(n)$ must have a zero-mean phase derivative.

Conclusion: On the space of the sequences $x(n)$ with a positive dc component (polarity) and zero-mean phase derivative, the complex logarithm defines an invertible homomorphic system.

■ 3.2.3. *Phase unwrapping*

■ 3.2.3a. *Principle*

The phase unwrapping involves computing a continuous phase from the set of principal phase samples. Various techniques have been developed. A basic one is Schafer's Algorithm, which is based on the the following:

- (1) whenever a jump -2π is detected while unwrapping along the positive ω -axis a constant 2π is added to the principal value at that point, and
- (2) whenever a jump of 2π is detected while unwrapping along the positive ω -axis a constant -2π is added to the principal value at that point, with a 'jump' defined as the difference between a new principal value and an old one.

A jump has a threshold defined in terms of the difference between the two principal values at adjacent frequencies; below this threshold the jump does not exist. This implies a frequency sampling fine enough to set the difference in the principal values of two adjacent samples be detected as a jump. However although this algorithm is simple to implement it does not provide accurate results in the case of a sharp phase curve, since there is only principal value phase information and this is not sufficient.

To overcome this, we have completed the phase unwrapping by a modified Tribolet Algorithm, which takes into account the information in the first derivative of the phase. Let us recall briefly the principle of the Tribolet Algorithm [11].

One calculates the phase at the frequency ω from the mean of the integral

$$\arg X(e^{j\omega}) = \int_0^{\omega} \frac{d}{d\omega} \arg X(e^{j\omega}) d\omega.$$

This integral is approximated by the trapezoidal rule. Assuming that the phase is known at the frequency ω_i , one estimates the phase at the frequency ω_{i+1} ($\omega_{i+1} > \omega_i$) by

$$\widehat{\arg}[X(e^{j\omega_{i+1}})/\omega_i] = \arg X(e^{j\omega_i}) + \frac{1}{2}\Delta\omega \left[\frac{d}{d\omega} \arg X(e^{j\omega_{i+1}}) + \frac{d}{d\omega} \arg X(e^{j\omega_i}) \right],$$

where $\Delta\omega = \omega_{i+1} - \omega_i$.

A phase estimate is called consistent if

$$\exists k(\omega_{i+1}) \ni |\widehat{\arg}[X(e^{j\omega_{i+1}})/\omega_i] - \text{Arg}[X(e^{j\omega_i})] + 2\pi k(\omega_{i+1})| < \text{THLD1} < \pi.$$

The idea of the algorithm is to adapt the step size $\Delta\omega$ until the phase estimate becomes consistent. The algorithm requires a second threshold THLD2 in order to control the phase increase between two consecutive frequency samples. The unwrapped phase $\widehat{\arg}X(e^{j\omega_{i+1}})$ at frequency f is used to estimate the phase at frequency ω_{i+2} and so on. One recalls that the phase derivative is given by

$$\frac{d}{d\omega} \arg X(e^{j\omega}) = \frac{X_I'(e^{j\omega})X_R(e^{j\omega}) - X_R'(e^{j\omega})X_I(e^{j\omega})}{|X(e^{j\omega})|^2}.$$

Thus it can be computed very fast using the FFT according that

$$X'_R(e^{j\omega}) + jX'_I(e^{j\omega}) = -j\text{FFT}\{nz(n)\}.$$

This algorithm works well as long as the spectrum does not have any zeros close to the unit circle. In this case the phase derivative given by the previous relationship and computed by FFT has singularities and presents big spikes. Thus the phase increase is no larger controlled. To improve the Tribolet algorithm, an idea has been suggested by [13]. It consists of fitting a curve to the phase derivatives before performing the numerical integration: one fits cubic splines $S(\omega)$, having continuous first and second derivatives, to the phase derivative. The phase is then given by

$$\arg X(e^{j\omega}) = \int_0^\omega S(e^{j\omega}) d\omega,$$

or, according to [14]

$$\begin{aligned} \widehat{\arg}[X(e^{j\omega_{i+1}})/\omega_i] &= \arg X(e^{j\omega_i}) + \frac{1}{2}\Delta\omega \left[\frac{d}{d\omega} \arg X(e^{j\omega_{i+1}}) + \frac{d}{d\omega} \arg X(e^{j\omega_i}) \right] \\ &\quad - \frac{1}{12}\Delta\omega^2 \left[\frac{d}{d\omega} S(e^{j\omega_{i+1}}) - \frac{d}{d\omega} S(e^{j\omega_i}) \right], \end{aligned}$$

where

$$\frac{d}{d\omega} S(e^{j\omega}) = \frac{d^2}{d^2\omega} \arg X(e^{j\omega}).$$

This can be also computed by FFT as

$$\begin{aligned} \frac{d^2}{d^2\omega} \arg X(e^{j\omega}) &= \frac{1}{|X(e^{j\omega})|^4} \left[|X(e^{j\omega})|^2 (X_R(e^{j\omega})X''_I(e^{j\omega}) \right. \\ &\quad \left. - X_I(e^{j\omega})X''_R(e^{j\omega})) + 2X_R(e^{j\omega})X_I(e^{j\omega}) \right. \\ &\quad \left. [(X'_R(e^{j\omega}))^2 - (X'_I(e^{j\omega}))^2] + 2X'_R(e^{j\omega})X'_I(e^{j\omega}) \right. \\ &\quad \left. [(X_I^2(e^{j\omega}) - X_R^2(e^{j\omega}))] \right] \end{aligned}$$

and

$$X''_R(e^{j\omega}) + jX''_I(e^{j\omega}) = -\text{FFT}\{n^2 z(n)\}.$$

■ 3.2.3b. Examples of phase unwrapping

(a) First example

Let $y(n)$ be a time series which is the convolution of two time series: $w(n)$ which is a CW pulse windowed by a Hanning window and $r(n)$ given by

$$r(n) = \delta(n - n_1) + \delta(n - n_2) + \delta(n - n_3).$$

The following processing is applied to the time series $y(n)$:

- (1) compute the spectrum of $y(n)$ by FFT;
- (2) band-pass filter the spectrum around the CW pulse frequency;
- (3) apply the band-pass mapping system;
- (4) compute the first and second derivatives of the shifted and stretched spectrum;
- (5) compute the unwrapped phase.

$y(n)$ is a 256 time-sample series. The normalized CW frequency is 0.25 and the Hanning window length is 64 time-samples. The time series $r(n)$ is given by

$$r(n) = \delta(n - 55) + \delta(n - 90) + \delta(n - 125).$$

The band-pass mapping is defined as in §subsect. 3.2.6:

$$Y[e^{j\omega}] = \begin{cases} Y[e^{j\omega}] \neq 0, & \text{for } \omega_1 < |\omega| < \omega_2, \\ Y_R[e^{j\omega}] \neq 0, & \text{for } |\omega| = \omega_1, \omega_2, \\ 0, & \text{otherwise.} \end{cases}$$

The spectra of $w(n)$, $r(n)$ and $y(n)$ after band-pass mapping are depicted in Figs. 9, 10 and 11 respectively. The phases of $w(n)$, $r(n)$ and $y(n)$, before unwrapping, are represented in Figs. 12, 13 and 14. The first and second derivatives of the CW pulse phase are represented in Figs. 15 and 16. The first and second derivatives of the medium response phase are represented in Figs. 17 and 18. The first and second derivatives of the received signal phase are depicted in Figs. 19 and 20 respectively. The unwrapped phase of the wavelet, the medium response, and the received signal before removal of the linear phase, are represented in Figs. 21, 22 and 23 respectively. The unwrapped phase of the wavelet, the medium response, and the received signal after removal of the linear phase, are represented in Figs. 24, 25 and 26 respectively.

Remark The band-pass mapping introduces some small instabilities into the phase around the cut-off frequencies ω_1 and ω_2 . The instabilities are well shown on the first and second phase derivatives of the wavelet phase.

(b) Second example

Field marine explosive data have been recorded at the output of a vertical array of 32 hydrophones. The received signal path is composed of a direct path followed by a refracted and a reflected path at the sea surface. The bottom interaction comes much later and is not accounted for in the present data. One is looking at the output of the hydrophone 17. The phase unwrapping is processed on the full frequency band (no band-pass mapping) and the results are shown in Figs. 27 and 28.

■ 3.2.4. Properties of the complex cepstrum

The complex cepstrum has some properties which are useful for the design of filters and transmitted signals. Some of these properties are summarized below.

Property 1: The complex cepstrum of a convolution of two (or more) signals is the sum of the individual complex cepstra.

Property 2: The complex cepstrum $\hat{y}(n)$ of a minimum phase sequence $y(n)$ is zero for $n \leq 0$, and the complex cepstrum of a maximum phase sequence is zero for $n \geq 0$. (See the definition of a minimum and maximum phase sequence in Appendix A).

Property 3: The complex cepstrum of a pulse whose spectrum is smooth tends to be concentrated around low frequency values.

Property 4: The complex cepstrum of a periodic impulse train is a periodic impulse train with the same period.

■ 3.2.5. Sensitivity of the complex cepstrum to the noise

The more critical part of the complex cepstrum is the unwrapping of the phase due to its sensitivity to the additive noise. In the following discussion we try to show how the behaviour of the signal phase depends of the signal-to-noise ratio and the noise phase. The received signal plus additive noise can be expressed as

$$s(t) = y(t) + n(t),$$

where $y(t)$ is the convolution of two or more signals and $n(t)$ is the additive noise. In the frequency domain this equation becomes

$$S(\omega) = Y(\omega) + N(\omega)$$

and

$$\log S(\omega) = \log[Y(\omega) + N(\omega)]. \quad (7)$$

Equation (7) can be rewritten as

$$\log S(\omega) = \log Y(\omega) + \log \left[1 + \frac{N(\omega)}{Y(\omega)} \right].$$

If we consider a signal-to-noise ratio which is relatively high, we can assume that

$$\frac{N(\omega)}{Y(\omega)} \ll 1,$$

and Eq. (7) can be expanded into its Taylor series as follows:

$$\log S(\omega) = \log Y(\omega) + \frac{N(\omega)}{Y(\omega)} - \frac{1}{2} \left(\frac{N(\omega)}{Y(\omega)} \right)^2 + \dots$$

If we consider the terms of the series of the second order and higher to be negligible the phase of $S(\omega)$ can be expressed as follows:

$$\Phi_Y(\omega) + \frac{N(\omega)}{Y(\omega)} \sin[\Phi_N(\omega) - \Phi_Y(\omega)], \quad (8)$$

where $\Phi_N(\omega)$ and $\Phi_Y(\omega)$ are respectively the phase of the noise and the signal. If we now consider that the signal-to-noise ratio is low such that

$$\frac{N(\omega)}{Y(\omega)} \gg 1,$$

Equation (7) can be approximated as

$$\log S(\omega) = \log N(\omega) + \frac{Y(\omega)}{N(\omega)},$$

and the phase of $S(\omega)$ is equal to

$$\Phi_N(\omega) + \frac{Y(\omega)}{N(\omega)} \sin[\Phi_Y(\omega) - \Phi_N(\omega)]. \quad (9)$$

Equations (8) and (9) show that the phase of the received signal $s(t)$ can become unpredictable (random) because of the noise. When the signal-to-noise ratio is low (Eq. 9) the phase is dominated by the phase of the noise. The part of the noise spectrum which is not overlapped by the signal spectrum can be removed by band-pass filtering in order to avoid the situation of a low signal-to-noise ratio.

Remark The use of band-pass filters before the homomorphic deconvolution leads to the notion of band-pass systems (see Subsubject. 3.2.6).

■ 3.2.6. *Definition of the band-pass mapping system*

In many applications the signals have band-pass characteristics. In general the signals are band-pass filtered before being sampled in order to increase the signal-to-noise ratio. The homomorphic deconvolution as described above cannot be applied directly to the band-pass signal: the logarithm is not defined in the frequency domain where the signal vanishes. Before applying any cepstrum analysis one must find a system which transforms the band-pass signal into a full-band signal. Such a system is called a *band-pass mapping system*.

■ 3.2.6a. *Principle*

This notion of a *band-pass mapping system* has been introduced by Tribolet [11]. Let $x(n)$ be a stable sequence and $X[e^{j\omega}]$ its fourier transform satisfying

$$X[e^{j\omega}] = \begin{cases} X[e^{j\omega}] \neq 0, & \text{for } \omega_1 < |\omega| < \omega_2 \\ X_R[e^{j\omega}] \neq 0, & \text{for } |\omega| = \omega_1, \omega_2 \\ 0, & \text{otherwise,} \end{cases}$$

where ω_1, ω_2 are the cut-off frequencies. Let BP denote the band-pass mapping system operator defined by

$$\tilde{x}(n) = BP[x(n)]$$

such that the fourier transform of $\tilde{x}(n)$ verifies

$$\tilde{X}[e^{j\tilde{\omega}}] = X[e^{j\omega}], \quad 0 \leq |\tilde{\omega}| \leq \pi, \quad (10)$$

where

$$\tilde{\omega}(\omega) = \pi \frac{\omega - \omega_1}{\omega_2 - \omega_1}, \quad \omega_1 \leq |\omega| \leq \omega_2.$$

Remark This frequency transformation is a scaling operation that shifts and stretches the signal's pass-band to occupy all of the frequency band.

Tribolet has verified that this band-pass mapping is an invertible homomorphic operation with convolution as input and output operations. The inverse operation is defined by

$$\omega' = \omega_1 + \tilde{\omega} \frac{\omega_2 - \omega_1}{\pi}, \quad \omega_1 \leq \omega' \leq \omega_2,$$

$$X'[(e^{j\omega})] = \begin{cases} \tilde{X}[e^{j\tilde{\omega}}], & \text{for } \omega_1 \leq |\omega| \leq \omega_2, \\ 0, & \text{otherwise.} \end{cases}$$

From Eq. (10), we have

$$X'[e^{j\omega'}] = X[e^{j\omega}], \quad \text{for } \omega = \omega',$$

and thus

$$x'(n) = x(n).$$

The block diagram of the band-pass complex cepstrum system D_c is illustrated in Fig. 6. The band-pass mapping system is illustrated in Fig. 7 using simulated data. The received signal is the convolution of a Hanning-windowed CW pulse with three Dirac.

■ 3.2.6b. *Implementation of the band-pass mapping system*

Let $x(n)$ be a N (power of 2) samples sequence and $X(n)$ the corresponding DFT sequence. One may suppose the sampled spectrum to be symmetrically band-pass filtered around the normalized frequency 0.5, which corresponds to the frequency sample $\frac{1}{4}N$; the sampled cut-off frequencies are $\frac{1}{4}N - N_1$ and $\frac{1}{4}N + N_1$. The band-pass mapping operation can be decomposed into the four following phases:

- (1) shift the band-pass spectrum to 0,
- (2) compute the $2N_1 + 1$ inverse DFT of the sequence $X(n)$ for $\frac{1}{4}N - N_1 < n < \frac{1}{4}N + N_1$ in order to get a $2N_1 + 1$ time series,
- (3) zero-pad this new time series to get a time sequence of N samples,
- (4) compute the N inverse FFT.

Operations 2, 3 and 4 correspond to the stretching of the spectrum (spectrum interpolation).

The inverse band-pass mapping operation can be broken down into the four following phases:

- (1) cut the N samples deconvolved sequence at the first $2N_1 + 1$ samples;
- (2) compute the $2N_1 + 1$ DFT of the $2N_1 + 1$ sequence;
- (3) shift the spectrum to the $\frac{1}{4}N - N_1$ frequency sample; set the spectrum value $X(n)$ at 0 for $1 < n < \frac{1}{4}N - N_1 - 1$ and $\frac{1}{4}N + N_1 + 1 < n < \frac{1}{4}N$;
- (4) compute the N inverse FFT.

■ 3.2.7. *Normalization of the signal before applying the complex cepstrum*

■ 3.2.7a. *Principle*

When the time series $\tilde{x}(n)$ does not fulfill the requirements that its dc component (polarity) is positive and its mean phase derivative is equal to zero, the input sequence $\tilde{x}(n)$ must be normalized in order to be able to apply the complex cepstrum.

We recall that if $x(n)$ has a mean phase derivative no null,

$$\frac{1}{2\pi} \int_{-\pi}^{+\pi} \frac{d}{d\omega} \arg \tilde{X}[e^{j\omega}] d\omega = \tau,$$

$$\frac{1}{\pi} \int_0^{+\pi} \frac{d}{d\omega} \arg \tilde{X}[e^{j\omega}] d\omega = \frac{1}{\pi} \arg X[e^{j\omega}]|_{\omega=\pi} = \tau.$$

The first part of the normalization consists of multiplying $\tilde{X}[e^{j\omega}]$ by $e^{(-j\omega\tau)}$.

$$\frac{1}{\pi} \int_0^{+\pi} \frac{d}{d\omega} \arg [\tilde{X}[e^{j\omega}]e^{(-j\omega\tau)}] d\omega = \frac{1}{\pi} \arg X[e^{j\omega}] - \frac{1}{\pi} \int_0^{\pi} \tau d\omega = \tau - \tau = 0.$$

The second part of the normalization consists of multiplying $\tilde{X}[e^{j\omega}]$ by the polarity s_{α} .

■ 3.2.7b. *Restoration of the linear phase components*

Consider a signal $x(t)$ which is the convolution of two signals $x_1(t)$ and $x_2(t)$ and the respective spectra for which are given by

$$X_1(f) = X_{1nl}(f)e^{-j2\pi f\tau_1} \quad ,$$

$$X_2(f) = X_{2nl}(f)e^{-j2\pi f\tau_2} \quad ,$$

where $X_{1nl}(f)$ and $X_{2nl}(f)$ are respectively the non-linear phase components of $X_1(f)$ and $X_2(f)$. Then take the logarithm of $X(f)$

$$\log X(f) = \log |X_{1nl}(f)| + j \arg X_{1nl}(f) + \log |X_{2nl}(f)|$$

$$+ j \arg X_{2nl}(f) - j2\pi f\tau_1 - j2\pi f\tau_2.$$

And then remove the the linear phase component:

$$\log X_{nl}(f) = \log |X_{1nl}(f)| + j \arg X_{1nl}(f) + \log |X_{2nl}(f)| + j \arg X_{2nl}(f).$$

This last relation shows that we get an infinity of solutions comprising all the signals with the same non-linear phase components. Assuming that we are able to separate \hat{x}_{1nl} and \hat{x}_{2nl} in the cepstral domain, we must restore the proper linear phase to each of the deconvolved signals \hat{x}_{1nl} and \hat{x}_{2nl} . This task becomes infeasible if we do not have *a priori* information on the original signals $x_1(t)$ and $x_2(t)$. For example, if we assume that one of the signals has no linear phase component, let us say $x_2(t)$, then τ_2 equals zero and the global linear phase is restored to $\hat{x}_1(t)$. At this point it is more a matter of experimental conditions, as we can see in the example treated in Appendix B. In the results concerning the active sonar simulation, the deconvolved

wavelet is rescaled in time by computing the cross-correlation with the transmitted pulse.

The same problem arises for the signal polarity.

The global complex cepstrum deconvolution system is depicted in Fig. 8a.

4. Deconvolution of the medium response by Wiener filtering

The goal of this section is to provide a method of deconvolving the medium impulse response. Since the homomorphic deconvolution was not the best one for estimating the medium response (see Appendix B) in the presence of additive noise, we use a digital Wiener filter. It belongs to the class of linear time-invariant filters with a criterion of minimization of the mean quadratic error [27,28]. It attempts to optimally transform a given signal to another, here the received signal, into the medium impulse response. It is stressed that the estimation of the length and the lag of the Wiener filter are not treated here; those are discussed in [16]. The Wiener filter assumes that we know the wavelet, and therefore we can use the wavelet deconvolved by the complex cepstrum as the input signal of the filter. We derive two different but complementary filters: a causal Wiener filter which assumes a minimum phase wavelet and an anti-causal filter which assumes a maximum phase wavelet. This section considers (a) the assumptions about the signals and (b) the derivation of the Wiener filter.

4.1. ASSUMPTIONS ABOUT THE SIGNALS

We recall that the received signal has the following form:

$$s(m) = r(m) * w(m) + n(m) = y(m) + n(m),$$

where

$$y(m) = r(m) * w(m).$$

$w(m)$ and $r(m)$ are respectively the wavelet and the medium response. The stationarity of the signals and the noise is assumed up to the second order. We know the second-order statistics $E[r(m)^2]$ and $E[r(m)s(m)]$, or equivalent statistics—as we will see further on. Under these assumptions we estimate the medium response by using an estimator which is a linear function of the observation $s(m)$ and is given by

$$\hat{r}(m) = s(m) * h(m).$$

The Wiener filter characterized by $h(m)$ is defined by the minimization of the mean quadratic error

$$e^2 = E \left(\left[\sum_{k=-\infty}^{+\infty} h(k)s(m-k) - r(m) \right]^2 \right),$$

where E indicates the expected value. The filter $h(m)$ is characterized by its length P and the located interval $[-L, P-L+1] : h(m; P, L)$. P and L are respectively called the order and the lag of the filter.

4.2. DERIVATION OF THE WIENER FILTER

■ 4.2.1. Derivation of the zero-lag Wiener filter for minimum phase signals

The zero-lag Wiener filter characterized by $h(m, P)$ is defined by the minimization of the mean quadratic error

$$e^2 = E \left(\left[\sum_{k=-\infty}^{+\infty} h(k)s(m-k) - r(m) \right]^2 \right).$$

The filter $h(m, P)$ is characterized by its length P and the located interval $[0, P-1]$.

Derivation of the normal equations Let us define the prediction error e_1 by

$$e_1 = \sum_{k=0}^{P-1} h(k)y(m-k) + \sum_{k=0}^{P-1} h(k)n(m-k) - r(m), \quad m \in [0, P-1].$$

Then we have

$$e^2 = E(e_1^T e_1).$$

Let H be the matrix

$$[h(0), h(1), \dots, h(P-1)],$$

Y the matrix

$$[y(m), y(m-1), \dots, y(m-P+1)],$$

and N the matrix

$$[n(m), n(m-1), \dots, n(m-P+1)].$$

The mean quadratic error can be rewritten in the following form for each m :

$$e^2 = E([YH^T + NH^T - r(m)]^T [YH^T + NH^T - r(m)]).$$

If we assume that the sequences $y(m)$ and $r(m)$ are uncorrelated with the noise $n(m)$ and if one expands the r.h.s. of this equality one gets

$$e^2 = HE[Y^T Y]H^T + HE[N^T N]H^T - 2E[r(m)Y]H^T + E[r(m)^2].$$

R_{yy} , R_{nn} and R_{ry} are respectively the autocorrelation matrix of the sequence $y(m)$, the autocorrelation matrix of the noise $n(m)$, and the correlation vector of the sequence $y(m)$ with the scalar $r(m)$. We denote $R_{yy}(k)$, $R_{nn}(k)$ and $R_{ry}(k)$ respectively the quantities $E[y(m+l)y(m+l+k)]$, $E[n(m+l)n(m+l+k)]$, $E[r(m)y(m+k)]$.

If we assume a white noise, R_{nn} is a diagonal matrix $R_{nn}(0)I$, where I is the unit matrix and the mean quadratic error e^2 is given by

$$e^2 = HR_{yy}H^T + R_{nn}(0)HH^T - 2R_{ry}H^T + E\{r(m)^2\}.$$

Now we want to minimize the mean quadratic error and, classically, e^2 has a global minimum if the two following conditions are fulfilled:

- (1) $\nabla_H e^2 = 0$,
- (2) $\nabla_H(\nabla_H e^2)$ is positive definite ,

where $\nabla_H e^2$ and $\nabla_H(\nabla_H e^2)$ are respectively the gradient and the hessian of the mean quadratic error e^2 .

The first condition leads to

$$2HR_{yy} + 2R_{nn}(0)H - 2R_{ry} = 0$$

and the second condition requires the matrix $R_{yy} + R_{nn}(0)I$ to be positive definite. Thus the minimum is reached when

$$2H(R_{yy} + R_{nn}(0)I) = R_{ry}. \tag{11}$$

The linear system (11) is called the set of normal equations for the Wiener filter $h(m, P)$, and explicitly the set of normal equations is

$$\sum_{k=0}^{P-1} h(k, P)[R_{yy}(m-k) + R_{nn}(0)\delta(m-k)] = R_{ry}(m), \quad m \in [0, P-1]. \tag{12}$$

Remark i If the matrix $R_{yy} + R_{nn}(0)I$ is positive definite, one can directly find the solution, and e^2 can be expanded into a quadratic form as follows:

$$e^2 = \left[H - R_{ry}(R_{yy} + R_{nn}(0)I)^{-1} \right] \left[R_{yy} + R_{nn}(0)I \right] \left[H^T - (R_{yy} + R_{nn}(0)I)^{-1} R_{ry}^T \right] - R_{ry}(R_{yy} + R_{nn}(0)I)^{-1} R_{ry}^T + E\{r(m)^2\}.$$

e^2 vanishes if and only if $H - R_{ry}(R_{yy} + R_{nn}(0)I)^{-1}$ vanishes and the filter coefficients are given by the exact solution

$$H = R_{ry}(R_{yy} + R_{nn}(0)I)^{-1}.$$

In Eq. (12) we cannot access the correlation matrices R_{yy} and R_{ry} , and so we replace them by well-known second-order statistics.

If we take the z -transform of both sides of Eq. (12), we get after some straightforward derivations

$$\sum_{k=0}^{P-1} h(k, P) z^{-k} \left[\sum_{m=-\infty}^{\infty} (R_{yy}(m) + R_{nn}(0)\delta(m)) z^{-m} \right] = \sum_{m=-\infty}^{\infty} R_{ry}(m) z^{-m}.$$

According to the Blackman and Tukey definition of the Power Spectral Density, one gets

$$\sum_{k=0}^{P-1} h(k, P) z^{-k} (\Gamma_{yy}(z) + R_{nn}(0)) = \Gamma_{ry}(z), \quad (13)$$

where $\Gamma_{yy}(z)$ is the power spectral density of the sequence $y(n)$ and $\Gamma_{ry}(z)$ is the cross-spectral density of the sequence $r(n)$ with the sequence $y(n)$.

If the sequence $r(n)$ is uncorrelated

$$\Gamma_{ry}(z) = \Gamma_{rr}(z)W(z)^* = R_{rr}(0)W(z)^*, \quad (14)$$

and

$$\Gamma_{yy}(z) = \Gamma_{rr}(z)\Gamma_{ww}(z) = R_{rr}(0)\Gamma_{ww}(z), \quad (15)$$

where $\Gamma_{rr}(z)$ and $\Gamma_{ww}(z)$ are respectively the power spectral density of the sequences $r(n)$, $w(n)$ and R_{rr} the correlation function of $r(n)$.

Then Eq. (13) can be rewritten

$$\sum_{k=0}^{P-1} h(k, P) z^{-k} \left(\Gamma_{ww}(z) + \frac{R_{nn}(0)}{R_{rr}(0)} \right) = W(z)^*. \quad (16)$$

Coming back in the time domain, Eq. (16) assumes the form

$$\sum_{k=0}^{P-1} h(k, P) \left(R_{ww}(m-k) + \frac{R_{nn}(0)}{R_{rr}(0)} \delta(m-k) \right) = w(-m), \quad m \in [0, P-1]. \quad (17)$$

In this new set it does not matter if we do not know the autocorrelation R_{ww} exactly as we can estimate it—through $w(t)$ being the wavelet deconvolved by the complex cepstrum. However we do not know $R_{nn}(0)/R_{rr}(0)$, and so we have to estimate it.

Estimation of $R_{nn}(0)/R_{rr}(0)$ The principle of this estimation is the eigenvalue decomposition of the correlation matrices $R_{yy} + R_{nn}(0)I$ [26] and R_{ww} . According to classical linear algebra these matrices can be decomposed into the following forms:

$$R_{yy} + R_{nn}(0)I = U_y \Sigma_y U_y^T,$$

in which Σ_y is the diagonal matrix $\text{diag}(\sigma_1, \sigma_2, \dots, \sigma_P)$, with σ_i the eigenvalues of $R_{yy} + R_{nn}(0)I$.

$$R_{ww} = U_w \Sigma_w U_w^T,$$

Σ_w is the diagonal matrix $\text{diag}(\alpha_1, \alpha_2, \dots, \alpha_P)$, where the α_i are the eigenvalues of R_{ww} . The columns of U_w are the orthonormalized eigenvectors associated with these eigenvalues. In our case the eigenvalues are given by

$$\sigma_i = \lambda_i + R_{nn}(0), \quad i \in [1, P],$$

with λ_i the eigenvalues of the correlation matrix R_{yy} . At this point let us assume that the rank of R_{yy} is smaller than P . Because of the equality (15) the eigenvalues λ_i and α_i are linked together by the relation

$$\lambda_i = R_{rr}(0)\alpha_i.$$

Thus the rank of the matrix R_{yy} is equal to the rank of the matrix R_{ww} . The previous assumption is equivalent to assuming that the order of the wavelet is smaller than P . On the basis of this assumption the estimation procedure is as follows:

- (1) estimate the correlation matrix $R_{yy} + R_{nn}(0)$; compute the eigenvalues σ_i and the eigenvectors of this matrix;
- (2) estimate the correlation matrix R_{ww} ; compute the eigenvalues α_i and the eigenvectors of this matrix;
- (3) estimate the rank Q of the correlation matrix R_{yy} ;
- (4) estimate $R_{nn}(0)$ by taking the average of the $P - Q$ smallest eigenvalues σ_i (the eigenvalues are arranged in decreasing order):

$$R_{nn}(0) = \frac{1}{(P - Q)} \sum_{i=Q+1}^P \sigma_i.$$

- (5) estimate the eigenvalues λ_i from $\lambda_i = \sigma_i - R_{nn}(0)$.
- (6) estimate $R_{rr}(0)$ by means of $R_{rr}(0) = Q^{-1} \sum_{i=1}^Q \lambda_i / \alpha_i$.
- (7) compute $R_{nn}(0)/R_{rr}(0)$.

The rank Q is estimated by applying the AIC Akaike test to the correlation matrix $R_{ww} + R_{nn}(0)/R_{rr}(0)I$ [15]. One recalls that this test consists of estimating the

order of a model at the minimum of the function

$$f(q) = -\Phi(q) + \frac{\text{(number of free parameters)}}{N}$$

where $\Phi(q)$ is the Maximum Likelihood Function of the order q , N is the number of observations and P the order of the correlation matrix. In our case the function $f(q)$ is (see Appendix C)

$$f(q) = (P - q) \ln \left(\frac{1}{P - q} \sum_{i=q+1}^P \sigma_i \right) - \sum_{i=q+1}^P \ln(\sigma_i) + \frac{q(P + 1 - 1/2q)}{N}. \quad (18)$$

Figure 29 represents the eigenvalues of the correlation matrix R_{ww} for different transmitted pulses of 16 time-samples length (in these simulations, the wavelet was exactly the transmitted pulse):

- CW signal windowed by a rectangular window,
- CW signal windowed by a rectangular window,
- CW signal windowed by a half-cycle sinusoidal window,
- CW signal windowed by a Hanning window,
- CW signal windowed by a Hamming window.

In Fig. 30 we present the eigenvalues of $R_{ww}(0)$ for the same pulses but of 64 time-samples length.

In Figs. 31 and 32 we present the Akaike functions $f(q)$ applied to the matrix $R_{vv} + R_{nn}(0)I$ for pulse lengths of 16 and 64 time-samples respectively.

In Figs. 33 and 34 we present the estimate of $R_{nn}(0)/R_{rr}(0)$ for the four windows mentioned above for respectively 16 and 64 time-samples length. These results shows that the Hanning window is the one which is best at discriminating the eigenvalues corresponding to the wavelet and the eigenvalues corresponding to the noise.

Solution of the normal equations Taking into account the Toeplitz form of $R_{ww} + R_{nn}(0)/R_{rr}(0)I$, the normal Eqs. (17) are solved by the Levinson Algorithm [16].

Stability of the filter Since the wavelet $w(n)$ is minimum phase, Eq. (15) ensures the stability of the Wiener filter defined by $h(k, P)$.

■ 4.2.2. *Derivation of the zero-lag Wiener filter for maximum phase signals*

The derivation is similar to the derivation for minimum phase signals. This time, the filter $h(m, P)$ is characterised by its length P and the located interval $[-P + 1, 0]$.

Derivation of the normal equations Here, the prediction error e_1 is defined by

$$e_1 = \sum_{k=0}^{-P+1} h(k)y(m-k) + \sum_{k=0}^{-P+1} h(k)n(m-k) - r(m), \quad m \in [-P + 1, 0]$$

and we want to minimise the mean quadratic error

$$e = E(e_1^T e_1).$$

Using the same derivations that for minimum phase signals, we get to the set of normal equations which define the Wiener filter $h(m, P)$

$$\sum_{k=0}^{-P+1} h(k, P) [R_{yy}(m-k) + R_{nn}(0)\delta(m-k)] = R_{ry}(m), \quad m \in [-P + 1, 0]. \quad (19)$$

If we assume that the sequence $r(n)$ is uncorrelated and by means of derivations similar at the minimum phase case, Eq. (17) becomes

$$\sum_{k=0}^{-P+1} h(k, P) \left(R_{ww}(k-m) + \frac{R_{nn}(0)}{R_{rr}(0)} \delta(k-m) \right) = w(-m), \quad m \in [-P + 1, 0]. \quad (20)$$

The estimation of $R_{nn}(0)/R_{rr}(0)$ is identical to the estimation for minimum phase signals. Since $R_{ww} + R_{nn}(0)/R_{rr}(0)I$ has a toeplitz form, the solutions of Eq. (20) are obtained by the Generalised Levinson Algorithm. Since the wavelet $w(n)$ is maximum phase, Eq. (20) ensures the stability of the Wiener filter defined by $h(k, P)$.

5. Combination of homomorphic deconvolution and Wiener filtering

As we saw in Sect. 4, the Wiener filter is well defined for a minimum or maximum phase input sequence, but it is rather unstable for a mixed phase sequence. Since the received signal and the wavelet are mixed phase in real life (see Appendix B), an idea is to factorize the received signal and the wavelet into their minimum and maximum phase components. Then, in order to improve the deconvolution method, we can apply a zero-lag causal Wiener filter to the minimum phase component and an zero-lag anticausal Wiener filter to the maximum phase component. This idea has already been used by Oppenheim et al. [10], using a linear predictor instead of a Wiener filter. (Note that we do not present any results here on the combination of homomorphic deconvolution and Wiener filtering.)

5.1. FACTORIZATION OF THE MIXED PHASE SIGNALS

Let us assume, as in the previous chapters, that the received signal $y(t)$ is the convolution of the wavelet $w(t)$ with the medium response $r(t)$

$$y(t) = w(t) * r(t),$$

or in the z -domain

$$Y(z) = W(z)R(z).$$

If we assume that $Y(z)$ is a rational transfer function, $W(z)$ can be factorized as follows:

$$W(z) = W_{\min p}(z)W_{\max p}(z),$$

where $W_{\min p}(z)$ and $W_{\max p}(z)$ are respectively the minimum and maximum phase components of $W(z)$. In the same way, $R(z)$ can be factorized as follows:

$$R(z) = R_{\min p}(z)R_{\max p}(z),$$

where $R_{\min p}(z)$ and $R_{\max p}(z)$ are respectively the minimum and maximum phase components of $R(z)$. Therefore, $Y(z)$ can be rewritten in the following form:

$$Y(z) = [W_{\min p}(z)R_{\min p}(z)][W_{\max p}(z)R_{\max p}(z)],$$

or

$$Y(z) = Y_{\min p}(z)Y_{\max p}(z),$$

where

$$Y_{\min p}(z) = W_{\min p}(z)R_{\min p}(z),$$

$$Y_{\max p}(z) = W_{\max p}(z)R_{\max p}(z).$$

In the cepstral domain, the previous equations become

$$\hat{y}(t) = \hat{y}_{\min p}(t) + \hat{y}_{\max p}(t),$$

$$= [\hat{w}_{\min p}(t) + \hat{r}_{\min p}(t)] + [\hat{w}_{\max p}(t) + \hat{r}_{\max p}(t)].$$

According to the properties of the complex cepstrum recalled in Sect. 3, $\hat{y}_{\min p}(t)$ is equal to zero for the negative frequencies and $\hat{y}_{\max p}(t)$ is equal to zero for the positive frequencies. Then, by applying the complex cepstrum, we are able to factorized $y(t)$ and $w(t)$ into their minimum and maximum phase components.

5.2. PROCEDURE TO DECONVOLVE THE WAVELET AND THE MEDIUM RESPONSE

We first apply the complex cepstrum to the received signal $y(t)$. We filter the complex cepstrum $\hat{y}(t)$ by means of two rectangular windows. The first window is defined for the positive frequencies in order to extract the cepstrum $\hat{y}_{\min p}(t)$. The second window is defined for the negative frequencies in order to extract $\hat{y}_{\max p}$. Then, we low-pass filter $\hat{y}_{\min p}(t)$ to separate $\hat{w}_{\min p}(t)$ and $\hat{r}_{\min p}(t)$, and we high-pass filter $\hat{y}_{\max p}(t)$ to separate $\hat{w}_{\max p}(t)$ and $\hat{r}_{\max p}(t)$. Thus we get both the minimum and maximum phase components of the received signal and the deconvolved wavelet. The next step of the procedure consists of simultaneously applying a causal Wiener filter $h_{\min}(t)$ to $y_{\min p}(t)$ with $w_{\min p}(t)$ in input and an anti-causal Wiener filter $h_{\max}(t)$ to $y_{\max p}(t)$ with $w_{\max p}(t)$ in input.

The medium response $r(t)$ is estimated by the inverse filter $h_{\min}(t) * h_{\max}(t)$ as follow:

$$\hat{r}(t) = h_{\min}(t) * h_{\max}(t) * y(t).$$

The deconvolution procedure is shown schematically in Fig. 8b. The system D , is nothing other than the complex cepstrum as defined in Sect. 3.

6. Results

6.1. RESULTS OBTAINED BY SIMULATIONS

The results presented in this section relate to active sonar reverberation. They are summary-type representative results, proving the feasibility of the methods, but also pointing out their limitations. The transmitted signals are windowed CW pulses and the reverberated signals are received on a horizontal towed array.

■ 6.1.1. Reverberation in active sonar

We assume that reverberation is measured in deep water with a low-frequency omnidirectional source and a towed, horizontal array. We are looking at reverberated signals after beamforming. The simulations try to be an accurate copy of the experiments carried out for backscattering studies in active sonar (surface, volume and bottom-layer backscattering).

The simulations are described in terms of two models.

■ 6.1.1a. First model

The scenario is depicted in Fig. 35. Remember that it is the simulated signals after beamforming that are simulated. The simulation does not take any beamforming processing into account.

Description of the signals

Transmitted signal The transmitted signal is a Hanning-windowed CW pulse. The pulse length is taken as a parameter of the simulation. The sampled CW pulse is modelled in time as

$$x(n) = \sin[2\pi f_0(n-1)][1 - \cos(2\pi((n-1)/L))],$$

where L is the pulse length expressed in time-samples and f_0 is the normalised frequency of the CW signal. The CW pulse is represented in Fig. 36.

Medium impulse response The reverberation model has three paths: the direct path, the reflection on the surface and the reflection on the bottom. We do not model the transfer function of the surface, nor the bottom transfer function. The

travel times along the three paths are three parameters of the simulation, and depend on the source depth and its distance from the array, and the array and water depths. τ_D, τ_S, τ_L are respectively the arrival times for the direct path, the surface reflected path, and the bottom-layer reflected path. The three discrete-time paths are modelled as three Dirac at the time-samples n_D, n_S and n_L (where $\tau_D = n_D \Delta t, \tau_S = n_S \Delta t, \tau_L = n_L \Delta t$; Δt is the time sampling interval) and is given by

$$r(n) = -r\delta(n - n_D) + r^2\delta(n - n_S) - r^3\delta(n - n_L)$$

Additive noise The noise is characterized by its spectrum and the signal-to-noise ratio, and is defined as the response of a linear filter to an input white gaussian noise (random normal sequence). Because of the frequency step feature of the complex cepstrum, we are interested in the SNR at each frequency. Hence, three SNRs are defined. One of these, called SNRT, is the transmitted signal-to-noise ratio and another, called SNRR, is the received signal-to-noise ratio. These two SNRs are processed in the full frequency band as follows:

$$\text{SNRT}_{\text{dB}} = 10 \log \left(\frac{\int_0^B |X(f)|^2 df}{\int_0^B |N(f)|^2 df} \right)$$

$$\text{SNRR}_{\text{dB}} = 10 \log \left(\frac{\int_0^B |S(f)|^2 df}{\int_0^B |N(f)|^2 df} \right)$$

where $X(f)$, $S(f)$, and $N(f)$ are respectively the spectrum of the transmitted signal $x(t)$, the received signal $s(t)$, and the noise $n(t)$; B is the frequency band. We recall that the normalized Hanning CW pulse bandwidth is given by the well-known relation

$$B_{\text{CW}} = 4\pi/L.$$

The third signal-to-noise ratio, called SNRF, is defined at each frequency of the filtered bandwidth as follows:

$$\text{SNRF}_{\text{dB}} = 10 \log \left(\frac{|S(f)|^2}{|N(f)|^2} \right).$$

Description of the processing An observation time of 256 time-samples has been used and the pulse length is equal to 64 time-samples. The normalized frequency f_0 of the CW signal is equal to 0.25. First of all the received signal is band-pass filtered in frequency with a rectangular window defined by the lowest normalized frequency f_{min} and the highest normalized frequency f_{max} . These two frequencies are given here as $f_{\text{min}} = 0.222$ and $f_{\text{max}} = 0.277$. Then we apply the band-pass

mapping and the complex cepstrum to get the deconvolved wavelet. The medium impulse response is deconvolved by both complex cepstrum and Wiener filtering.

Results and their interpretation For a given pulse length and multipath configuration, we first look at the effect of the noise on the deconvolved signal accuracy. The results are summarized in Table 1 (the pulse length is 64 time-samples, the delays τ_D, τ_S, τ_L are respectively equal to 80, 110 and 170 time-samples).

Table 1

Classification of the results with the number of the corresponding figure. Active sonar simulation: Hanning CW pulse with 3 multiples

SNRR (dB)	Received signal	Power spectrum	Deconvolved wavelet	Deconvolved medium response (cepstrum)	Deconvolved medium response (Wiener)
13	Fig. 38	Fig. 39	Fig. 40	Fig. 41	Fig. 42
8	Fig. 43	Fig. 44	Fig. 45	failed	Fig. 46
3	Fig. 47	Fig. 48	Fig. 49	failed	Fig. 50
- 1	Fig. 51	Fig. 52	Fig. 53	failed	failed
- 6	Fig. 54	Fig. 55	Fig. 56	failed	failed
- 11	Fig. 57	Fig. 58	Fig. 59	failed	failed

We conclude that the wavelet is rather well deconvolved up to a SNRR of -6 dB and seems relatively insensitive to additive noise. The wavelet can be rescaled by correlation with the transmitted pulse. The correlation function of the deconvolved wavelet with the CW pulse for a received signal-to-noise ratio of 15 dB is depicted in Fig. 37. On the other hand, the medium impulse response suffers more from the additive noise, as we can see in Fig. 41. The complex cepstrum cannot deconvolve the medium response at lower signal-to-noise ratio. These results agree with the mathematical derivation in Appendix B, where it is shown that the medium impulse response deconvolved by the complex cepstrum is more affected by additive noise than the wavelet is. The Wiener filter, with the original pulse as input, can acceptably separate the three multipaths shown in Fig. 42. It does so successfully up to a SNR of 3 dB (the corresponding SNRR values are given in Table 2). In Figs. 42, 46 and 50, we see that the Wiener filter resolution is not 'optimal', as a consequence of the fact that we add a 'white noise' parameter to the zero-lag element of the auto-correlation matrix in order to stabilize the computation of the inverse [24]. Here, the white noise parameter is equal to 0.005. The ill-conditioned problem arises because the order of the received signal is smaller than the order of the linear system, as

shown by the Akaike test in the Sect. 4. Another reason is the non-minimum phase characteristic of the transmitted pulse.

Table 2
Signal-to-noise ratio of the received signal at each frequency of the bandwidth: Hanning CW pulse with 3 multiples

Normalised frequency	SNRF (dB)
0.222	- 90
0.223	6
0.230	8
0.234	4
0.238	4
0.242	12
0.246	17
0.250	18
0.254	17
0.258	24
0.261	17
0.265	14
0.269	12
0.273	- 9
0.277	- 4
SNRT = 10 dB SNRR = 3 dB	

■ 6.1.1b. *Second model*

Description of the signals

Transmitted signal The same transmitted pulse described in the previous section is used.

Medium impulse response Five equi-spaced multiples defined by the time delays $\tau_1, \tau_2, \tau_3, \tau_4,$ and τ_5 , with values, respectively, of 80, 110, 140, 170 and 200 time-samples.

Additive noise The same characteristics as that in the previous section.

Description of the processing The same processing as that in the previous section.

Results and their interpretation The results are summarized in Table 3.

Table 3

Signal-to-noise ratio of the received signal at each frequency of the bandwidth: Hanning CW pulse with 3 multiples

SNRR (dB)	Received signal	Power spectrum	Deconvolved wavelet	Deconvolved medium response (cepstrum)	Deconvolved medium response (Wiener)
16	Fig. 61	Fig. 62	Fig. 63	Fig. 64	Fig. 65
11	Fig. 66	Fig. 67	Fig. 68	Fig. 69	Fig. 70
6	Fig. 71	Fig. 72	Fig. 73	Fig. 74	Fig. 75
1	Fig. 76	Fig. 77	Fig. 78	Fig. 79	Fig. 80
- 4	Fig. 81	Fig. 82	Fig. 83	failed	failed

Table 4

Location of the poles of $H_0(z)$ given in polar coordinates

Pole (no.)	Radius	Angle (dg)	Pole (no.)	Radius	Angle (dg)
1	0.1	0	11	0.7	100
2	0.2	10	12	0.75	110
3	0.3	20	13	0.8	120
4	0.3	30	14	0.8	130
5	0.4	40	15	0.8	140
6	0.45	50	16	0.85	150
7	0.5	60	17	0.85	160
8	0.55	70	18	0.9	170
9	0.6	80	19	0.95	180
10	0.65	90	20	0.5	180

We conclude that the wavelet is well deconvolved up to a SNRR of 0 dB. The deconvolved wavelet can be rescaled by correlation with the transmitted pulse (as in the previous model). Figure 60 depicts this correlation function for a SNRR of 15 dB. The deconvolutions of the medium impulse response by the complex cepstrum and Wiener filtering are equivalent, and successful up to 0 dB. The time delay in the medium response deconvolved by the complex cepstrum is due to the linear phase not being recovered properly, but the relative positions of the multiples are correct.

6.2. RESULTS OBTAINED WITH EXPERIMENTAL DATA

■ 6.2.1. Reverberation in active sonar

Experiment configuration The purpose of the experiment was to measure reverberation with an activated towed array at low frequency. The geometrical configuration is depicted in Fig. 84 [23]. The towed array has 32 hydrophones spaced at one half-wavelength (1.96 m for the measurements processed here). The array depth was around 100 m and was separated from the towship by 900 m. The water depth was around 3500 m.

Signal characteristics The transmitted signal was a Hanning-windowed CW pulse. Its duration was 2 s at a frequency of 370 kHz. The signal received on the array is beamformed and band-pass filtered in frequency. The sampling frequency at the beamformer output was 70 Hz, and the observation time was 3.65 s (256 time-samples). The resolution in time provided by this transmitted signal is

$$t_r = \frac{1}{\text{bandwidth}},$$

or in this case

$$t_r = 1.438 \text{ s.}$$

The blocks of recorded data are characterized by the number of the beam, the number of the ping, and the range.

Description of the processing The processing was the same as that for the simulated data of Subsubsect. 6.1.1a.

Results Figure 85 depicts the transmitted pulse in time. The received signal corresponding to beam 6, ping 9 and range 8 is represented in Fig. 86. The wavelet

deconvolved by means of the complex cepstrum is represented in Fig. 87. When we compared the deconvolved medium response for two different inputs of the Wiener filter (the deconvolved wavelet and the transmitted pulse). The results depicted Figs. 88 and 89 were obtained. The results are similar in both figures, except that we get a better resolution with the transmitted pulse (Fig. 89). The deconvolved wavelet looks like the transmitted pulse, which is a promising result. However, the pulse length reduces the credibility of the results significantly, is obviously not the type of signal one should use to study reverberation. (In order to measure surface, volume and bottom backscattering, the transmitted pulse must have a significant bandwidth, and instead of using CW pulses of 2 s it would be more sensible to transmit pulses of 0.1 s, for example.)

■ 6.2.2. Explosive data

Experiment configuration The data come from an acoustic propagation experiment made by the Centre's Environmental Acoustics Group in the Tyrrhenian sea. The aim of the experiment was to estimate the transfer function of the ocean over a broad acoustic frequency range. The broadband signal arising from an explosive source was recorded (a) at a range of 4.5 km with a vertical array of 32 hydrophones spaced at 2 m, and (b) close to the source with a portable array of 4 hydrophones. The experiment configuration, with its various geometrical parameters, is presented in Fig. 90. Before any kind of processing one can expect at least four arrivals: one direct, one by reflection and one by refraction at the sea surface, and later one by reflection at the seabed. Since it is a deep water environment, we do not consider the bottom reflection.

Signal characteristics The explosive is a broad band source. The power spectrum of the signal received on hydrophone 17 of the vertical array is depicted in Fig. 93. The sampling frequency was 6 kHz. Therefore, according to Fig. 93 the received signal bandwidth was almost 2.5 kHz. The time series at the output of each hydrophone is represented on Fig. 91.

Description of the processing The observation time was 170 ms (or 1024 time-samples). We processed the full frequency band (no band-pass mapping). The wavelet was deconvolved by the complex cepstrum, and the paths reflected and paths refracted at the surface were resolved by Wiener filtering.

Results The received time series for hydrophones 4 and 17 are depicted on Figs. 92 and 94. The deconvolved wavelets are presented in Figs. 95 and 96. The minimum phase property of the wavelet can be studied in Fig. 97, which shows the partial

energy of the two deconvolved wavelets. The partial energy is defined as follows [22]

$$E_p(m) = \sum_{n=1}^m |w(n)|^2.$$

The two deconvolved wavelets carry the same quantity of energy. The wavelet for hydrophone 4 has more energy at the beginning; the wavelet for hydrophone 17 has more energy at the end. Their power spectra are identical, as we can see in Figs. 98 and 99. It seems that some poles or zeros of the transfer function of the wavelet has been transferred outside of the unit circle. We can see that the wavelets are not minimum phase, most definitely for the wavelet corresponding to hydrophone 17. If we compare the results to a theoretical wavelet, it seems the original shot has been perturbed by the propagation medium and perhaps also the layer conditions (the sea-surface was flat during the experiment and introduced only a time-delay). If we use the deconvolved wavelet in order to resolve the reflected and refracted paths, we have no success. Therefore, we use the first arrival as the input of the Wiener filter. The deconvolved reflected and refracted arrivals corresponding to hydrophones 4 and 17 are presented respectively in Figs. 100 and 101. The results for the entire vertical array are presented in Fig. 102, with the direct arrival taken as the time origin.

These results confirm the hypothesis of three main arrivals, one direct, one refracted and one reflected. The assumed propagation model is depicted in Fig. 102b, which also shows the mean sound-velocity profile estimated from the measurements.

7. Conclusions

The study carried out in this report has pointed out the importance of the phase information in the understanding of propagation and reverberation mechanisms. Since the phase behaviour is rather complicated due, in part to its randomness, we need some accurate signal processing methods to perform the analysis. By modelling the propagation medium, the bottom-layer, and the surface as linear filters one may apply techniques such as deconvolution and identification methods.

The complex cepstrum used to deconvolve the wavelet does not postulate a minimum or maximum phase characteristic for the signals, and therefore is very useful in propagation and reverberation application, for which the signals are mostly mixed phase. Although the complex cepstrum requires a relatively high signal-to-noise ratio, because of the phase unwrapping, its application to seismic and active sonar reverberation is meaningful. The results obtained and presented in Sect. 6 with simulated data are quite satisfactory up to a signal-to-noise ratio of -5 dB for the wavelet, but only up to 5 dB for the medium response. These results confirm the derivation made in Appendix B, proving that the complex cepstrum does not succeed in deconvolving the medium response as well as it does for the wavelet, due to the presence of additive noise. We have seen that the deconvolved wavelet carries a lot of information on the medium and a further focus would be to fit a parametric model and control its behaviour with the propagation conditions. This can be done by using autoregressive (AR) or autoregressive-moving average (ARMA) modelling of the wavelet.

The results shown in Sect. 6, on explosive measured data, emphasize the importance of the phase. We have seen that the deconvolved wavelet at two separate hydrophones of the vertical array can have the same power spectrum but not the same energy distribution (shown by the partial energy curves). The transfer function treated in Appendix A is an example of how an all-pass filter can modify the energy distribution inside a signal, transforming it from a minimum phase signal to a mixed phase signal. This can arise when the transmitted pulse goes through a layer which has an all-pass-filter transfer function (Appendix B). In this environmental technique like the power cepstrum method is not powerful enough. One deficiency underlined in this report, concerning the complex cepstrum technique, is the restoration of the linear phase once the different components have been deconvolved. In the described simulations in Sect. 6, this equipment has been solved by computing the crosscorrelation between the deconvolved wavelet and the transmitted pulse. However, some more attention has to be put on this particular but significant part of the complex cepstrum.

The combination of homomorphic deconvolution and Wiener filtering is well adapted to reverberation studies in that it capitalises on the individual advantages of both the techniques. The homomorphic deconvolution handles the mixed phase characteristics of the wavelet while the Wiener filter provides high resolution of the medium response, as, for example time-of-arrivals estimation. Some results using this promising mixed technique will be the subject of a subsequent report.

References

- [1] RICE, R.B. Inverse convolution filters. *Geophysics*, **27**, 1962: 4-18.
- [2] ROBINSON, E.A. Multichannel z-transforms and minimum delay. *Geophysics*, **31**, 1966: 473-500.
- [3] ROBINSON, E.A. and TREITEL, S. Principles of digital Wiener filtering. *Geophysical Prospecting*, **15**, 1967: 311-333.
- [4] MAKHOUL, J. Linear prediction: a tutorial review. *Proceedings of the IEEE*, **63**, 1975: 561-580.
- [5] ATAL, B.S. and HANAUER, S.L. Speech analysis and synthesis by linear prediction of the speech wave. *Journal of the Acoustical Society of America*, **50**, 1971: 637-655.
- [6] MARKEL, J.D., GRAY, A.H. and WAKITA, H. Linear prediction of speech-theory and practice, Monograph 10. Santa Barbara, CA, Speech Communication Research Laboratory, 1973.
- [7] OPPENHEIM, A.V. Superposition in a class of non-linear systems, TR-432. Cambridge, MA, MIT, 1965.
- [8] OPPENHEIM, A.V., SCHAFER, R.W. and STOCKHAM, T.G. Nonlinear filtering of multiplied and convolved signals. *Proceedings of the IEEE*, **56**, 1968: 1264-1291.
- [9] OPPENHEIM, A.V. and SCHAFER, R.W. Digital Signal Processing. Englewood Cliffs, NJ, Prentice-Hall, 1975.
- [10] OPPENHEIM, A.V., KOPEC, G.E. and TRIBOLET, J.M. Signal analysis by homomorphic prediction. *IEEE Transactions on Acoustics, Speech and Signal Processing*, **24**, 1976: 327-332.
- [11] TRIBOLET, J.M. Seismic Application of Homomorphic Signal Processing. Englewood Cliffs, NJ, Prentice-Hall, 1978.
- [12] GRIFFITHS, L.J., SMOLKA, F.R. and TREMBLY, L.D. Adaptive deconvolution: a new technique for processing time-varying seismic data. *Geophysics*, **42**, 1977: 742-759.
- [13] BHANU, B. and McCLELLAN, J.H. On the computation of the complex cepstrum. *IEEE transactions on Acoustics, Speech and Signal Processing*, **28**, 1980: 583-585.
- [14] BHANU, B. Computation of the complex cepstrum thesis, Cambridge, MA, MIT, 1977.
- [15] AKAIKE, H.A. A new look at the statistical model identification. In: CHILDERS, D.G., ed. Modern Spectrum Analysis. Piscataway, NJ, IEEE Press, 1978: pp. 234-241.
- [16] TREITEL, S. and ROBINSON, E.A. The Design of High-Resolution Digital Filters. *IEEE Transactions on Geoscience Electronics*, **4**, 1966: 25-38.
- [17] LEVINSON, N. The Wiener RMS (root mean square) error criterion in filter design and prediction. *Journal of Mathematical Physics*, **25**, 1947: 261-278.
- [18] URICK, R.J. Principles of Underwater Sound, 2nd edition. New York, NY, McGraw-Hill, 1975.

- [19] BREKHOVSKIKH, L. and LYSANOV, Yu. *Fundamentals of Ocean Acoustics*. Berlin, Springer, 1982.
- [20] FORTUIN, L. The sea surface as a random filter for underwater sound waves. *Journal of the Acoustical Society of America*, **62**, 1972: 302-315.
- [21] BOGERT, B., HEALY, H. and TUKEY, J. The frequency analysis of time series for echoes. *In: ROSENBLATT, M. ed. Proceedings of the symposium on Time Series Analysis*. New York, NY, Wiley, 1963: pp. 209-243.
- [22] ROBINSON, E.A. and TREITEL, S. *Geophysical Signal Analysis*. Englewood Cliffs, NJ, Prentice-Hall, 1980.
- [23] MARANDINO, D. and GOLDSBERRY, T.G. Evaluation of low-frequency bottom backscattering strength vs grazing angle by means of multiple beamforming. *In: AKAL, T. and BERKSON, J.M. eds. Ocean Seismo-Acoustics, Low-frequency Underwater Acoustics. Proceedings of the symposium organised by SACLANTCEN, held June 10-14, 1985, Lerici, Italy*. New York, NY, Plenum, 1986: pp. 355-364.
- [24] JURKEVICS, A. and WIGGINS, R. A critique of seismic deconvolution methods. *Geophysics*, **49**, 1984: 2109-2116.
- [25] TREITEL, S. and ROBINSON, E.A. Seismic Wave Propagation in layer media in terms of communication theory. *Geophysics*, **31**, 1966: 17-32.
- [26] WILKINSON, J.H. and REINSCH, C. *Linear Algebra*. Berlin, Springer, 1971.
- [27] ARQUES, P.Y. *Décisions en Traitement du Signal*. Paris, Masson, 1982.
- [28] VAN TREES, H.L. *Detection, Estimation and Modulation Theory, part I*. New York, NY, Wiley, 1968.
- [29] VEZZOSI, G. and NICOLAS, P. Séparation de fronts d'ondes corrélés. *In: GROUPE D'ETUDE DU TRAITEMENT DU SIGNAL. Neuvième colloque sur le traitement du signal, Nice, 16-20 mai 1983. Nice, France, GRETSI, 1983: pp. 277-282.*

Appendix A

Minimum-phase signals and their properties

The notion of minimum-phase signals is of considerable importance in signal processing [9]. In this section it will be shown that the fourier transform of a minimum-phase signal can be recovered from its magnitude or its phase. Because most of the digital filters are defined in term of magnitude, it is important to know the phase in order to design stable filters. The minimum-phase condition gives some nice properties to the complex cepstrum [8] and allow us to design inverse filters [16].

Before giving the definition of a minimum phase signal, let us recall the definition of a causal signal in order to make an analogy between the complex cepstrum of a minimum-phase sequence and a causal signal.

A.1. DEFINITION OF A CAUSAL SIGNAL-PROPERTY OF ITS FOURIER TRANSFORM

The values of a causal signal $x(t)$ are null for the negative values of t . We can always write $x(t)$ as a sum of an odd function $x_{\text{odd}}(t)$ and even function $x_{\text{even}}(t)$:

$$x(t) = x_{\text{odd}}(t) + x_{\text{even}}(t),$$

where

$$x_{\text{even}}(t) = \frac{1}{2}(x(t) + x(-t)), \quad (\text{A.1})$$

$$x_{\text{odd}}(t) = \frac{1}{2}(x(t) - x(-t)). \quad (\text{A.2})$$

For the positive values of t we have

$$x_{\text{even}}(t) = x_{\text{odd}}(t) = \frac{1}{2}x(t),$$

and for the negative values

$$x_{\text{odd}}(t) = -x_{\text{even}}(t) = -\frac{1}{2}x(-t),$$

and we can rewrite

$$x_{\text{odd}}(t) = \text{sig}(t)x_{\text{even}}(t), \quad (\text{A.3})$$

$$x_{\text{even}}(t) = \text{sig}(t)x_{\text{odd}}(t). \quad (\text{A.4})$$

By taking the fourier transform of both of the sides of the equality (Eq. A.1) and calling respectively $X_{\text{even}}(f)$ and $X(f)$ the fourier transform of $x_{\text{even}}(t)$ and $x(t)$, we have

$$\begin{aligned} X_{\text{even}}(f) &= \int_{-\infty}^{+\infty} x_{\text{even}}(t) e^{-j2\pi t} dt = \frac{1}{2} \int_{-\infty}^{+\infty} x(t) e^{-j2\pi t} dt + \frac{1}{2} \int_{-\infty}^{+\infty} x(-t) e^{-j2\pi t} dt \\ &= \frac{1}{2} \int_{-\infty}^{+\infty} x(t) e^{-j2\pi t} dt - \frac{1}{2} \int_{-\infty}^{+\infty} x(t) e^{j2\pi t} dt \\ &= \frac{1}{2} [X(f) - \bar{X}(f)] = i \text{Im} X(f). \end{aligned}$$

By taking the fourier transform of both the sided of Eq. (A.2) and calling $X_{\text{odd}}(f)$ the fourier transform of $x_{\text{odd}}(t)$, we get

$$\begin{aligned} X_{\text{odd}}(f) &= \frac{1}{2} \int_{-\infty}^{+\infty} x(t) e^{-j2\pi t} dt - \frac{1}{2} \int_{-\infty}^{+\infty} x(-t) e^{j2\pi t} dt \\ &= \frac{1}{2} [X(f) + \bar{X}(f)] = \text{Re} X(f). \end{aligned}$$

If we take now the fourier transform of (A.3) we have

$$\begin{aligned} X_{\text{odd}}(f) &= \text{fourier transform}[\text{sig}(t)] * X_{\text{even}}(f), \\ &= \frac{1}{\pi i} \text{vp} \left(\frac{1}{f} \right) * i \text{Im} X(f), \end{aligned}$$

where $\text{vp}(1/f)$ is the Cauchy principal value of $\int_{-\infty}^{+\infty} (1/f) df$.

Then

$$X_{\text{odd}}(f) = \frac{1}{i\pi} \text{vp} \int_{-\infty}^{+\infty} \frac{i \text{Im} X(\nu)}{f - \nu} d\nu$$

or

$$\text{Re} X(f) = \frac{1}{\pi} \text{vp} \int_{-\infty}^{+\infty} \frac{\text{Im} X(\nu)}{f - \nu} d\nu = \text{hilbert transform}[\text{Im} X(f)].$$

If we take the fourier transform of (A.4), we have

$$\begin{aligned} X_{\text{even}}(f) &= \frac{1}{\pi i} \text{vp} \left(\frac{1}{f} \right) * \text{Re} X(f), \\ &= -i \frac{1}{\pi} \text{vp} \int_{-\infty}^{+\infty} \frac{\text{Re} X(\nu)}{f - \nu} d\nu \\ &= \text{inverse hilbert transform}[\text{Re}(X(f))]. \end{aligned}$$

By performing the inverse process we show that if $\text{Im } X(f)$ and $\text{Re } X(f)$ are related through a hilbert transform, the signal $x(t)$ is causal.

Therefore a causal signal is characterized by the fact that the real part and the imaginary part of its fourier transform are related through a hilbert transform.

The z -transform of a causal sequence $x(n)$ converges in the domain

$$(R, +\infty)$$

but this necessary condition is not sufficient to steady the causality of $x(n)$. A necessary and sufficient condition is given by the following theorem.

Theorem: $X(z)$ is the z -transform of a causal sequence $x(n)$ if and only if $X(z)$ is bounded when z reaches the infinity.

A.2. DEFINITION OF A MINIMUM-PHASE SIGNAL

■ A.2.1. Definition

Let $\hat{X}(z)$ be defined by

$$\hat{X}(z) = \log X(z) = \log |X(z)| + i \arg X(z),$$

and let $\hat{x}(n)$ be the inverse z -transform of $\hat{X}(z)$; $\hat{x}(n)$ is by definition the complex cepstrum of $x(n)$ [see Sect. 3].

The minimum-phase condition is that the complex cepstrum $\hat{x}(n)$ is causal or, according to the previous section, that

$$\log |X(z)| = \text{hilbert transform}[\arg X(z)]. \quad (\text{A.5})$$

For a minimum-phase signal $x(t)$, the phase of $X(f)$ is uniquely defined from the magnitude $\log |X(f)|$. Another condition is that there is causal, stable inverse system $X^{-1}(z)$ such that

$$X^{-1}(z)X(z) = 1$$

There is a consequential property of the minimum-phase sequences $x(n)$: the poles and the zeros of the z -transform $X(z)$ are inside the unit circle.

■ A.2.2. Justification of the terminology 'minimum-phase signal' [22]

Let $X(z)$ be the z -transform of any signal $x(t)$. $X(z)$ can be written as a product of two functions

$$X(z) = X_0(z)G_{s.p.}(z), \quad (\text{A.5})$$

where $X_0(z)$ is the z -transform of a minimum-phase signal $x_0(t)$ and $G_{a.p.}(z)$ the transfer function of an all-pass filter. The role of $G_{a.p.}(z)$ is to transfer M zeros of $X_0(z)$ outside the unit circle without modifying the magnitude response $|X_0(z)|$ and $X(z)$ can be rewritten in the following form

$$X(z) = G_0(z) \prod_{m=1}^M (z - z_m),$$

where z_m are the M zeros of $X(z)$ outside the unit circle. To render the terminology 'minimum-phase' explicit, let $G_{a.p.}(z)$ be an all all-pass transfer function of order one with only one real zero. $G_{a.p.}(z)$ is given by

$$G_{a.p.}(z) = \frac{z + \bar{c}}{1 + cz} \quad \text{with } |c| \leq 1.$$

$G_{a.p.}(z)$ has a zero (Z) at $z_1 = -\bar{c}$ and a pole (P) at $z_2 = \frac{-1}{c}$. The zero-pole diagram of $G_{a.p.}(z)$ is presented in Fig. 103.

The phase-lag angle of $G_{a.p.}(z)$ is given by

$$\Phi(z) = -(\Phi_Z(z) - \Phi_P(z)) = \Phi_P(z) - \Phi_Z(z),$$

where $\Phi_Z(z)$ and $\Phi_P(z)$ are respectively the angles of the vectors \overline{PM} and \overline{ZM} with the axis O_x . For the normalized frequency f in the range $[0, \frac{1}{2}]$ the phase-lag is always positive. Let $\Phi_X(z)$ and $\Phi_{X_0}(z)$ be the phases of $X(z)$ and $X_0(z)$, and we have

$$\Phi_X(z) = \Phi_{X_0}(z) - \Phi(z)$$

or

$$-\Phi_X(z) = -\Phi_{X_0}(z) + \Phi(z), \tag{A.7}$$

and therefore the phase-lag angle of the function $X(z)$ is always greater than the phase-lag angle of the function $X_0(z)$. The all-pass transfer function $G_{a.p.}(z)$ can be decomposed into a product of M all-pass transfer functions of order one, and consequently following (A.7) the phase-lag angle of any function $X(z)$ is always greater than the phase-lag angle of the function $X_0(z)$, which is why $x_0(t)$ is called a minimum phase-lag signal or by abbreviation minimum-phase signal.

Remark Given two functions $X_1(z)$ and $X_2(z)$, one has

$$|X_1(z)| = |X_2(z)| \quad \text{and} \quad \Phi_{X_1}(z) \neq \Phi_{X_2}(z)$$

if

$$X_1(z) = X_0(z)G_{a.p.1}(z)$$

$$X_2(z) = X_0(z)G_{a.p.2}(z).$$

Hence for a given magnitude $|X(z)| = |X_1(z)| = |X_2(z)|$, the phase-lag is not defined uniquely. It is uniquely defined if $x_1(t)$ and $x_2(t)$ are minimum phase.

Now, let us consider examples of minimum-phase and mixed-phase signals. Let $X_0(z)$ be the z-transform of a minimum-phase signal $x_0(t)$. $X_0(z)$ is represented by an all-pole model of order 20 as follows

$$X_0(z) = \prod_{i=1}^{20} \frac{z}{(z - P_i)}$$

where P_i represents the poles of the z-transform located inside the unit circle. Their positions are shown in Fig. 104 and the exact values given in Table 4. The signal $x_0(t)$ is represented in Fig. 107. Let $x_1(t)$ be the signal obtained by applying an all-pass filter to $x_0(t)$. The all-pass filter is defined by its transfer function in the z-domain by

$$G_{a.p.1}(z) = \prod_{i=1}^7 \frac{(z - P_i)}{(1 - P_i^* z)}$$

The all-pass filter moves the seven first poles of $X_0(z)$ outside the unit circle. The poles of $X_1(z)$ are represented in Fig. 105; the signal $x_1(t)$ is represented in Fig. 108. Let $x_2(t)$ the signal obtained by applying to $x_0(t)$ the all-pass filter defined by

$$G_{a.p.2}(z) = \prod_{i=1}^{10} \frac{(z - P_i)}{(1 - P_i^* z)}$$

This all-pass filter moves the ten first poles of $H_0(z)$ outside of the unit circle. The poles of $X_2(z)$ are represented in Fig. 106; and $x_2(t)$ in Fig. 109. The partial energies of the three signals are compared in Fig. 110. We recall that the partial energy of a signal $x(t)$ is defined by

$$E(m) = \sum_{i=1}^m x(i)^2.$$

The minimum-phase signal is the one which has the energy concentrated at the beginning.

Thus the all-pass filter can partially model some bottom-layers and incidentally show their influence on a propagating wavelet.

A.3. RELATION BETWEEN THE POWER CEPSTRUM AND THE COMPLEX CEPSTRUM

We recall that the power cepstrum proposed by Bogert, Healy and Tukey, is defined by

$$\tilde{x}(t) = [\text{fourier transform}(\log |X(f)|^2)]^2$$

where $X(f)$ is the fourier transform of $x(t)$. Because $\hat{X}(f) = \log X(f) = \log |X(f)| + i \arg X(f) = \hat{X}_R(f) + i\hat{X}_I(f)$ we have

$$\log |X(f)|^2 = 2\hat{X}_R(f),$$

because $X_R(f)$ is an even function of the frequency f

$$\tilde{x}(t) = \begin{cases} \left| \int_{-\infty}^{+\infty} 2\hat{X}_R(f) e^{-j2\pi ft} df \right|^2; \\ \left| \int_{-\infty}^{+\infty} 2\hat{X}_R(f) e^{j2\pi ft} df \right|^2. \end{cases}$$

The integral $\int_{-\infty}^{+\infty} \hat{X}_R(f) e^{j2\pi ft} df$ is the even part of the complex cepstrum $\hat{x}(t)$, denoted by $\hat{x}_{\text{even}}(t)$. Consequently we have the relation

$$|\hat{x}_{\text{even}}(t)|^2 = \frac{1}{4} \tilde{x}(t).$$

One can always decompose the complex cepstrum $\hat{x}(t)$ to the sum of its even part and its odd part

$$\hat{x}(t) = \hat{x}_{\text{even}}(t) + \hat{x}_{\text{odd}}(t),$$

where $\hat{x}_{\text{even}}(t) = \frac{1}{2}(\hat{x}(t) + \hat{x}(-t))$ and $\hat{x}_{\text{odd}}(t) = \frac{1}{2}(\hat{x}(t) - \hat{x}(-t))$.

If the complex cepstrum vanishes for the negative values of t ,

$$\hat{x}_{\text{even}}(t) = \frac{1}{2} \hat{x}(t)$$

and then

$$|\hat{x}(t)|^2 = \tilde{x}(t). \quad (\text{A.8})$$

We will see that the complex cepstrum vanishes for the negative values of t in the case of minimum signals.

We can conclude that for a minimum phase input sequence, the power cepstrum and the complex cepstrum are equivalent.

Appendix B

An example derivation of the complex cepstrum

In this section we consider a two-path propagation model with reflection at the bottom and the surface. The backscattering mechanism at each of the boundaries is modelled by a linear filter. The objective is to show how the modelling of the propagation medium affects the complex cepstrum technique (with regard to the fundamental notion of minimum phase signals) and to point out the limitation of this technique for deconvolution of the medium response. The propagation model is simple and highlights the parameters which have a determining effect on the method.

B.1. DERIVATION OF THE COMPLEX CEPSTRUM FOR THE TWO-PATHS
DISTORTION CHANNEL PLUS NOISE

■ B.1.1. Expression of the complex cepstrum

The general scenario is described in Fig. 111. Here, we consider the case where the direct path is not taken into account. In practice, this means that the observation time starts with the direct arrival. Under this assumption, the received signal assumes the form

$$s(t) = h_i(t - \tau_i) * x(t) + h_s(t - \tau_s) * x(t) + n(t),$$

where we recall that $h_i(t)$ and $h_s(t)$ are respectively the impulse response associated with the bottom layer and the surface and the additive noise $n(t)$; τ_i and τ_s are the reflected time arrivals with respect to the direct arrival. In the frequency domain the equality becomes

$$S(\omega) = H_i(\omega)X(\omega)e^{-j\omega\tau_i} + H_s(\omega)X(\omega)e^{-j\omega\tau_s} + N(\omega). \quad (\text{B.1})$$

Equation (B.1) can be factorized into the following form:

$$S(\omega) = X(\omega)H_i(\omega)e^{-j\omega\tau_i} \left[1 + \frac{H_s(\omega)}{H_i(\omega)}e^{-j\omega(\tau_s - \tau_i)} + \frac{N(\omega)}{H_i(\omega)X(\omega)}e^{j\omega\tau_i} \right].$$

By normalizing $S(\omega)$ (removing the linear phase $e^{-j\omega\tau_i}$ and taking the complex logarithm of both sides of the initial equality), we have

$$\hat{S}(\omega) = \hat{X}(\omega) + \hat{H}_i(\omega) + \log \left[1 + \frac{H_s(\omega)}{H_i(\omega)}e^{-j\omega(\tau_s - \tau_i)} + \frac{N(\omega)}{H_i(\omega)X(\omega)}e^{j\omega\tau_i} \right],$$

where

$$\hat{S}(\omega) = \log S(\omega), \quad \hat{X}(\omega) = \log X(\omega), \quad \hat{H}_1(\omega) = \log H_1(\omega).$$

Under the assumption that

$$\left| \frac{H_s(\omega)}{H_1(\omega)} e^{-j\omega(\tau_s - \tau_l)} + \frac{N(\omega)}{H_1(\omega)X(\omega)} e^{j\omega\tau_l} \right| < 1,$$

the logarithm can be expanded into its Taylor series and $\hat{S}(\omega)$ takes the form

$$\begin{aligned} \hat{S}(\omega) = & \hat{X}(\omega) + \hat{H}_1(\omega) + \frac{H_s(\omega)}{H_1(\omega)} e^{-j\omega(\tau_s - \tau_l)} + \frac{N(\omega)}{H_1(\omega)X(\omega)} e^{j\omega\tau_l} \\ & - \frac{1}{2} \left[\frac{H_s(\omega)}{H_1(\omega)} \right]^2 e^{-j\omega 2(\tau_s - \tau_l)} - \frac{1}{2} \left[\frac{N(\omega)}{H_1(\omega)X(\omega)} \right]^2 e^{j\omega 2\tau_l} \\ & - \frac{H_s(\omega)N(\omega)}{H_1(\omega)^2 X(\omega)} e^{-j\omega\tau_s}. \end{aligned}$$

Remark 1 The medium response introduces a linear phase term $e^{-j\omega\tau_l}$ and therefore the mean phase derivative of $s(t)$ is not equal to 0. After deconvolution this linear phase must be restored to the deconvolved medium response.

The complex cepstrum is obtained by taking the inverse fourier transform of $\hat{S}(\omega)$ and is given by

$$\begin{aligned} \hat{s}(t) = & \hat{x}(t) + \hat{h}_1(t) + h_2[t - (\tau_s - \tau_l)] + h_3(t + \tau_l) - \frac{1}{2}h_2(t) * h_2[t - 2(\tau_s - \tau_l)] \\ & - \frac{1}{2}h_3(t) * h_3(t + 2\tau_l) - h_4(t - \tau_s), \end{aligned} \quad (\text{B.2})$$

where $h_2(t)$, $h_3(t)$ and $h_4(t)$ are respectively the inverse fourier transforms of

$$\frac{H_s(\omega)}{H_1(\omega)}, \quad \frac{N(\omega)}{H_1(\omega)X(\omega)}, \quad \frac{H_s(\omega)N(\omega)}{H_1(\omega)^2 X(\omega)}.$$

Remark 2 The expression (B.2) of the complex cepstrum reveals that the received signal is not minimum phase (the complex cepstrum has negative components introduced by the noise). This illustrates that we must be very careful when we want to apply inverse filtering.

B.2. DERIVATION OF THE COMPLEX CEPSTRUM OF THE HANNING-WINDOWED CW PULSE

Let us now calculate the complex cepstrum of the transmitted signal $x(t)$. Here $x(t)$ is a Hanning-windowed CW pulse given by

$$x(t) = 0.5(1 - \cos 2\pi t/T) \cos \omega_0 t,$$

where ω_0 is the CW pulsation and T is the length of the Hanning window. The spectrum $X(\omega)$ of $x(t)$ is

$$X(\omega) = [0.5Q_0(\omega) + 0.25Q_0(\omega + 2\pi/2T) + 0.25Q_0(\omega - 2\pi/2T)] \\ * \frac{1}{2} [\delta(\omega - \omega_0) + \delta(\omega + \omega_0)],$$

where

$$Q_0(\omega) = T \frac{\sin \omega T}{\omega T}.$$

Alternatively

$$X(\omega) = 0.25Q_0(\omega - \omega_0) + 0.125Q_0(\omega - \omega_0 + 2\pi/2T) \\ + 0.125Q_0(\omega - \omega_0 - 2\pi/2T) + 0.25Q_0(\omega + \omega_0) \\ + 0.125Q_0(\omega + \omega_0 + 2\pi/2T) + 0.125Q_0(\omega + \omega_0 - 2\pi/2T).$$

The first sidelobe of $X(\omega)$ is quite low compared to the principal lobe ($X(\text{first lobe})/X(\omega_0) = 0.00843$) and thus, one does not make a serious error if one derives the complex logarithm of $X(\omega)$ from only the principal lobes $0.5Q_0(\omega - \omega_0)T$ and $0.5Q_0(\omega + \omega_0)T$. Under this assumption $X(\omega)$ is given by

$$\hat{X}(\omega) = \log \frac{1}{2} \left[T \frac{\sin(\omega - \omega_0)T}{(\omega - \omega_0)T} + T \frac{\sin(\omega + \omega_0)T}{(\omega + \omega_0)T} \right].$$

We now apply the band-pass mapping defined in Subsubsect. 3.2.6. We recall that it consists of band-pass filtering the spectrum $X(\omega)$ followed by the mapping transformation. Here the spectra is filtered around the frequencies $-\omega_0$ and ω_0 in such a way that

$$X_{\text{filtered}}(\omega) = \begin{cases} X(\omega), & \text{if } 0 \leq |(\omega - \omega_0)T| \leq \pi \quad \text{and} \quad 0 \leq |(\omega + \omega_0)T| \leq \pi; \\ , & \text{otherwise.} \end{cases}$$

■ B.2.1. Derivation of $\hat{X}(\omega)$ for $0 \leq |(\omega - \omega_0)T| \leq \pi$

For the values of ω close to ω_0 , one can assume that the quantity

$$T \frac{\sin(\omega + \omega_0)T}{(\omega + \omega_0)T}$$

is negligible and write

$$\hat{X}_{\omega_0}(\omega) = \log \frac{1}{2}T + \log \left[\frac{\sin(\omega - \omega_0)T}{(\omega - \omega_0)T} \right].$$

(This condition is fulfilled when ω_0 is much larger than $1/T$.) If one now applies band-pass mapping, the frequency ω is transformed into ω' by

$$\omega' = \pi \frac{\omega - (\omega_0 - \pi/T)}{\omega_0 + \pi/T - (\omega_0 - \pi/T)} = \pi \frac{\omega - (\omega_0 - \pi/T)}{2\pi/T},$$

and therefore

$$\omega = 2\omega'/T + \omega_0 - \pi/T.$$

The expression of $X_{\omega_0}(\omega)$ becomes, with respect to ω' ,

$$X_{\omega_0}(\omega') = \frac{1}{2}T \frac{\sin(2\omega' - \pi)}{2\omega' - \pi}.$$

And then the logarithm can be expanded in series as follows:

$$\hat{X}_{\omega_0}(\omega') = \log \frac{1}{2}T + \sum_{n=1}^{\infty} \frac{(-1)^n 2^{2n-1} B_n}{n(2n)!} (2\omega' - \pi)^{2n},$$

where B_n are the bernoulli numbers.

B.2.2. Derivation of $\hat{X}(\omega)$ for $0 \leq |(\omega + \omega_0)T| \leq \pi$

For the values of ω close to $-\omega_0$, one can assume that the quantity

$$T \frac{\sin(\omega - \omega_0)T}{(\omega - \omega_0)T}$$

is negligible and write

$$\hat{X}_{-\omega_0}(\omega) = \log \frac{1}{2}T + \log \left[\frac{\sin(\omega + \omega_0)T}{(\omega + \omega_0)T} \right].$$

If one now applies band-pass mapping, the frequency ω is transformed into ω' by

$$\omega' = \pi \frac{\omega - (-\omega_0 + \pi/T)}{-\omega_0 + \pi/T - (-\omega_0 - \pi/T)} = \pi \frac{\omega + \omega_0 - \pi/T}{2\pi/T}$$

and therefore

$$\omega = 2\omega'/T - \omega_0 + \pi/T.$$

The expression of $X_{\omega_0}(\omega)$ becomes, with respect to ω' ,

$$X_{\omega_0}(\omega') = \frac{1}{2}T \frac{\sin(-2\omega' + \pi)}{-2\omega' + \pi}.$$

Then the logarithm can be expanded into series as follows:

$$\hat{X}_{-\omega_0}(\omega') = \log \frac{1}{2}T + \sum_{n=1}^{\infty} \frac{(-1)^n 2^{2n-1} B_n}{n(2n)!} (2\omega' - \pi)^{2n}.$$

The sum $\hat{X}_{\omega_0}(\omega') + \hat{X}_{-\omega_0}(\omega')$ is called $\hat{X}_{BP}(\omega')$.

■ B.2.3. Inverse fourier transform of $\hat{X}_{BP}(\omega')$

Let $\hat{x}_{BP}(t)$ be the inverse fourier transform of $\hat{X}_{BP}(\omega')$, given by

$$\begin{aligned} \hat{x}_{BP}(t) &= \int_{-\pi}^{\pi} \hat{X}_{BP}(\omega') e^{j\omega' t} d\omega' \\ &= \int_{-\pi}^0 \hat{X}_{-\omega_0}(\omega') e^{j\omega' t} d\omega' + \int_0^{\pi} \hat{X}_{\omega_0}(\omega') e^{j\omega' t} d\omega'. \end{aligned}$$

Let $I_{-\omega_0}$ be the integral $\int_{-\pi}^0 \hat{X}_{-\omega_0}(\omega') e^{j\omega' t} d\omega'$ and I_{ω_0} the integral $\int_0^{\pi} \hat{X}_{\omega_0}(\omega') e^{j\omega' t} d\omega'$. $I_{-\omega_0}$ is given by

$$I_{-\omega_0} = \log \frac{1}{2}T \int_{-\pi}^0 e^{j\omega' t} d\omega' + \sum_{n=1}^{\infty} \frac{(-1)^n 2^{2n-1} B_n}{n(2n)!} \int_{-\pi}^0 (2\omega' + \pi)^{2n} e^{j\omega' t} d\omega'.$$

And if the variable ω' is changed into the variable $\omega = 2\omega' + \pi$ the integral $I_{-\omega_0}$ becomes

$$\begin{aligned} I_{-\omega_0} &= 2e^{-j\pi t} \left[\log \frac{1}{2}T \int_{-\pi}^{\pi} e^{j\omega/2t} d\omega \right. \\ &\quad \left. + \sum_{n=1}^{\infty} \frac{(-1)^n 2^{2n-1} B_n}{n(2n)!} \int_{-\pi}^{\pi} \omega^{2n} e^{j\omega/2t} d\omega \right]. \end{aligned}$$

I_{ω_0} is given by

$$I_{\omega_0} = \log \frac{1}{2}T \int_0^{\pi} e^{j\omega' t} d\omega' + \sum_{n=1}^{\infty} \frac{(-1)^n 2^{2n-1} B_n}{n(2n)!} \int_0^{\pi} (2\omega' - \pi)^{2n} e^{j\omega' t} d\omega'.$$

And if the variable ω' is changed into the variable $\omega = 2\omega' - 2\pi$ the integral I_{ω_0} becomes

$$I_{\omega_0} = 2e^{j\pi t} \left[\log \frac{1}{2} T \int_{-\pi}^{\pi} e^{j\omega t/2} d\omega + \sum_{n=1}^{\infty} \frac{(-1)^n 2^{2n-1} B_n}{n(2n)!} \int_{-\pi}^{\pi} \omega^{2n} e^{j\omega t/2} d\omega \right].$$

Consequently $\hat{x}_{PB}(t)$ assumes the form

$$\hat{x}_{PB}(t) = 4 \cos\left(\frac{1}{2}\pi t\right) \left[\log T \omega \frac{\sin\left(\frac{1}{2}\pi t\right)}{\frac{1}{2}\pi t} + \sum_{n=1}^{\infty} \frac{(-1)^n 2^{2n-1} B_n}{n(2n)!} \int_{-\pi}^{\pi} \omega^{2n} e^{j\omega t/2} d\omega \right]. \quad (B.3)$$

This can be simplified as follows. When $I = \int_{-\pi}^{\pi} \omega^{2n} e^{j\omega t/2} dt$ is integrated by parts it has the following form:

$$I = 2e^{j\omega t/2} \left[\frac{\omega^{2n}}{jt} + \frac{4n\omega^{2n-1}}{t^2} - \frac{8n(2n-1)\omega^{2n-2}}{jt^3} - \dots - \frac{(-1)^{n-2}(2n)!2^{2n-2}\omega^2}{jt^{2n-1}} + \frac{(-1)^{n-1}(2n)!2^{2n}\omega}{t^{2n}} + \frac{(-1)^{n2^{2n+1}}}{jt^{2n+1}} \right],$$

and consequently the integral $I_{\pi} = \int_{-\pi}^{\pi} \omega^{2n} e^{j\omega t/2} dt$ is given by

$$I_{\pi} = \pi^{2n+1} \frac{\sin\left(\frac{1}{2}\pi t\right)}{\frac{1}{2}\pi t} + \frac{4n\pi^{2n} \cos\left(\frac{1}{2}\pi t\right)}{t \frac{1}{2}\pi t} - \frac{8n(2n-1)\pi^{2n-1} \sin\left(\frac{1}{2}\pi t\right)}{t^2 \frac{1}{2}\pi t} - \dots - \frac{(-1)^{n-2}(2n)!2^{2n-1}\pi^3 \sin\left(\frac{1}{2}\pi t\right)}{t^{2n-2} \frac{1}{2}\pi t} + \frac{(-1)^{n-1}(2n)!2^{2n}\pi \cos\left(\frac{1}{2}\pi t\right)}{t^{2n-1} \frac{1}{2}\pi t},$$

or

$$I_{\pi} = \pi \left[\left(\pi^{2n} - \frac{8n(2n-1)\pi^{2n-1}}{t^2} \dots - \frac{(-1)^{n-2}(2n)!2^{2n-1}\pi^3}{t^{2n-2}} \right) \frac{\sin\left(\frac{1}{2}\pi t\right)}{\frac{1}{2}\pi t} + \left(\frac{4n\pi^{2n-1}}{t} + \dots + \frac{(-1)^{n-1}(2n)!2^{2n}\pi}{t^{2n-1}} \right) \frac{\cos\left(\frac{1}{2}\pi t\right)}{\frac{1}{2}\pi t} \right].$$

And if we define the variables $C_n(t)$ and $D_n(t)$ as

$$C_n(t) = \pi^{2n} - \frac{8n(2n-1)\pi^{2n-1}}{t^2} \dots - \frac{(-1)^{n-2}(2n)!2^{2n-1}\pi^3}{t^{2n-2}},$$

$$D_n(t) = \frac{4n\pi^{2n-1}}{t} + \dots + \frac{(-1)^{n-1}(2n)!2^{2n}\pi}{t^{2n-1}}.$$

The simplified form of $\hat{x}_{PB}(t)$ becomes

$$\begin{aligned} \hat{x}_{PB}(t) = & 4 \cos(\pi t) \pi \sum_{n=1}^{\infty} \frac{(-1)^n 2^{2n-1} B_n}{n(2n)!} \left(C_n(t) \frac{\sin(\frac{1}{2}\pi t)}{\frac{1}{2}\pi t} + D_n(t) \frac{\cos(\frac{1}{2}\pi t)}{\frac{1}{2}\pi t} \right) \\ & + 4 \cos(\pi t) \log \frac{1}{2} T \frac{1}{2} \pi \frac{\sin(\frac{1}{2}\pi t)}{\frac{1}{2}\pi t}. \end{aligned} \quad (B.4)$$

B.3. DERIVATION OF THE COMPLEX CEPSTRUM OF THE BOTTOM IMPULSE RESPONSE

We consider $H_l(\omega)$ as the transfer function of one finite-thickness layer given by [25]

$$H_l(\omega) = -e^{-j\omega\tau} \frac{(1 - \sqrt{r_0}e^{j\omega\tau})(1 + \sqrt{r_0}e^{j\omega\tau})}{(1 - \sqrt{r_0}e^{-j\omega\tau})(1 + \sqrt{r_0}e^{-j\omega\tau})},$$

where τ is the time delay across the layer and r_0 ($r_0 < 1$) is the reflection coefficient of the first layer boundary. One must normalize $H_l(\omega)$ by removing the component $-e^{-j\omega\tau}$ and we end up with the simplified form of $H_l(\omega)$:

$$H_l(\omega) = \frac{(1 - \sqrt{r_0}e^{j\omega\tau})(1 + \sqrt{r_0}e^{j\omega\tau})}{(1 - \sqrt{r_0}e^{-j\omega\tau})(1 + \sqrt{r_0}e^{-j\omega\tau})}.$$

If one derives the complex cepstrum in the full frequency band, the following expression is obtained for $\hat{h}_l(t)$:

$$\begin{aligned} \hat{h}_l(t) = & -r_0\delta(t + 2\tau) - \frac{1}{2}r_0^2\delta(t + 4\tau) - \frac{1}{3}r_0^3\delta(t + 6\tau) \\ & + \dots + r_0\delta(t - 2\tau) + \frac{1}{2}r_0^2\delta(t - 4\tau) + \frac{1}{3}r_0^3\delta(t - 6\tau) + \dots \end{aligned}$$

Under the assumption that the terms higher or equal to $\frac{1}{3}r_0^3$ can be neglected, one arrives at the complex cepstrum expression of the second order:

$$\hat{h}_l(t) = -r_0\delta(t + 2\tau) - \frac{1}{2}r_0^2\delta(t + 4\tau) + r_0\delta(t - 2\tau) + \frac{1}{2}r_0^2\delta(t - 4\tau).$$

The problem is that the bottom transfer function has been band-pass filtered as the Hanning-windowed CW pulse. Consequently the same band-pass mapping must be used before deriving the complex cepstrum. We recall that the frequency transform is defined by

$$\omega' = \begin{cases} \frac{\pi}{2\pi/T} \frac{\omega - (-\omega_0 + \pi/T)}{2\pi/T} & \text{for } 0 \leq |(\omega - \omega_0)T| \leq \pi, \\ \frac{\pi}{2\pi/T} \frac{\omega - (\omega_0 + \pi/T)}{2\pi/T} & \text{for } 0 \leq |(\omega + \omega_0)T| \leq \pi. \end{cases}$$

Let us now derive the expression of $H_1(\omega')$ around the two frequencies ω_0 and $-\omega_0$.

■ B.3.1. Derivation of $H_1(\omega')$ for $0 \leq |(\omega - \omega_0)T| \leq \pi$

$H_1(\omega')$ is given by

$$H_1(\omega') = \frac{[1 - \sqrt{r_0} e^{j(2\omega'/T + \omega_0 - \pi/T)\tau}] [1 + \sqrt{r_0} e^{j(2\omega'/T + \omega_0 - \pi/T)\tau}]}{[1 - \sqrt{r_0} e^{-j(2\omega'/T + \omega_0 - \pi/T)\tau}] [1 + \sqrt{r_0} e^{-j(2\omega'/T + \omega_0 - \pi/T)\tau}]}$$

Let us call α the quantity $\omega_0 - \pi/T$, and take the logarithm of both sides of the equation and expand it into its Taylor series

$$\begin{aligned} \hat{H}_1(\omega') &= -\sqrt{r_0} e^{j(2\omega'/T + \alpha)\tau} - \frac{1}{2} r_0 e^{j2(2\omega'/T + \alpha)\tau} \\ &\quad - \frac{1}{3} r_0 \sqrt{r_0} e^{j3(2\omega'/T + \alpha)\tau} - \dots + \sqrt{r_0} e^{j(2\omega'/T + \alpha)\tau} \\ &\quad - \frac{1}{2} r_0 e^{j2(2\omega'/T + \alpha)\tau} + \frac{1}{3} r_0 \sqrt{r_0} e^{j3(2\omega'/T + \alpha)\tau} \\ &\quad + \dots + \sqrt{r_0} e^{-j(2\omega'/T + \alpha)\tau} + \frac{1}{2} r_0 e^{-j2(2\omega'/T + \alpha)\tau} \\ &\quad + \frac{1}{3} r_0 \sqrt{r_0} e^{-j3(2\omega'/T + \alpha)\tau} - \dots - \sqrt{r_0} e^{-j(2\omega'/T + \alpha)\tau} \\ &\quad + \frac{1}{2} r_0 e^{-j2(2\omega'/T + \alpha)\tau} - \frac{1}{3} r_0 \sqrt{r_0} e^{-j3(2\omega'/T + \alpha)\tau} + \dots \end{aligned}$$

All the odd terms disappear and the expression becomes

$$\begin{aligned} \hat{H}_1(\omega) &= -r_0 e^{j2(2\omega'/T + \alpha)\tau} - \frac{1}{2} r_0^2 e^{j4(2\omega'/T + \alpha)\tau} \\ &\quad - \frac{1}{3} r_0^3 e^{j6(2\omega'/T + \alpha)\tau} + \dots + r_0 e^{-j2(2\omega'/T + \alpha)\tau} \\ &\quad + \frac{1}{2} r_0^2 e^{-j4(2\omega'/T + \alpha)\tau} + \frac{1}{3} r_0^3 e^{-j6(2\omega'/T + \alpha)\tau} + \dots \end{aligned}$$

■ B.3.2. Derivation of $H_1(\omega')$ for $0 \leq |(\omega + \omega_0)T| \leq \pi$

By the same kind of derivation as in the previous case, one ends up with the following expression for $\hat{H}_1(\omega')$:

$$\begin{aligned} \hat{H}_1(\omega') &= -r_0 e^{j2(2\omega'/T - \alpha)\tau} - \frac{1}{2} r_0^2 e^{j4(2\omega'/T - \alpha)\tau} \\ &\quad - \frac{1}{3} r_0^3 e^{j6(2\omega'/T - \alpha)\tau} + \dots + r_0 e^{-j2(2\omega'/T - \alpha)\tau} \\ &\quad + \frac{1}{2} r_0^2 e^{-j4(2\omega'/T - \alpha)\tau} + \frac{1}{3} r_0^3 e^{-j6(2\omega'/T - \alpha)\tau} + \dots \end{aligned}$$

■ B.S.3. Derivation of the complex cepstrum $\hat{h}_1(t)$

Take the inverse fourier transform of $\hat{H}_1(\omega')$

$$\begin{aligned} \hat{h}_1(t) &= \int_{-\pi}^{\pi} \hat{H}_1(\omega') e^{j\omega' t} d\omega' \\ &= \int_{-\pi}^0 \hat{H}_1(\omega') e^{j\omega' t} d\omega' + \int_0^{\pi} \hat{H}_1(\omega') e^{j\omega' t} d\omega' \end{aligned}$$

and derive the integrals corresponding to the terms r_0 of $\hat{H}_1(\omega')$, since the derivation of the higher order terms (r_0^2, r_0^3, \dots) is similar. Define first the function $g(t)$ as

$$\begin{aligned} g(t) &= - \int_{-\pi}^0 e^{j2(\omega'/T - \alpha)\tau} e^{j\omega' t} d\omega' \\ &\quad + \int_{-\pi}^0 e^{-j2(\omega'/T - \alpha)\tau} e^{j\omega' t} d\omega' \\ &\quad - \int_0^{\pi} e^{j2(\omega'/T + \alpha)\tau} e^{j\omega' t} d\omega' \\ &\quad + \int_0^{\pi} e^{-j2(\omega'/T + \alpha)\tau} e^{j\omega' t} d\omega', \end{aligned}$$

which gives

$$\begin{aligned} g(t) &= \frac{\pi}{j\pi(t - 4\tau/T)} e^{j2\alpha\tau} [1 - e^{-j(t-4\tau/T)}] \\ &\quad + \frac{\pi}{j\pi(t - 4\tau/T)} e^{-j2\alpha\tau} [e^{j(t-4\tau/T)} - 1] \\ &\quad - \frac{2\pi}{j\pi(t + 4\tau/T)} e^{j2\alpha\tau} [e^{j(t+4\tau/T)} - 1] \\ &\quad - \frac{2\pi}{j\pi(t + 4\tau/T)} e^{-j2\alpha\tau} [1 - e^{-j(t+4\tau/T)}], \end{aligned}$$

or

$$\begin{aligned} g(t) &= 2\pi \left[\cos(2\alpha\tau) \frac{\sin \pi(t - 4\tau/T)}{\pi(t - 4\tau/T)} + \sin(2\alpha\tau) \frac{\sin^2 \frac{1}{2}\pi(t - 4\tau/T)}{\frac{1}{2}\pi(t - 4\tau/T)} \right] \\ &\quad - 2\pi \left[\cos(2\alpha\tau) \frac{\cos \pi(t + 4\tau/T)}{\pi(t + 4\tau/T)} - \sin(2\alpha\tau) \frac{\sin^2 \frac{1}{2}\pi(t + 4\tau/T)}{\frac{1}{2}\pi(t + 4\tau/T)} \right]. \end{aligned}$$

Now define the functions $\hat{h}_1(t + 4\tau/T)$ and $\hat{h}_2(t - 4\tau/T)$ as follows:

$$\hat{h}_1(t + 4\tau/T) = -2\pi \left[\cos(2\alpha\tau) \frac{\cos \pi(t + 4\tau/T)}{\pi(t + 4\tau/T)} - \sin(2\alpha\tau) \frac{\sin^2 \frac{1}{2}\pi(t + 4\tau/T)}{\frac{1}{2}\pi(t + 4\tau/T)} \right],$$

$$\hat{h}_2(t - 4\tau/T) = 2\pi \left[\cos(2\alpha\tau) \frac{\sin \pi(t - 4\tau/T)}{\pi(t - 4\tau/T)} + \sin(2\alpha\tau) \frac{\sin^2 \frac{1}{2}\pi(t - 4\tau/T)}{\frac{1}{2}\pi(t - 4\tau/T)} \right].$$

The derivations of the integrals of higher order are completed in the same way and finally the complex cepstrum assumes the form

$$\begin{aligned} \hat{h}_l(t) = & r_0 \hat{h}_1(t + 4\tau/T) + \frac{1}{2} r_0^2 \hat{h}_1(t + 8\tau/T) + \frac{1}{3} r_0^3 \hat{h}_1(t + 12\tau/T) \\ & + \dots + r_0 \hat{h}_2(t - 4\tau/T) + \frac{1}{2} r_0^2 \hat{h}_2(t - 8\tau/T) + \frac{1}{3} r_0^3 \hat{h}_2(t - 12\tau/T) + \dots \end{aligned}$$

In the second order, the complex cepstrum will have the form

$$\hat{h}_l(t) = r_0 \hat{h}_1(t + 4\tau/T) + \frac{1}{2} r_0^2 \hat{h}_1(t + 8\tau/T) + r_0 \hat{h}_2(t - 4\tau/T) + \frac{1}{2} r_0^2 \hat{h}_2(t - 8\tau/T).$$

Let us now discuss the expression for the complex cepstrum with respect to the different parameters involved. The most important is the time delay τ whose value determines whether or not we will be able to separate the bottom complex cepstrum from the 'boundary reflections'. τ is obviously a function of the layer depth and the layer sound velocity (i.e. it depends on bottom composition). Figure 112a, [18], represents the sound velocity in the layer function of the porosity of the layer components. Figure 112b, [19], shows the dependence of the sound velocity function on relative density, porosity and reflection coefficient. Let us consider two relatively opposite situations. The first one consists of a layer of low density, high porosity and low coefficient of reflection. Let us take the case where these three parameters have respectively the values 1.3, 80(%) and 0.1. According to Fig. 112b the corresponding velocity equals 1400 m/s if one assumes a water sound velocity of 1500 m/s. Let the layer depths be respectively equal to 50 m and 100 m. The incidence angle θ_{ab} being 60° , the time delays τ are respectively 0.041 s and 0.082 s. The corresponding complex cepstra $\hat{h}_l(t)$ are depicted in Figs. 113a and b. The second case corresponds to a layer of high density, low porosity and high reflection coefficient with parameter values respectively of 2.1, 32(%) and 0.4. Thus the sound velocity within the layer is 1800 m/s, and for the same layer thicknesses and incidence angle as previously, the time delays are 0.032 s and 0.064 s. The complex cepstra $\hat{h}_l(t)$ are presented in Figs. 114a and b.

It is meaningful to assume that the time delay 4τ is much smaller than τ_1 and therefore $\hat{h}_l(t)$ can be band-pass-filtered.

B.4. DERIVATION OF THE SURFACE IMPULSE RESPONSE AFTER BAND-PASS MAPPING

We consider the case of low frequencies and a very smooth surface. Under these assumptions the surface transfer function assumes the form (Fraunhofer diffraction), [20],

$$H_s(\omega, t) = -e^{i\Psi},$$

where

$$\Psi = \frac{2\omega}{c} \cos \theta_s \zeta(R_s, t_s).$$

θ_s is the incidence angle of the wave with respect to the normal to the surface; $\zeta(R_s, t_s)$ is the surface profile at the point of specular reflection. $\zeta(R_s, t_s)$ is a random function of the sea surface elevation (surface roughness). Our purpose is to derive the impulse response $h_s(t)$ after the band-pass mapping has been applied. As before let us distinguish the two cases $0 \leq |\omega - \omega_0|T \leq \pi$ and $0 \leq |\omega + \omega_0|T \leq \pi$.

■ **B.4.1. Derivation of $H_s(\omega)$ for $0 \leq |\omega - \omega_0|T \leq \pi$**

The frequency transform is defined by

$$\omega = 2\omega'/T + \omega_0 - \pi/T.$$

Thus,

$$H_s(\omega') = \exp \left[-j \frac{2}{c} \left(\frac{2\omega'}{T} + \omega_0 - \frac{\pi}{T} \right) \cos \theta_s \zeta(R_s, t_s) \right],$$

$$H_s(\omega') = \exp \left[-j \frac{2\alpha}{c} \cos \theta_s \zeta(R_s, t_s) \right] \exp \left[-j \frac{4\omega'}{cT} \cos \theta_s \zeta(R_s, t_s) \right],$$

where $\alpha = \omega_0 - \pi/T$.

■ **B.4.2. Derivation of $H_s(\omega)$ for $0 \leq |\omega + \omega_0|T \leq \pi$**

The frequency transform is defined by

$$\omega = \frac{2\omega'}{T} - \omega_0 + \frac{\pi}{T}$$

Thus,

$$H_s(\omega') = \exp \left[-j \frac{2}{c} \left(\frac{2\omega'}{T} - \omega_0 + \frac{\pi}{T} \right) \cos \theta_s \zeta(R_s, t_s) \right],$$

$$= \exp \left[j \frac{2\alpha}{c} \cos \theta_s \zeta(R_s, t_s) \right] \exp \left[-j \frac{4\omega'}{cT} \cos \theta_s \zeta(R_s, t_s) \right].$$

Take the inverse fourier transform to get $h_s(t)$

$$h_s(t) = \int_{-\pi}^{\pi} H_s(\omega') e^{j\omega' t} d\omega'$$

$$h_s(t) = \int_{-\pi}^0 H_s(\omega') e^{j\omega' t} d\omega' + \int_0^{\pi} H_s(\omega') e^{j\omega' t} d\omega'$$

By replacing $H_s(\omega')$ by its values $h_s(t)$ becomes

$$h_s(t) = \exp \left[j \frac{2\alpha}{c} \cos(\theta_s) \zeta(R_s, t_s) \right] \int_{-\pi}^0 \exp \left[j\omega' \left(t - \frac{4 \cos \theta_s}{cT} \zeta(R_s, t_s) \right) \right] d\omega'$$

$$+ \exp \left[-j \frac{2\alpha}{c} \cos(\theta_s) \zeta(R_s, t_s) \right] \int_0^{\pi} \exp \left[j\omega' \left(t - \frac{4 \cos \theta_s}{cT} \zeta(R_s, t_s) \right) \right] d\omega'$$

i.e.

$$h_s(t) = \exp \left[j \frac{2\alpha}{c} \cos(\theta_s) \zeta(R_s, t_s) \right] \left[\frac{1 - \exp \left[-j\pi \left(t - \frac{4 \cos \theta_s}{cT} \zeta(R_s, t_s) \right) \right]}{j \left(t - \frac{4 \cos \theta_s}{cT} \zeta(R_s, t_s) \right)} \right]$$

$$- \exp \left[-j \frac{2\alpha}{c} \cos(\theta_s) \zeta(R_s, t_s) \right] \left[\frac{1 - \exp \left[j\pi \left(t - \frac{4 \cos \theta_s}{cT} \zeta(R_s, t_s) \right) \right]}{j \left(t - \frac{4 \cos \theta_s}{cT} \zeta(R_s, t_s) \right)} \right]$$

Finally we end up with

$$h_s(t) = \cos \left[\frac{2\alpha}{c} \cos(\theta_s) \zeta(R_s, t_s) \right] \pi \frac{\sin \left[\pi \left(t - \frac{4 \cos \theta_s}{cT} \zeta(R_s, t_s) \right) \right]}{\pi \left(t - \frac{4 \cos \theta_s}{cT} \zeta(R_s, t_s) \right)}$$

$$+ \sin \left[\frac{2\alpha}{c} \cos(\theta_s) \zeta(R_s, t_s) \right] \pi \frac{\sin^2 \left[\frac{1}{2} \pi \left(t - \frac{4 \cos \theta_s}{cT} \zeta(R_s, t_s) \right) \right]}{\frac{1}{2} \pi \left(t - \frac{4 \cos \theta_s}{cT} \zeta(R_s, t_s) \right)}$$

Let us assume that the random function $\zeta(R_s, t_s)$ is described by the roughness parameter, which is the random wave height. If $h = h_0 h_r$, where h_0 is the basic wave height and h_r is a random number following a normal distribution with zero mean and unit standard deviation, and the incidence angle is equal to 60° , the surface impulse response shown in Fig. 115 is obtained.

The problem now is to properly filter the complex cepstrum in order to deconvolve the wavelet and the medium response (boundary reflection). If the time delay τ_s is small with respect to the signal $x(t)$ length, then $\hat{h}_s(t - \tau_s) - \frac{1}{2} h_s(t) * h_s(t - 2\tau_s)$ will be overlapped by $\hat{x}(t)$ (in our example the time delay τ_s is equal to 0.133 s). It would thus be reasonable to filter in such a way that

$$\hat{s}_w(t) = \hat{x}(t) + \hat{h}_t(t), \quad (\text{B.5})$$

i.e.

$$\begin{aligned} \hat{s}_m(t) = & h_2[t - (\tau_s - \tau_l)] - \frac{1}{2}h_2(t) * h_2[t - 2(\tau_s - \tau_l)] + h_3(t + \tau_l) \\ & - \frac{1}{2}h_3(t) * h_3(t + 2\tau_l) - h_4(t - \tau_s). \end{aligned} \quad (B.6)$$

$\hat{s}_w(t)$ is the band-pass-filtered cepstrum around $t = 0$ and represents an estimation of the complex cepstrum of the wavelet; $\hat{s}_m(t)$ is equal to $\hat{s}(t) - \hat{s}_m(t)$ and represents an estimation of the complex cepstrum of the so-called medium response (boundary reflection).

Remark 3 The complex cepstrum component corresponding to the medium response is more sensitive to the noise than the wavelet component: in our case the noise effect on the deconvolved wavelet is null.

Let us assume that the complex cepstrum is filtered in such a way that $\hat{s}_w(t)$ and $\hat{s}_m(t)$ are given by Eqs. (B.5) and (B.6). We now apply the inverse homomorphic transform to get the deconvolved wavelet and the deconvolved medium response.

B.5. DERIVATION OF THE DECONVOLVED WAVELET

Take the fourier transform of both sides of Eq. (B.5)

$$\hat{S}_w(\omega) = \hat{X}(\omega) + \hat{H}_1(\omega).$$

Take the complex exponential of both sides of the previous equation

$$S_w(\omega) = X(\omega)H_1(\omega).$$

Take the inverse fourier transform to get the deconvolved wavelet given by

$$s_w(t) = x(t) * h_1(t). \quad (B.7)$$

B.6. DERIVATION OF THE DECONVOLVED MEDIUM RESPONSE

Before proceeding with the derivation, we stress that $\hat{s}_m(t)$ is strongly perturbed by the noise component $n(t)$ (Eq. (B.6)). Since we recall that $\hat{s}_m(t)$ is given by

$$\begin{aligned} \hat{s}_m(t) = & h_2[t - (\tau_s - \tau_1)] + h_3(t + \tau_1) - \frac{1}{2}h_2(t) * h_2[t - 2(\tau_s - \tau_1)] \\ & - \frac{1}{2}h_3(t) * h_3(t + 2\tau_1) - h_4(t - \tau_s). \end{aligned}$$

Take the fourier transform

$$\begin{aligned} \widehat{S}_m(\omega) = & H_2(\omega)e^{-j\omega(\tau_s - \tau_1)} + H_3(\omega)e^{j\omega\tau_1} - \frac{1}{2}H_3(\omega)^2e^{j\omega 2\tau_1} \\ & - \frac{1}{2}H_2(\omega)^2e^{-j\omega 2(\tau_s - \tau_1)} - H_4(\omega)e^{-j\omega\tau_s}. \end{aligned}$$

$H_3(\omega)e^{j\omega\tau_1} - \frac{1}{2}H_3(\omega)^2e^{j\omega 2\tau_1}$ can be considered as the Taylor expansion of $\log[1 + H_3(\omega)e^{j\omega\tau_1}]$ to the second order. $H_2(\omega)e^{-j\omega(\tau_s - \tau_1)} - \frac{1}{2}H_2(\omega)^2e^{-j\omega 2(\tau_s - \tau_1)}$ can be considered as the Taylor expansion of $\log[1 + H_2(\omega)e^{-j\omega(\tau_s - \tau_1)}]$ to the second order. Thus, $\widehat{S}_m(\omega)$ will have the form

$$\begin{aligned} \widehat{S}_m(\omega) = & \log[1 + H_2(\omega)e^{-j\omega(\tau_s - \tau_1)}] \\ & + \log[1 + H_3(\omega)e^{j\omega\tau_1}] - H_4(\omega)e^{-j\omega\tau_s}. \end{aligned}$$

Take the complex exponential of both sides of the previous equation and reintroduce the linear phase component $e^{-j\omega\tau_1}$

$$\begin{aligned} S_m(\omega) = & [1 + H_2(\omega)e^{-j\omega(\tau_s - \tau_1)}e^{-j\omega\tau_1} + H_3(\omega)] \\ & \exp[-H_4(\omega)e^{-j\omega\tau_s}]. \end{aligned}$$

Let $H_p(\omega)$ be the perturbation $\exp[-H_4(\omega)e^{-j\omega\tau_s}]$ and take the inverse fourier transform of the previous equation to get the deconvolved medium response before restitution of the linear phase component

$$s_m(t) = [\delta(t) + h_2[t - (\tau_s - \tau_1)] * [\delta(t - \tau_1) + h_3(t)] * h_p(t). \quad (\text{B.8})$$

B.7. APPLICATION TO PARTICULAR CASES

We now consider the reflected paths to be solely reflections at the bottom and bottom-surface without any modification of the transfer function of the transmitted signal up to a time delay. In other words the bottom transfer function $H_b(\omega)$ and the surface transfer function $H_s(\omega)$ verify

$$H_b(\omega) = 1$$

$$H_s(\omega) = 1 \quad \text{for any } 0 \leq \omega \leq \pi.$$

We also assume that the signal-to-noise ratio is high enough to allow all terms containing $N(\omega)/X(\omega)$ to be neglected. Under these assumptions the relations (B.7) and (B.8) assume the simplified form

$$s_w(t) = x(t) \tag{B.9}$$

$$s_m(t) = [\delta(t) + \delta[t - (\tau_s - \tau_l)] * \delta(t - \tau_l)]. \tag{B.10}$$

B.8. CONCLUSIONS

The derivation of the complex cepstrum using this simple propagation model evokes two major observations:

- (1) The received signal after reverberation is not minimum phase (Eq. (B.2)).
- (2) The derivation of the layer complex cepstrum shows that it is difficult in the cepstral domain to separate by rectangular windowing the transmitted pulse from the layer response, because they occupy the same cepstral space (Figs. 113a,b and 114a,b). Therefore, what we deconvolve is the wavelet, from the boundary reflections, and incidentally obtain some information about the layer.

The location of the source and the array (closer to the surface or closer to the bottom) allows us to estimate the bottom impulse response or the surface impulse response.

Appendix C

Estimation of the rank of the correlation matrix R_{xx}

C.). TEST OF AIC AKAIKE

The method developed in this appendix has been already used in passive array processing [29]. The purpose was to estimate the number of sources from the cross-spectral matrix measured at the output of the array.

Let $X = (X_1, X_2, \dots, X_N)$ be a series of independent, zero-mean, gaussian vector random variables of order P and variance matrix

$$R_{xx} = \alpha I + R_{ss}.$$

Their probability density is given by

$$p(X/\alpha, R_{ss}) = 2\pi^{-NP/2} (\det R_{xx})^{-N/2} \exp\left(-\frac{1}{2} \sum_{n=1}^N X_n^T R_{xx}^{-1} X_n\right).$$

Let us define the likelihood function by

$$\begin{aligned} \Phi(X/\alpha, R_{ss}) &= \frac{-2}{N} \ln p(X/\alpha, R_{ss}) - P \ln 2\pi \\ &= \ln \det R_{xx} + \sum_{n=1}^N X_n^T R_{xx}^{-1} X_n \\ &= \ln \det(\alpha I + R_{ss}) + \frac{1}{2} \text{tr}(\alpha I + R_{ss})^{-1} \hat{R}_{xx} \end{aligned}$$

where

$$\hat{R}_{xx} = \frac{1}{N} \sum_{n=1}^N X_n X_n^T.$$

One wants to estimate, in the maximum likelihood sense, the two unknowns (α, R_{ss}) , which is equivalent to minimizing the function $\Phi(X/\alpha, R_{ss})$

■ C.1.1. Minimization of the likelihood function $\Phi(X/\alpha, R_{xx})$

Let us assume that the matrix R_{xx} is of rank Q . R_{xx} can be expanded into its eigenvalues and eigenvectors decomposition

$$R_{xx} = \sum_{i=1}^Q \lambda_i u_i u_i^T.$$

The inverse of $\alpha I + R_{xx}$ is given by

$$(\alpha I + R_{xx})^{-1} = \frac{1}{\alpha} \left[I - \sum_{i=1}^Q \frac{\lambda_i}{\alpha + \lambda_i} u_i u_i^T \right],$$

and then

$$\text{tr}(\alpha I + R_{xx})^{-1} \hat{R}_{xx} = \frac{1}{\alpha} \left[\text{tr} \hat{R}_{xx} - \sum_{i=1}^Q \frac{\lambda_i}{\alpha + \lambda_i} u_i^T \hat{R}_{xx} u_i \right],$$

and

$$\det(\alpha I + R_{xx}) = \alpha^{P-Q} \prod_{i=1}^Q (\alpha + \lambda_i).$$

Thus the function $\Phi(X/\alpha, R_{xx})$ will have the form

$$\Phi(X/\alpha, \lambda_i, u_i) = (P - Q) \ln \alpha + \sum_{i=1}^Q \ln(\alpha + \lambda_i) + \frac{1}{2\alpha} \left[\text{tr} \hat{R}_{xx} - \sum_{i=1}^Q \frac{\lambda_i}{\alpha + \lambda_i} u_i^T \hat{R}_{xx} u_i \right].$$

To globally the function $\Phi(X/\alpha, \lambda_i, u_i)$ minimize one minimizes it for each of the three variables with other two fixed.

C.1.1a. Minimization of Φ with respect to $u_i, i \in [1, Q]$, with $\lambda_i, i \in [1, Q]$, and α fixed

This is equivalent to maximizing the quantity

$$\sum_{i=1}^Q \frac{\lambda_i}{\alpha + \lambda_i} u_i^T \hat{R}_{xx} u_i.$$

One recalls that a quadratic form $u \hat{R}_{xx} u^T$, $\|u\| \leq 1$, is maximum if u is the eigenvector of \hat{R}_{xx} corresponding to the largest eigenvalue. Because we have the sum of Q quadratic forms, the maximum is reached for the Q eigenvectors \hat{u}_i of \hat{R}_{xx} . Thus the minimum of the function Φ is given by

$$\Phi(X/\alpha, \lambda_i, \hat{u}_i) = (P - Q) \ln \alpha + \sum_{i=1}^Q \ln(\alpha + \lambda_i) + \frac{1}{2\alpha} \left[\text{tr} \hat{R}_{xx} - \sum_{i=1}^Q \frac{\lambda_i}{\alpha + \lambda_i} \right], \quad (\text{C.1})$$

where $\hat{\sigma}_i, i \in [1, Q]$, are the eigenvalues of \hat{R}_{xx} arranged in decreasing order.

C.1.1b. Minimization of Φ with respect to $\lambda_i, i \in [1, Q]$, with $\hat{u}_i, i \in [1, Q]$, and α fixed

Noting that

$$\frac{\lambda_i}{(\alpha + \lambda_i)} = 1 - \frac{\alpha}{(\alpha + \lambda_i)}$$

and

$$\text{tr} \hat{R}_{xx} = \sum_{i=1}^P \hat{\sigma}_i.$$

it follows that

$$\Phi(X/\alpha, \lambda_i, \hat{u}_i) = (P - Q) \ln \alpha + \sum_{i=1}^P \ln(\alpha + \lambda_i) + \frac{1}{2\alpha} \sum_{i=Q+1}^N \hat{\sigma}_i + \frac{1}{2} \sum_{i=1}^Q \frac{\hat{\sigma}_i}{\alpha + \lambda_i}.$$

The function is minimum for the gradient equal to zero and the hessian positive. It can be easily verified that the hessian is always positive. The gradient equals zero when

$$\frac{1}{(\alpha + \lambda_i)} - \frac{\hat{\sigma}_i}{(\alpha + \lambda_i)^2} = 0, \quad 1 \leq i \leq P,$$

which gives us the solution

$$\hat{\lambda}_i = \hat{\sigma}_i - \alpha.$$

The minimum of the function Φ assumes the form

$$\Phi(X/\alpha, \hat{\lambda}_i, \hat{u}_i) = (P - Q) \ln \alpha + \sum_{i=1}^Q \ln(\hat{\sigma}_i) + \frac{1}{2\alpha} \sum_{i=Q+1}^N \hat{\sigma}_i + \frac{Q}{2}.$$

C.1.1c. Minimization of Φ with respect to $\alpha, \hat{u}_i, i \in [1, Q]$ with $\hat{\lambda}_i, i \in [1, Q]$ fixed As previously, Φ is minimum for

$$\frac{P - Q}{\alpha} - \frac{1}{\alpha^2} \sum_{i=Q+1}^P \hat{\sigma}_i = 0,$$

and the solution is given by

$$\hat{\alpha} = \frac{1}{(P - Q)} \sum_{i=Q+1}^P \hat{\sigma}_i.$$

The global minimum of Φ is given by

$$\begin{aligned} \Phi(X/\hat{\alpha}, \hat{\lambda}_i, \hat{u}_i) &= (P - Q) \ln \left[\frac{1}{(P - Q)} \sum_{i=Q+1}^P \hat{\sigma}_i \right] + \sum_{i=1}^Q \ln \hat{\sigma}_i + \frac{P}{2} \\ &= \phi(Q) + \frac{P}{2} + \ln \det \hat{R}_{xx}, \end{aligned} \quad (C.2)$$

where

$$\phi(Q) = (P - Q) \ln \left[\frac{1}{(P - Q)} \sum_{i=Q+1}^P \hat{\sigma}_i \right] - \sum_{i=Q+1}^P \ln \hat{\sigma}_i.$$

C.2. AKAIKE CRITERION, APPLICATION TO THE ESTIMATION OF THE RANK OF R_{xx}

The Akaike estimate of the order of a model at the minimum of the function is

$$f(q) = -\Phi(q) + \frac{\text{number of free parameters}}{N}$$

where $\Phi(q)$ is the maximum likelihood function of the model at the order q . In our case $\Phi(q)$ is given by Eq. (C.2). Using the Choleski decomposition, we have

$$R_{xx} = LL^T,$$

where L is a lower-triangular matrix with P rows and Q columns. Then the number of free parameters is

$$P + (P - 1) + (P - 2) + \dots + (P - Q + 1) = QP - \frac{1}{2}Q^2 = Q(P - \frac{1}{2}Q),$$

and the function $f(q)$ takes the following form

$$f(Q) = (P - Q) \ln \left[\frac{1}{(P - Q)} \sum_{i=Q+1}^P \hat{\sigma}_i \right] - \sum_{i=Q+1}^P \ln \hat{\sigma}_i + \frac{Q(P - \frac{1}{2}Q)}{N},$$

in which the constant term has been removed.

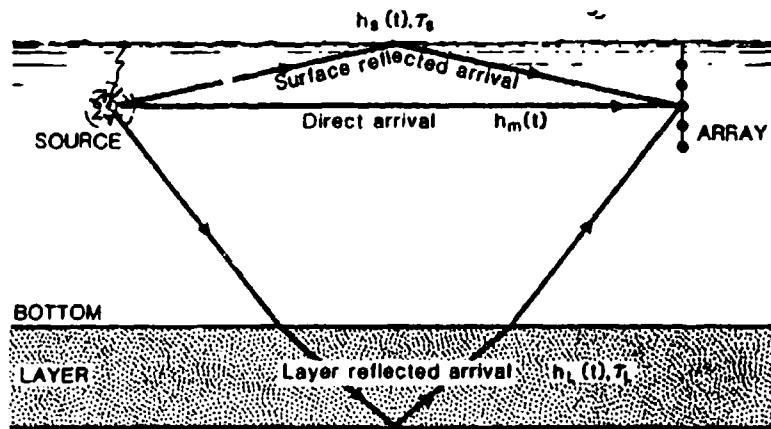


Fig. 1. Three-path propagation model (source and array close to the surface).

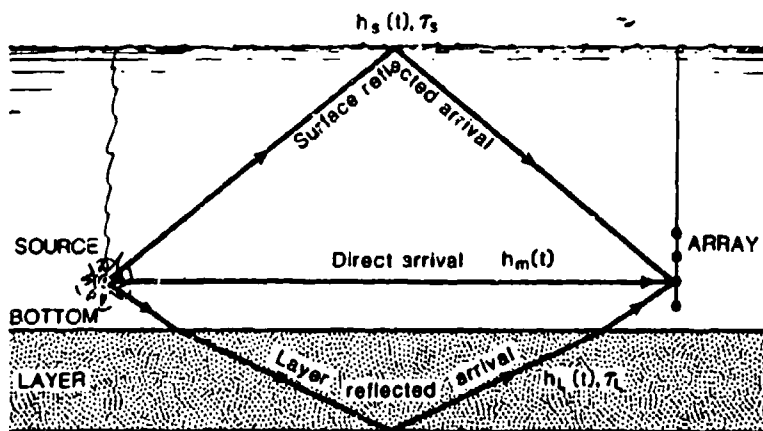


Fig. 2. Three-path propagation model (source and array close to the bottom).

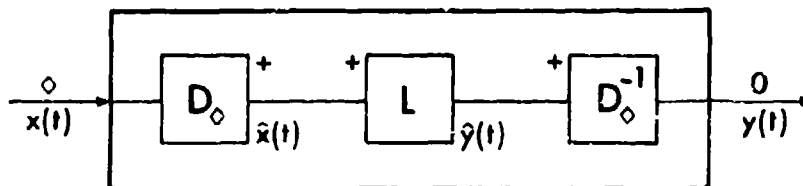


Fig. 3. Canonical representation of a homomorphic system.

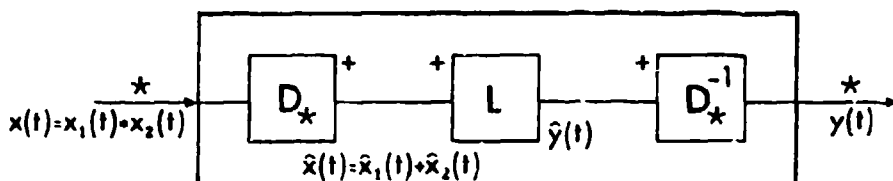


Fig. 4. Canonical representation of a homomorphic deconvolution system.

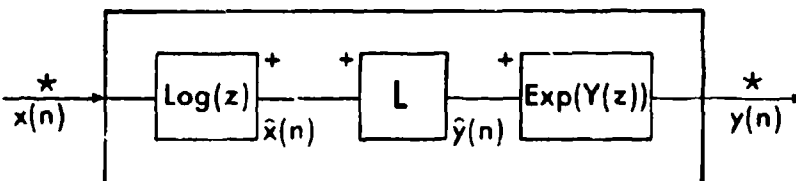


Fig. 5. Characteristic system D_0 of a homomorphic deconvolution.

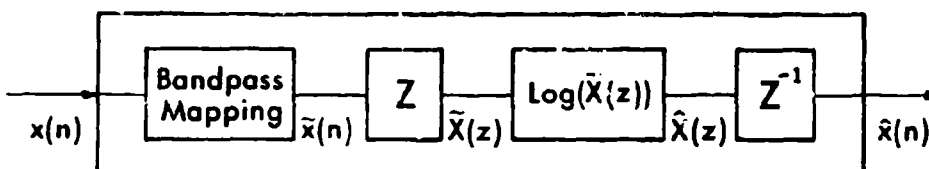


Fig. 6. Bandpass complex cepstrum system D_0 .

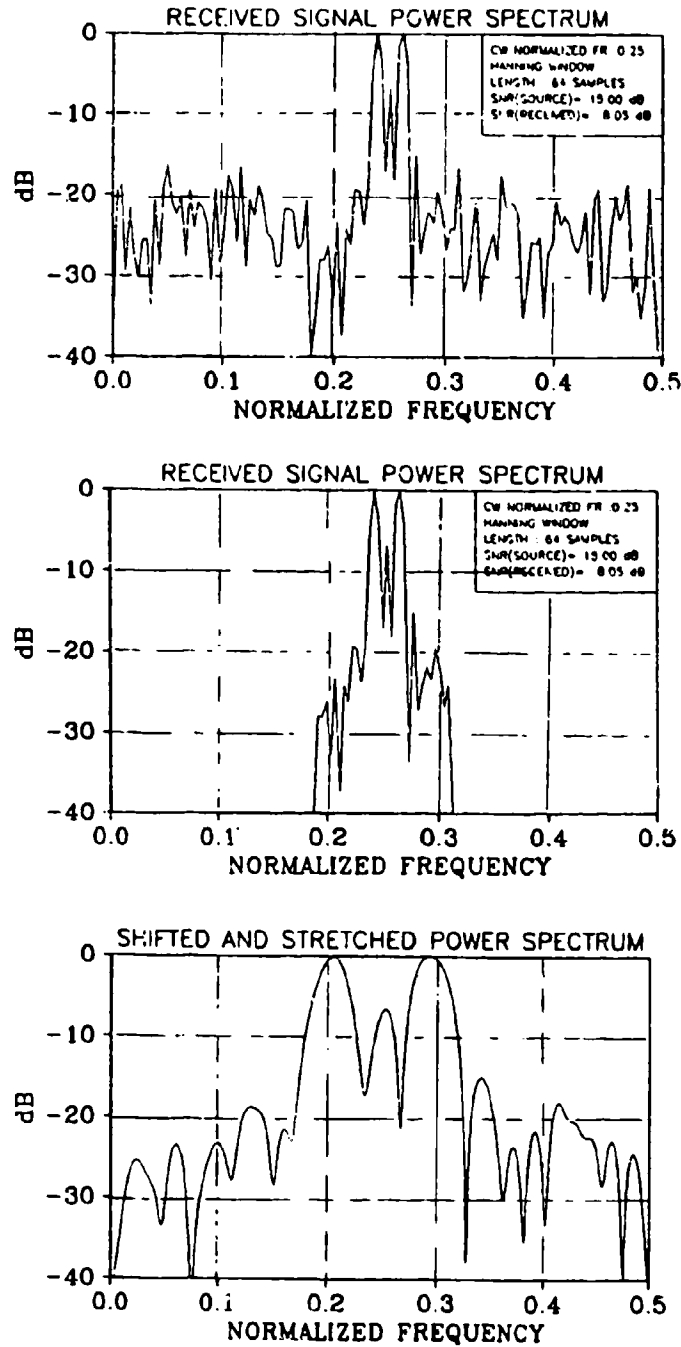


Fig. 7. Example of band-pass mapping.

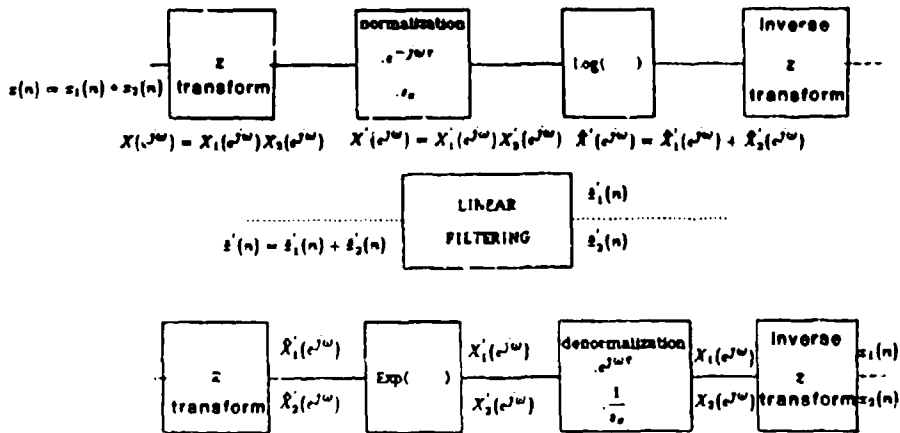


Fig. 8a. Global complex cepstrum deconvolution.

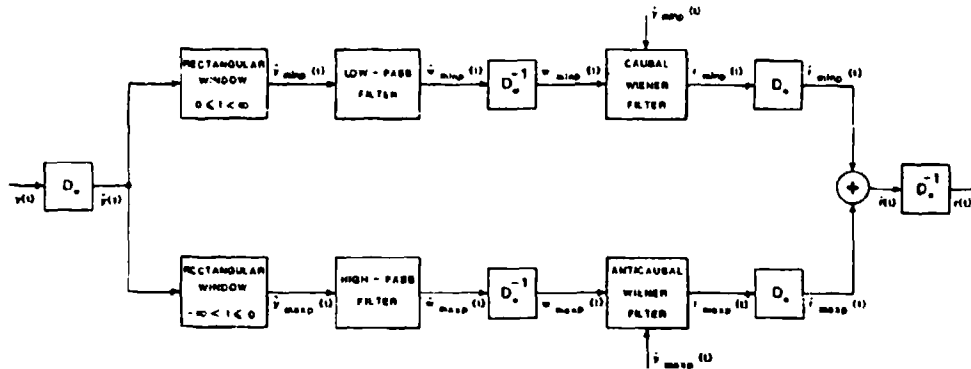


Fig. 8b. Deconvolution procedure by combination of homomorphic and Wiener filtering.

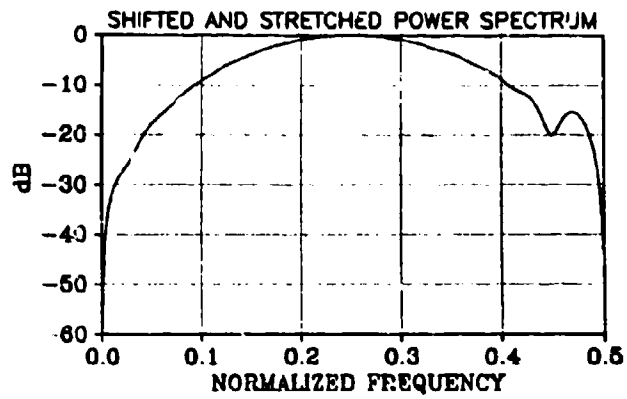


Fig. 9. Spectrum of the CW pulse after band-pass mapping.

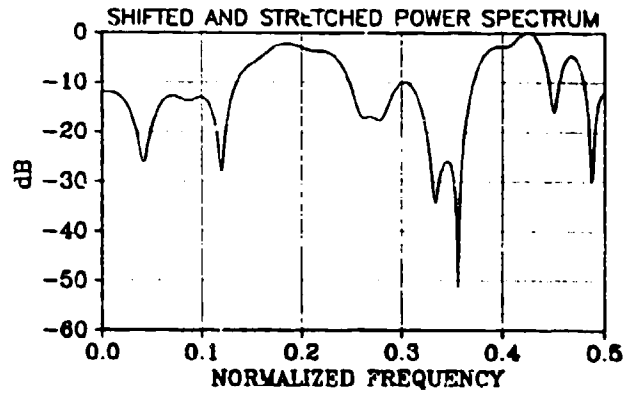


Fig. 10. Spectrum of the medium response after band-pass mapping.

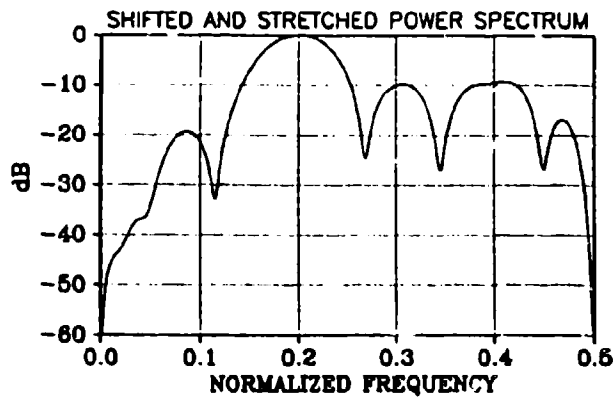


Fig. 11. Spectrum of the received signal after band-pass mapping.

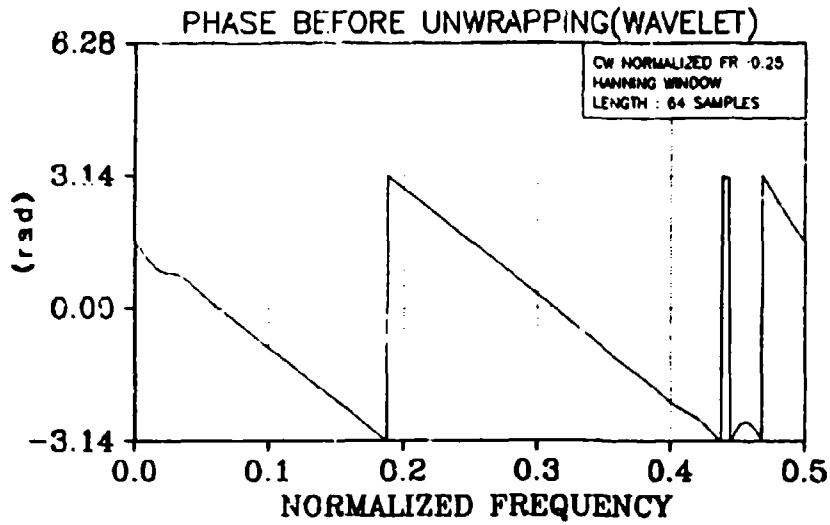


Fig. 12. Phase of the CW pulse before unwrapping.

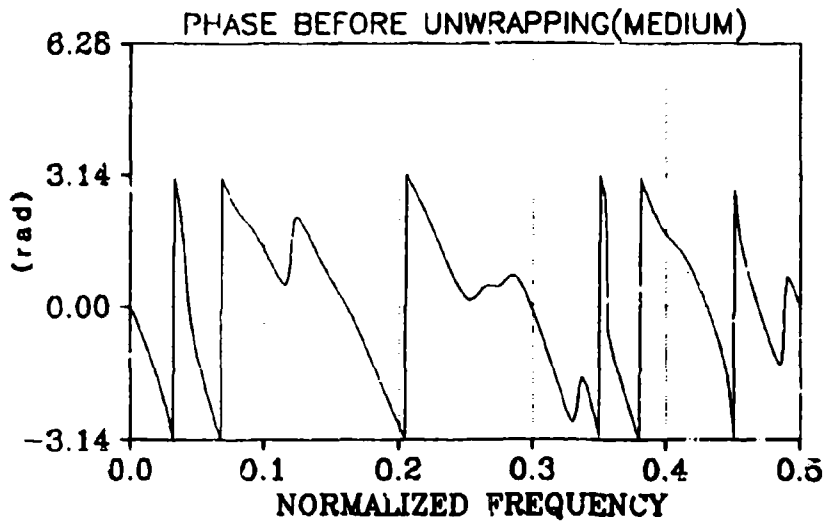


Fig. 13. Phase of the medium response before unwrapping.

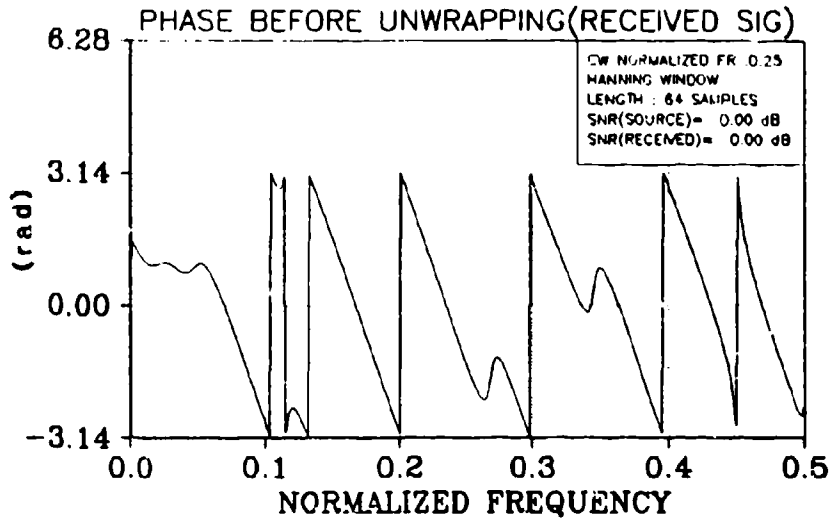


Fig. 14. Phase of the received signal before unwrapping.

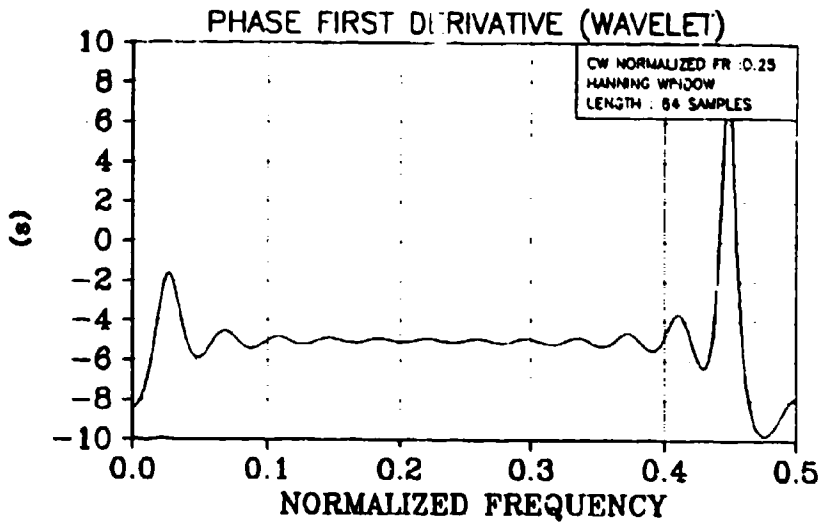


Fig. 15. First derivative of the phase of the CW pulse.

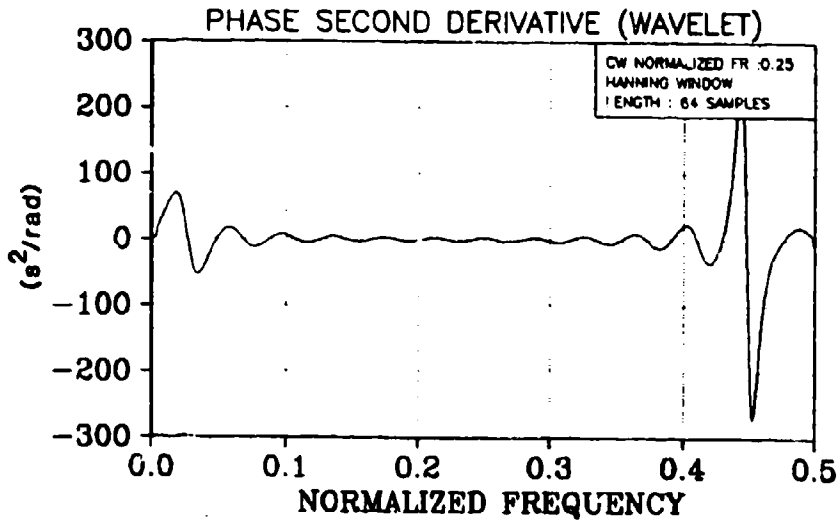


Fig. 16. Second derivative of the phase of the CW pulse.

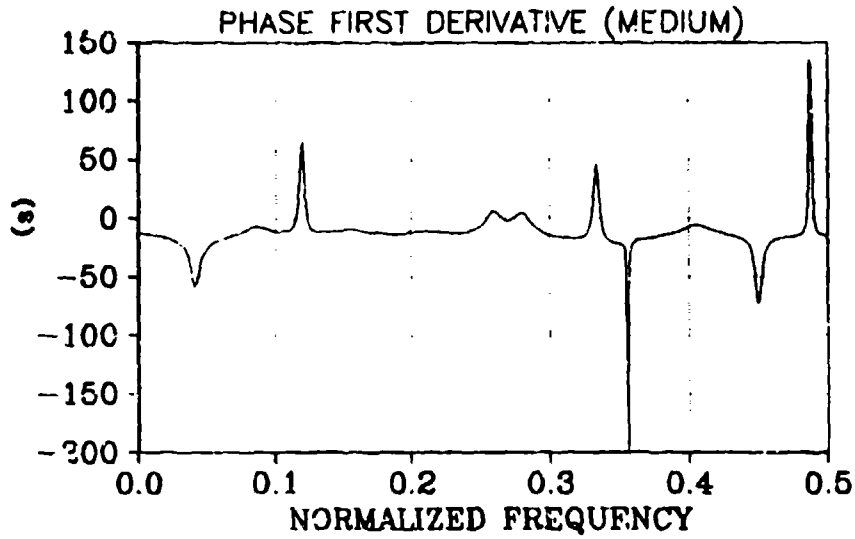


Fig. 17. First derivative of the phase of the medium response.

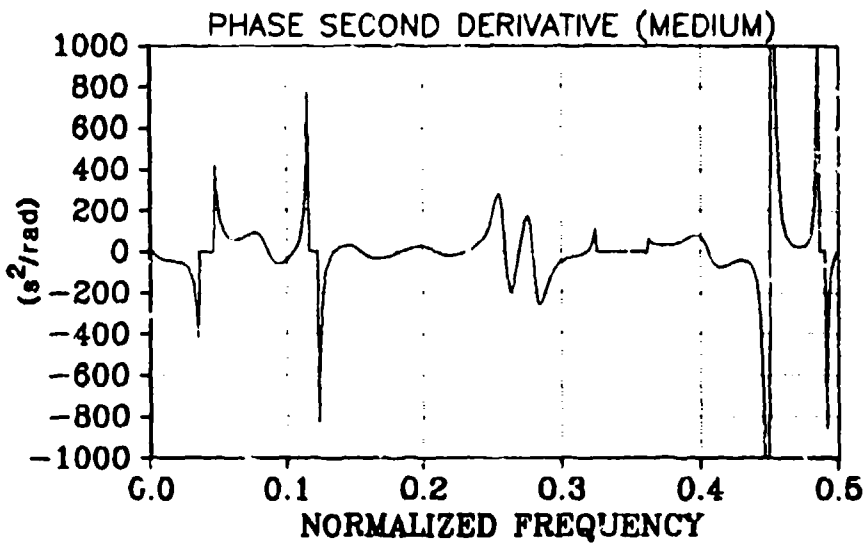


Fig. 18. Second derivative of the phase of the medium response.

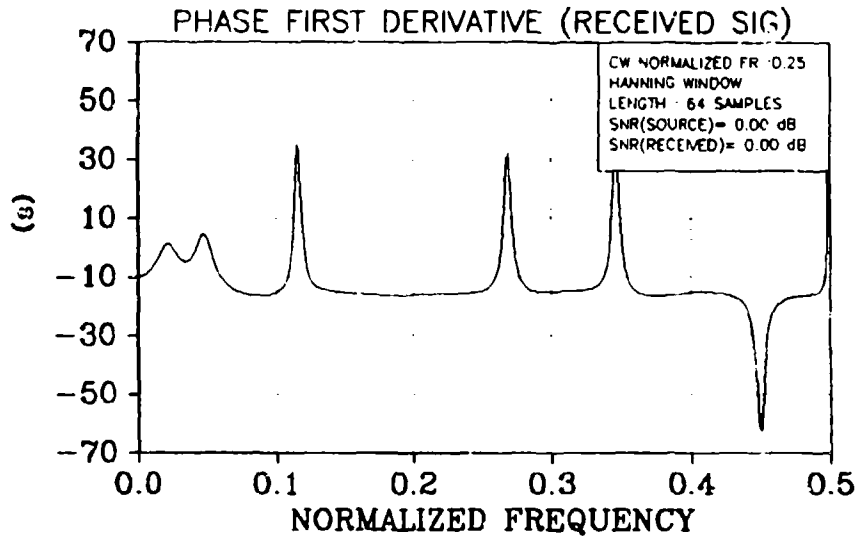


Fig. 19. First derivative of the phase of the received signal.

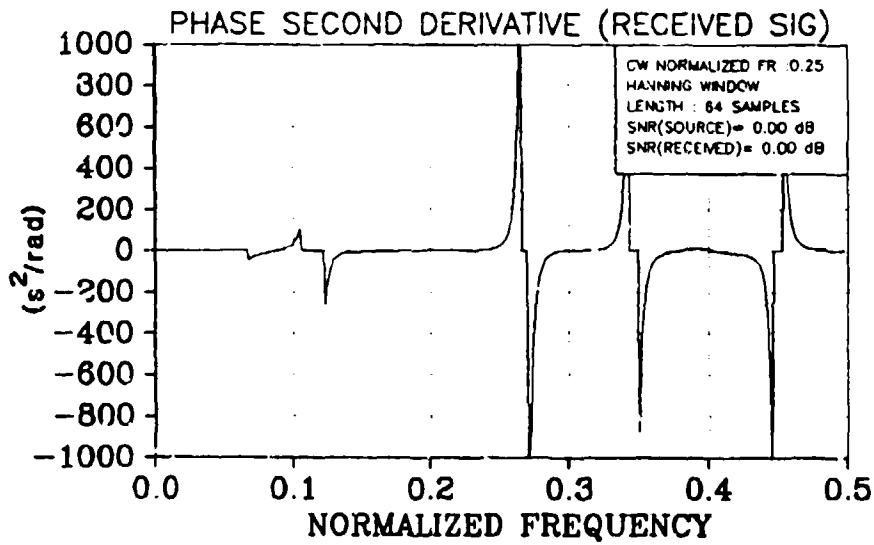


Fig. 20. Second derivative of the phase of the received signal.

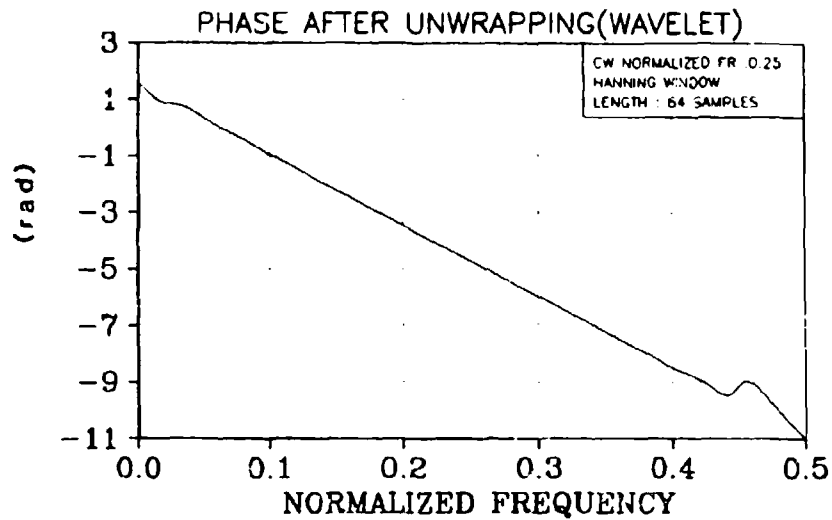


Fig. 21. Phase of the CW pulse after unwrapping (before linear phase removal!).

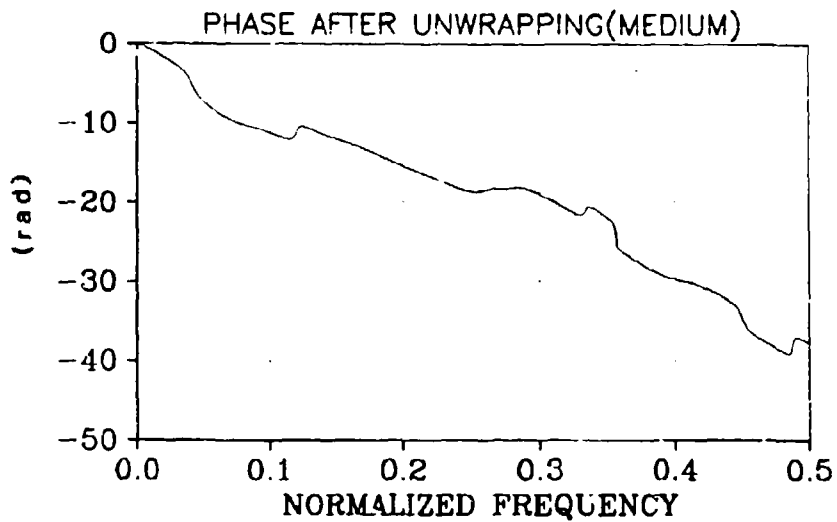


Fig. 22. Phase of the medium response after unwrapping (before linear phase removal).

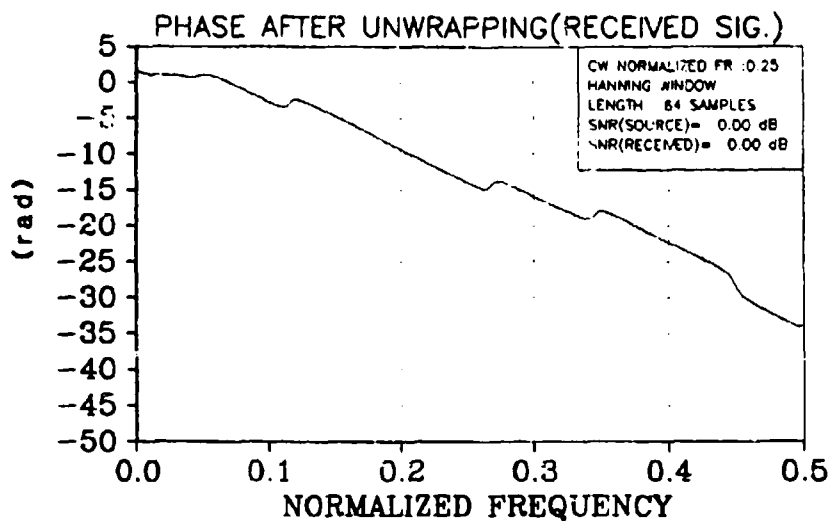


Fig. 23. Phase of the received signal after unwrapping (before linear phase removal).

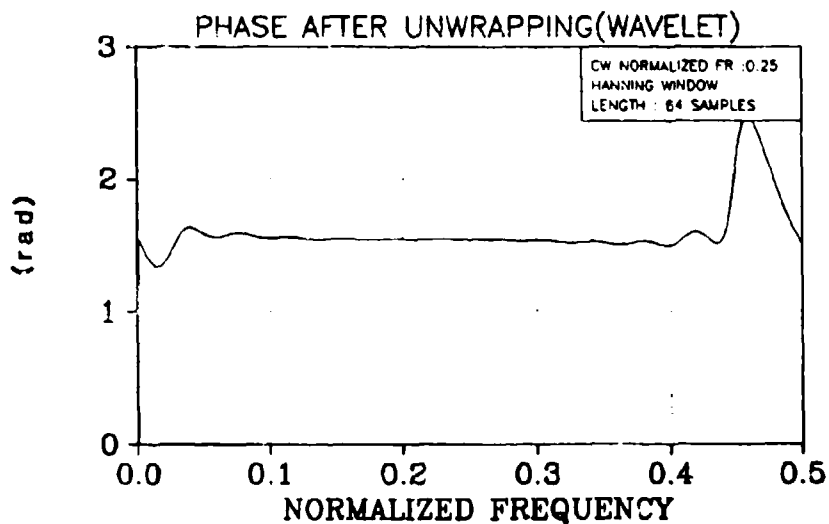


Fig. 24. Phase of the CW pulse after unwrapping (after linear phase removal).

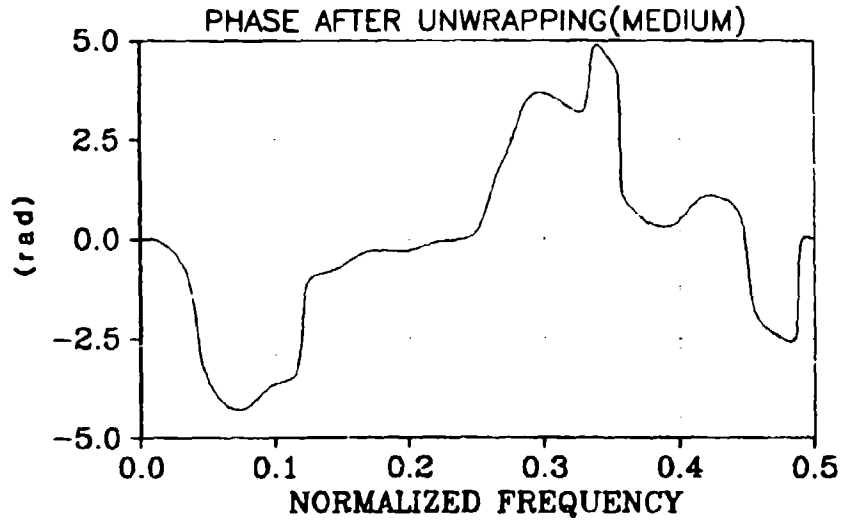


Fig. 25. Phase of the medium response after unwrapping (after linear phase removal).

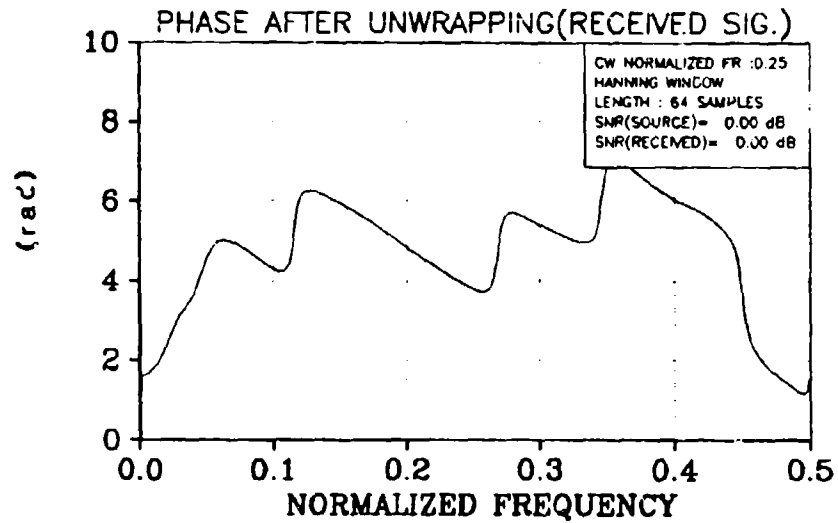


Fig. 26. Phase of the received signal after unwrapping (after linear phase removal).

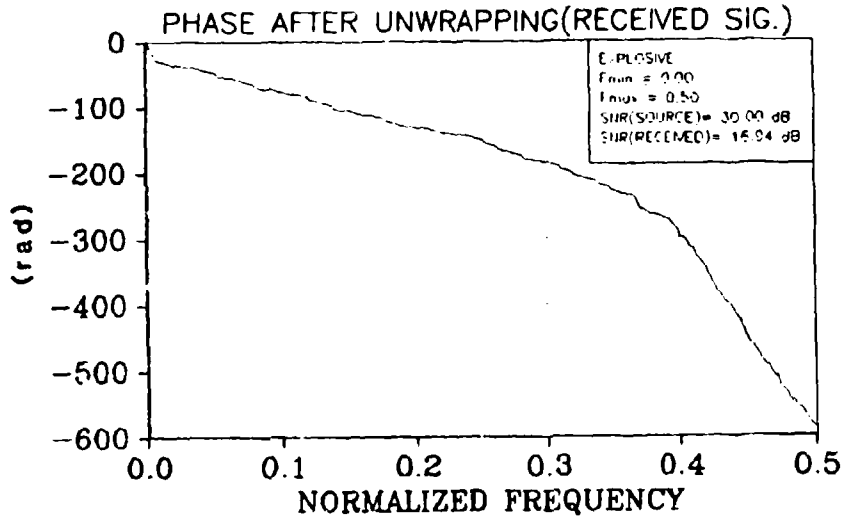


Fig. 27. Phase of the received signal (explosive) after unwrapping (before linear phase removal).

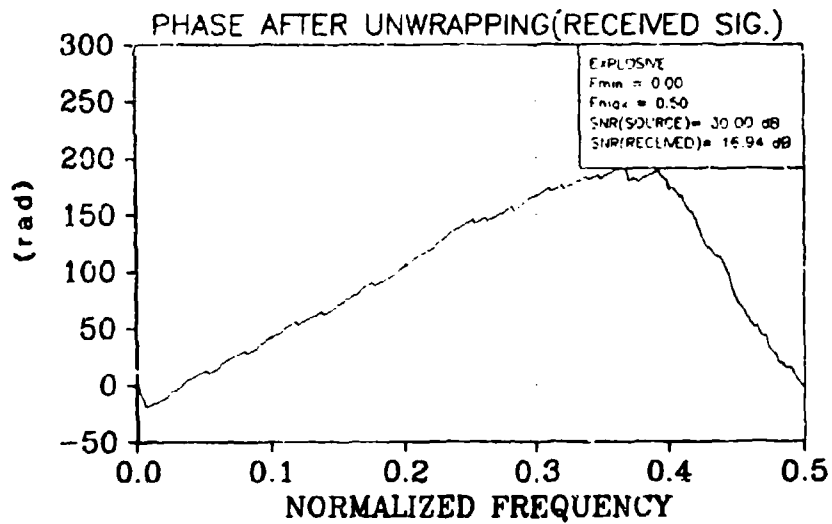


Fig. 28. Phase of the received signal (explosive) after unwrapping (after linear phase removal).

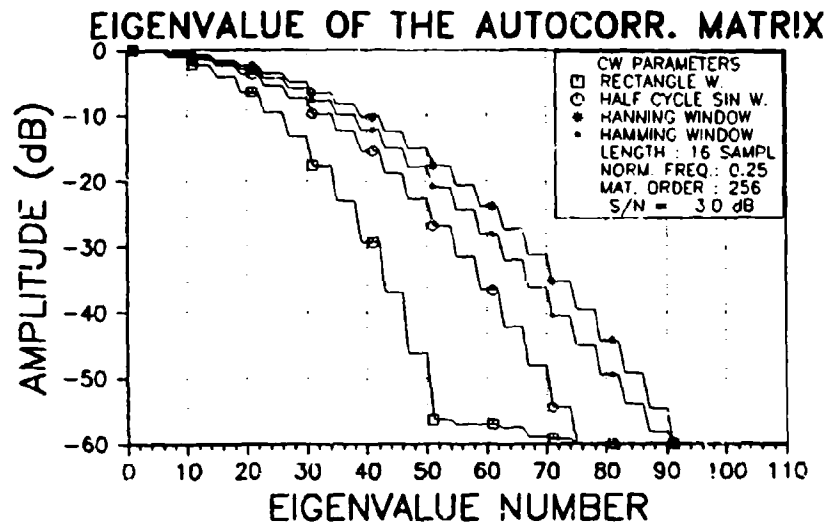


Fig. 29. Eigenvalues of the autocorrelation matrix of the received signal (transmitted pulse: 16 time-samples CW pulse).

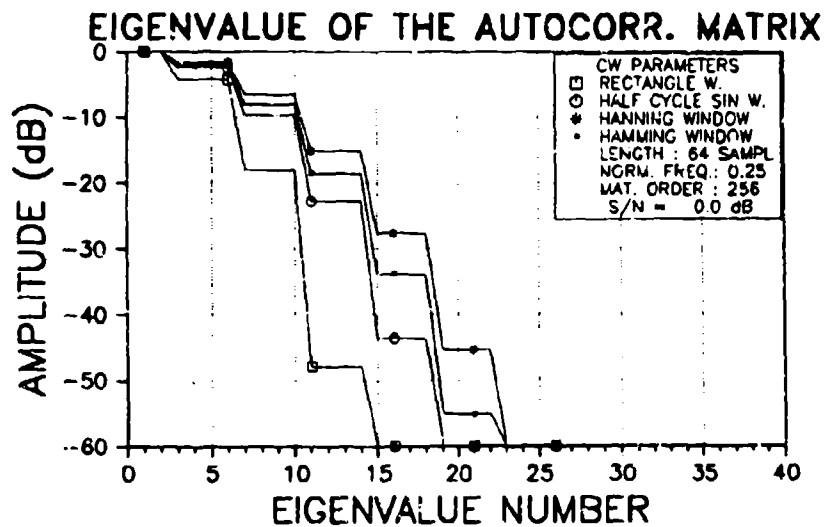


Fig. 30. Eigenvalues of the autocorrelation matrix of the received signal (transmitted pulse: 64 time-samples CW pulse).

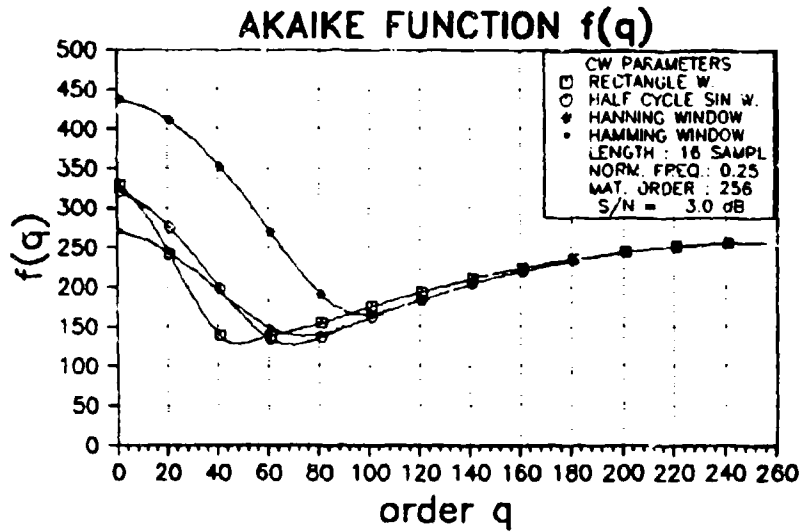


Fig. 31. Akaike function (transmitted pulse: 16 time-samples CW pulse).

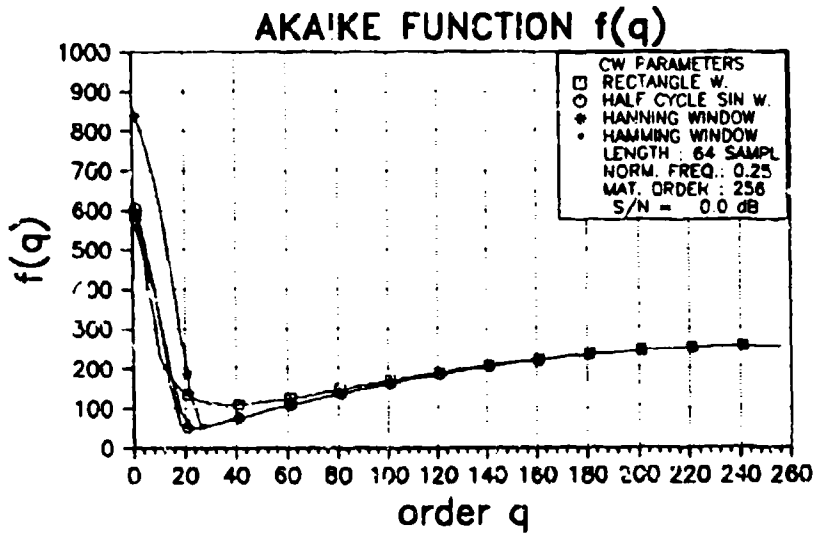


Fig. 32. Akaike function (transmitted pulse: 64 times-samples CW pulse).

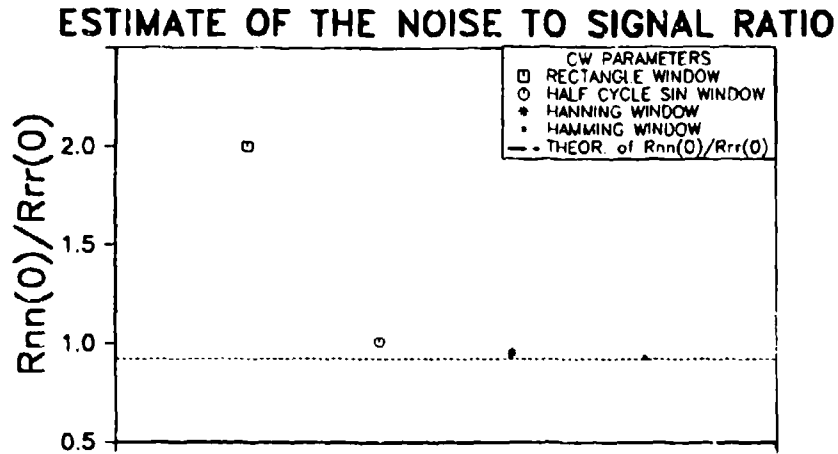


Fig. 33. Estimate of the noise-to-signal ratio (transmitted pulse: 16 time-samples CW pulse).

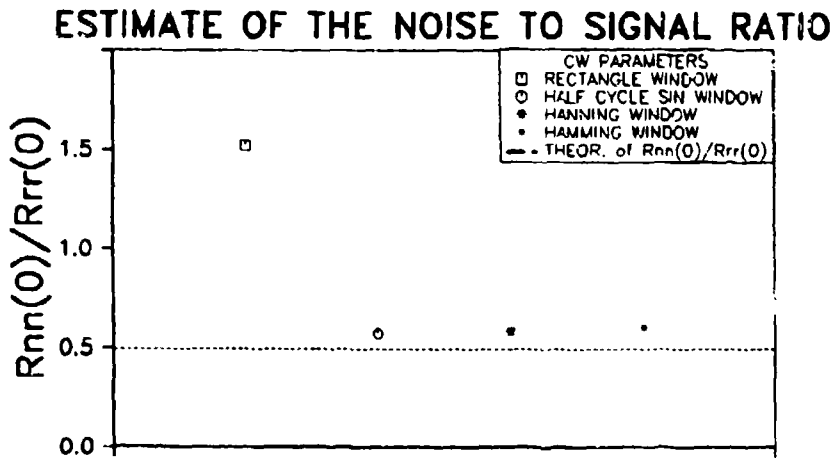


Fig. 34. Estimate of the noise-to-signal ratio (transmitted pulse: 64 time-samples CW pulse).

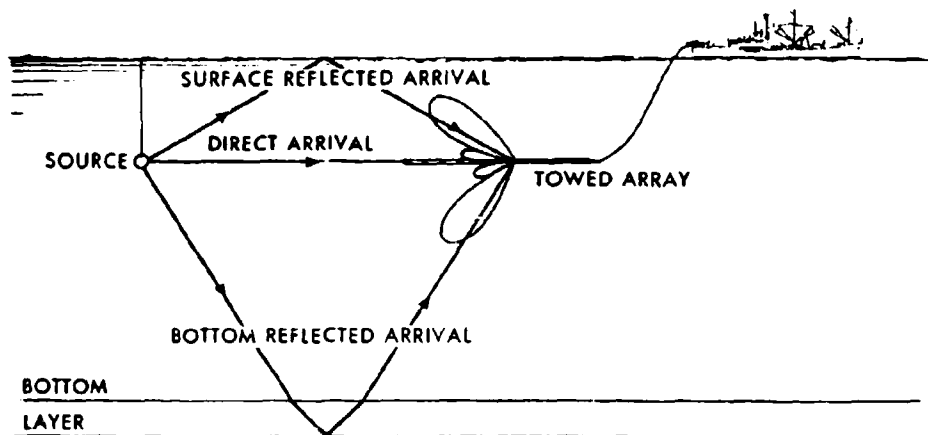


Fig. 35. Configuration of the active sonar backscattering simulation.

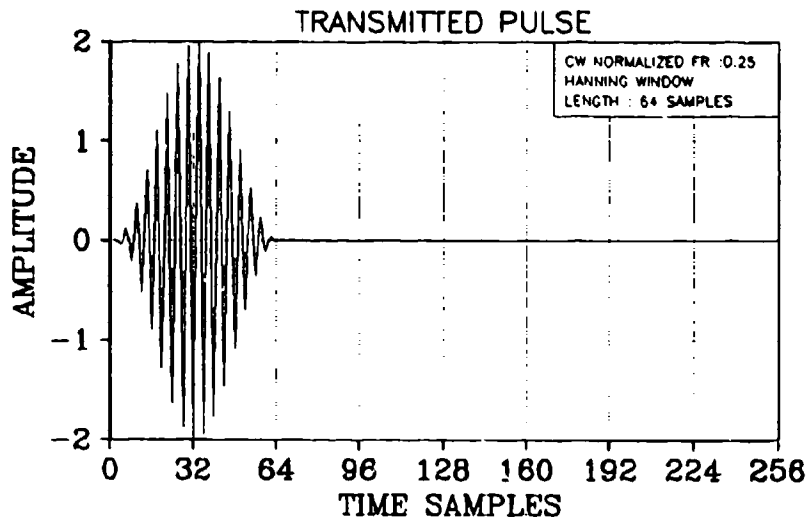


Fig. 36. Transmitted pulse (Hanning-windowed CW pulse).

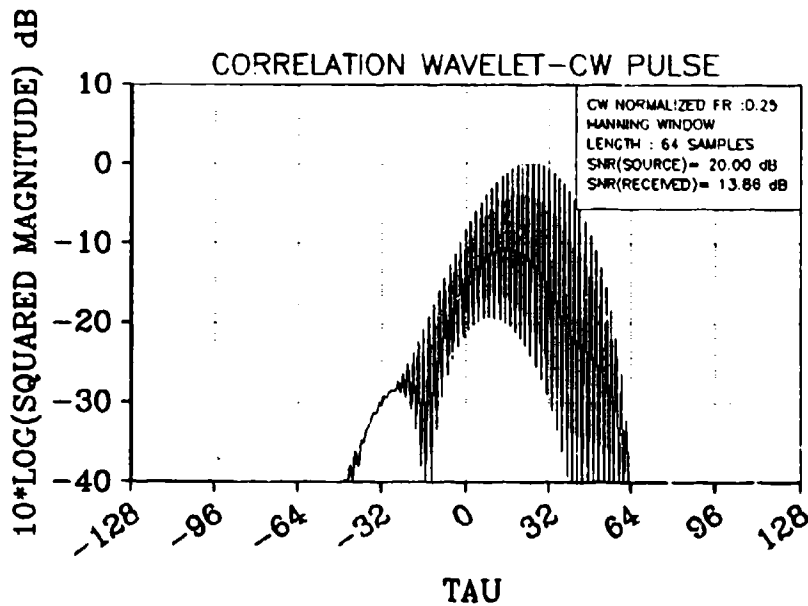


Fig. 37. Cross-correlation between the transmitted pulse and the deconvolved wavelet (Hanning-windowed CW pulse; 3 multiples; $\tau = 80, 110, 170$; SNRR = 14 dB).

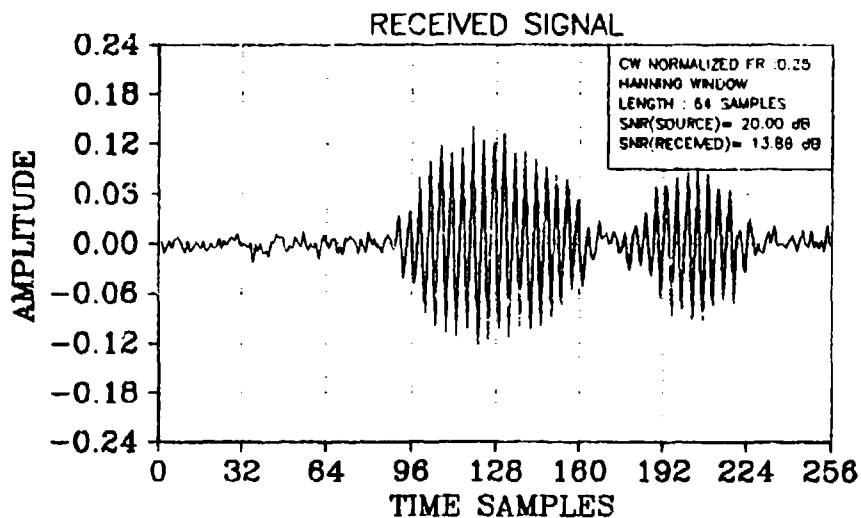


Fig. 38. Received signal (Hanning-windowed CW pulse; 3 multiples; $\tau = 80, 110, 170$; SNRR = 14 dB).

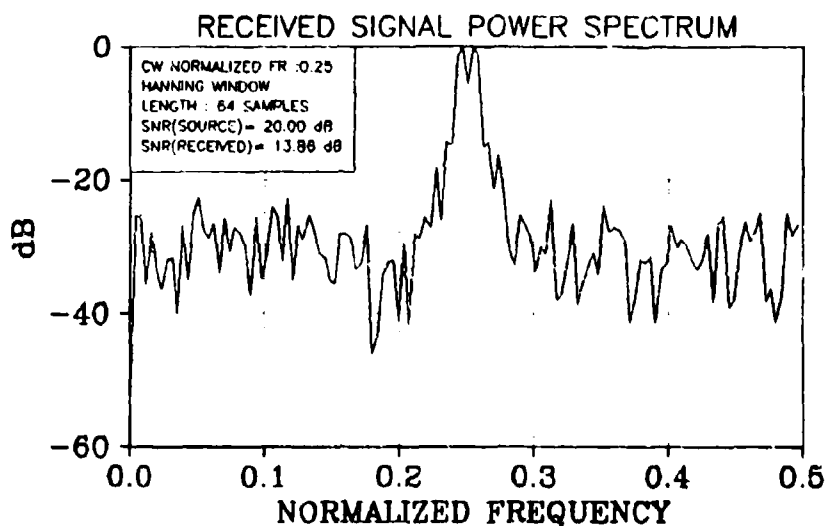


Fig. 39. Received signal power spectrum (Hanning-windowed CW pulse; 3 multiples; $\tau = 80, 110, 170$; SNRR = 14 dB).

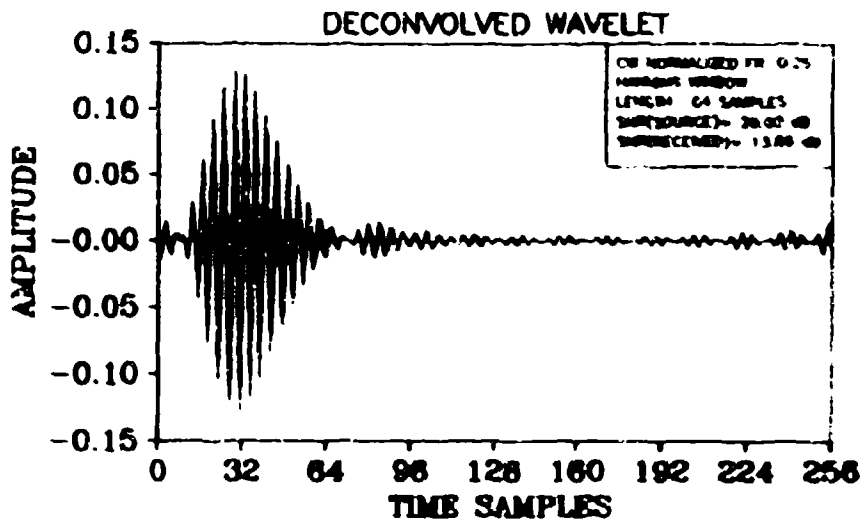


Fig. 40. Deconvolved wavelet (Hanning-windowed CW pulse; 3 multiples; $\tau = 80, 110, 170$; SNRR = 14 dB).

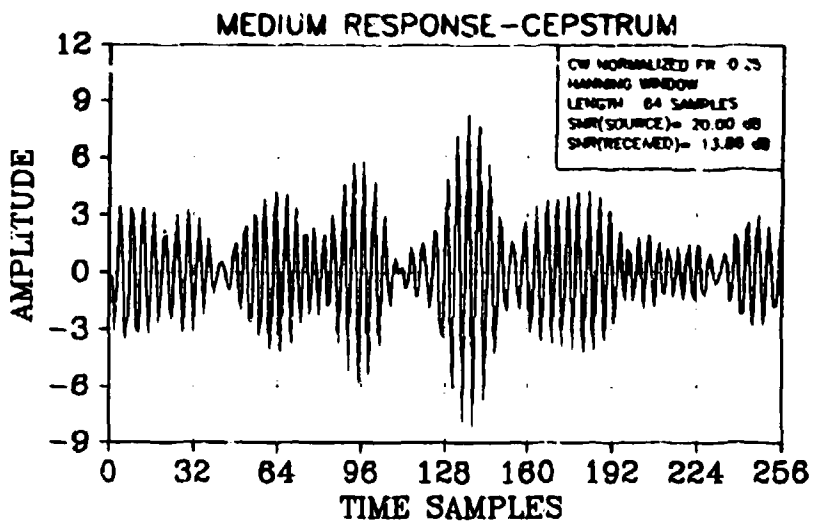


Fig. 41. Deconvolved medium response by cepstrum (Hanning-windowed CW pulse; 3 multiples; $\tau = 80, 110, 170$; SNRR = 14 dB).

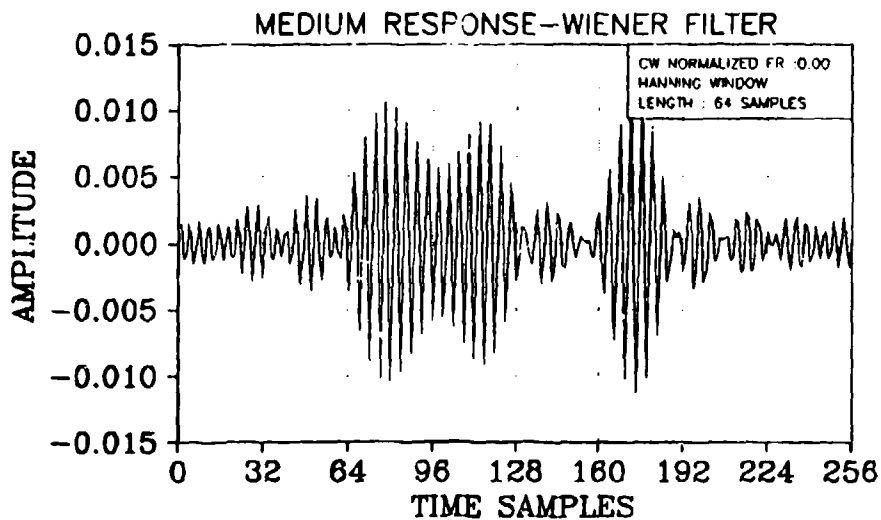


Fig. 42. Deconvolved medium response by Wiener filtering (Hanning-windowed CW pulse; 3 multiples; $\tau = 80, 110, 170$; SNRR = 14 dB).

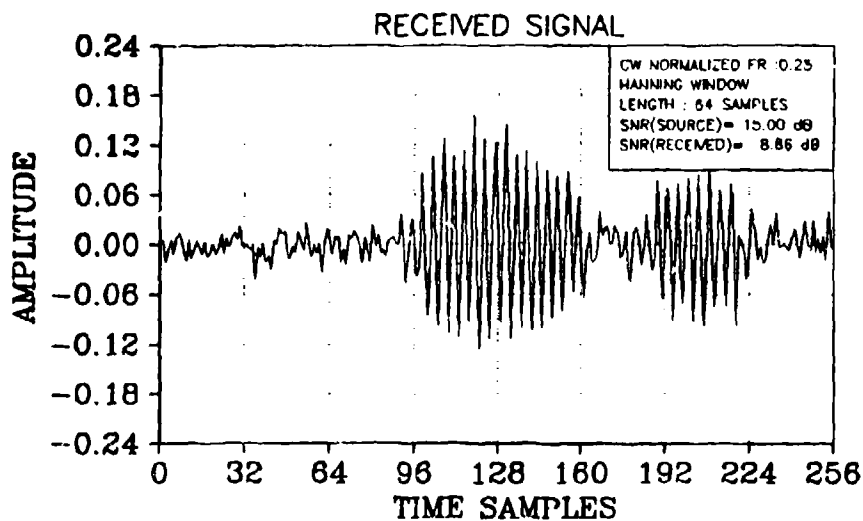


Fig. 43. Received signal (Hanning-windowed CW pulse; 3 multiples; $\tau = 80, 110, 170$; SNRR = 9 dB).

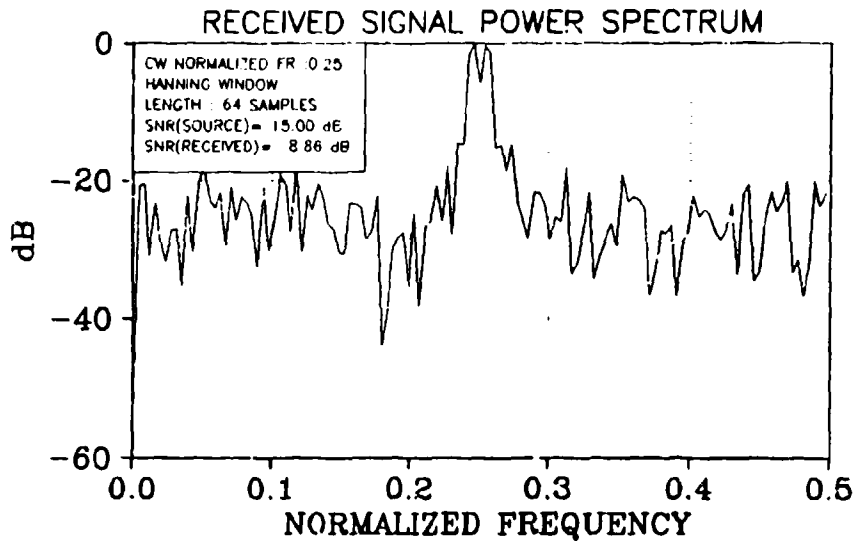


Fig. 44. Received signal power spectrum (Hanning-windowed CW pulse; 3 multiples; $\tau = 80, 110, 170$; SNRR = 9 dB).

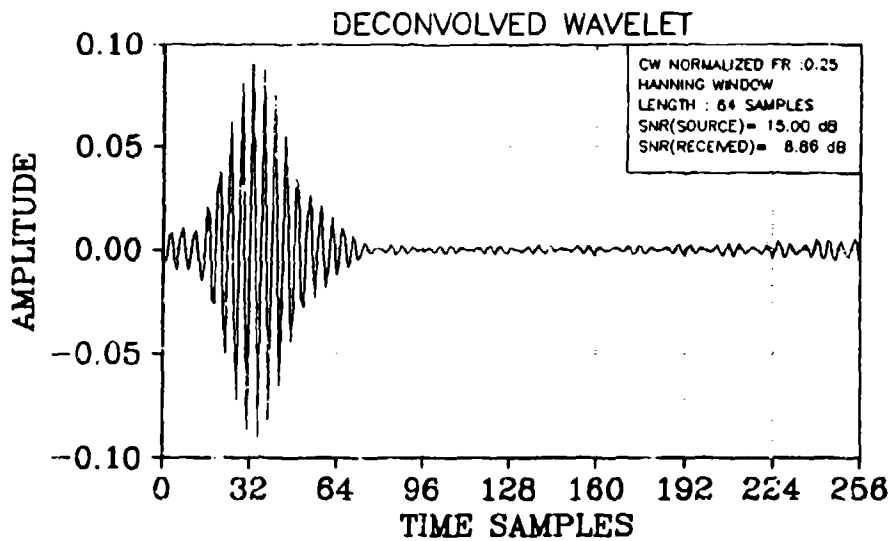


Fig. 45. Deconvolved wavelet (Hanning-windowed CW pulse; 3 multiples; $\tau = 80, 110, 170$; SNRR = 9 dB).

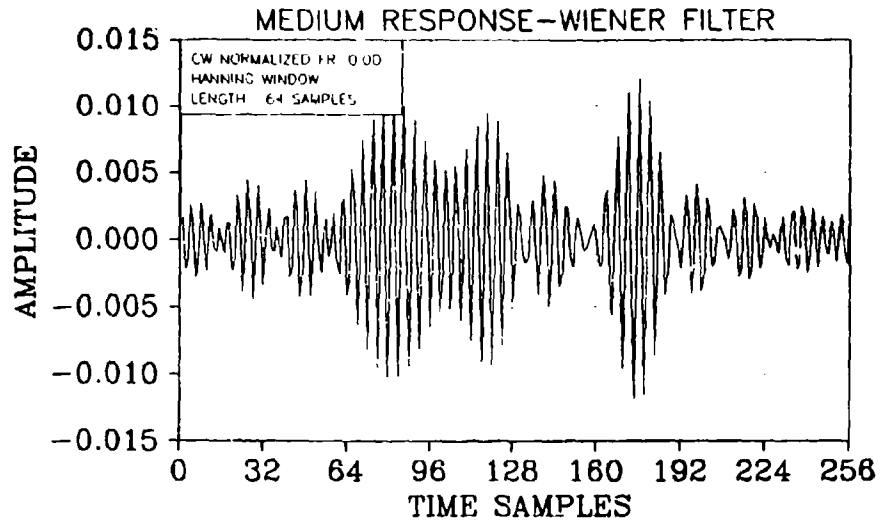


Fig. 46. Deconvolved medium response by Wiener filtering (Hanning-windowed CW pulse; 3 multiples; $\tau = 80, 110, 170$; SNRR = 9 dB).

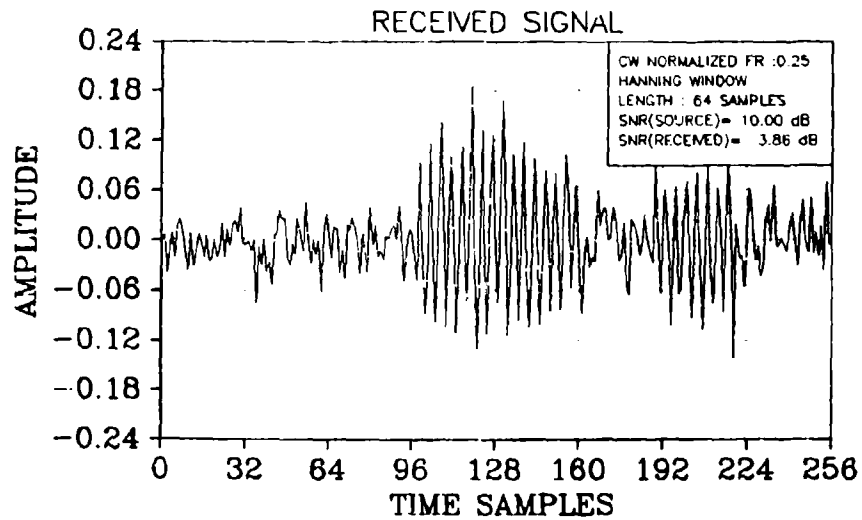


Fig. 47. Received signal (Hanning-windowed CW pulse; 3 multiples; $\tau = 80, 110, 170$; SNRR = 4 dB).

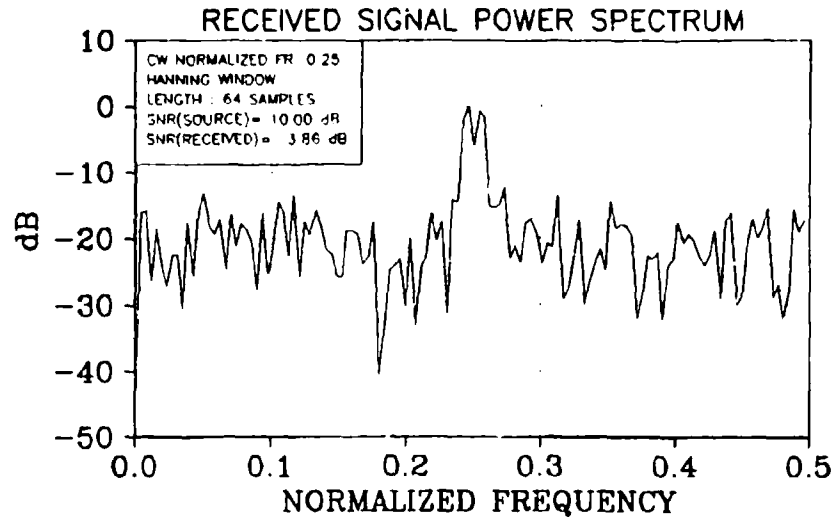


Fig. 48. Received signal power spectrum (Hanning-windowed CW pulse; 3 multiples; $\tau = 80, 110, 170$; SNRR = 4 dB).

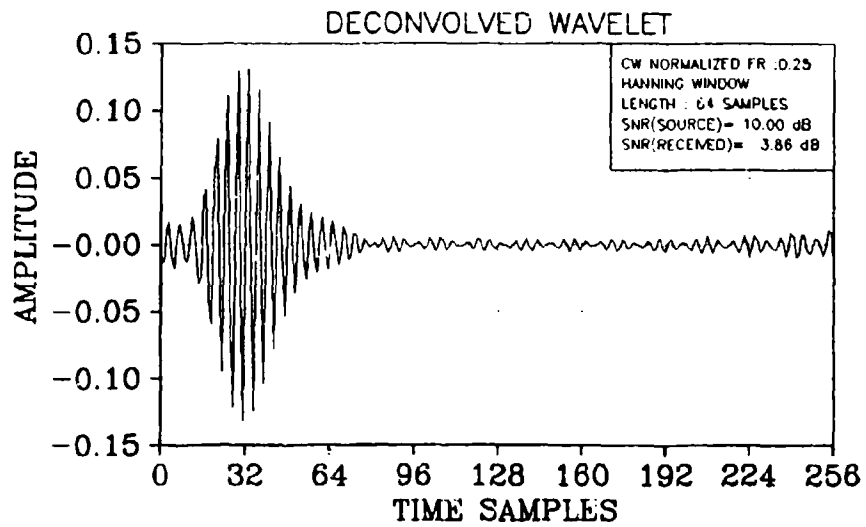


Fig. 49. Deconvolved wavelet (Hanning-windowed CW pulse; 3 multiples; $\tau = 80, 110, 170$; SNRR = 4 dB).

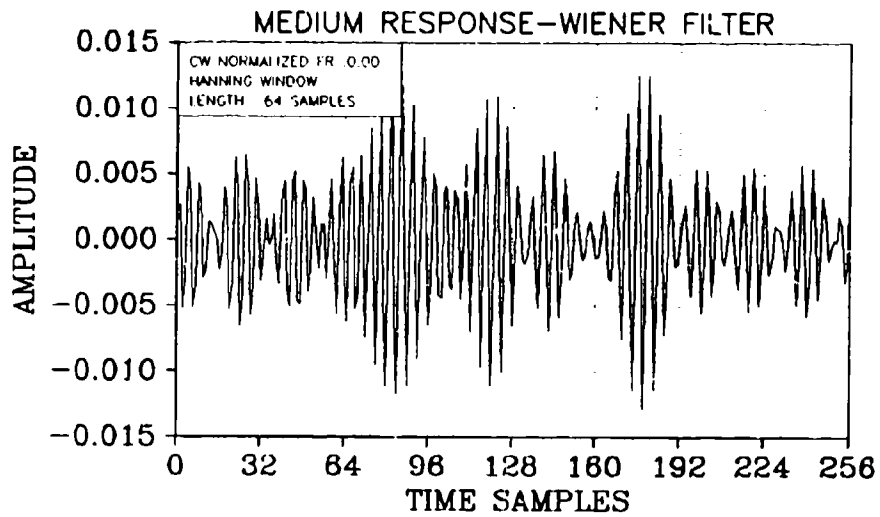


Fig. 50. Deconvolved medium response by Wiener filtering (Hanning-windowed CW pulse; 3 multiples; $\tau = 80, 110, 170$; SNRR = 4 dB).

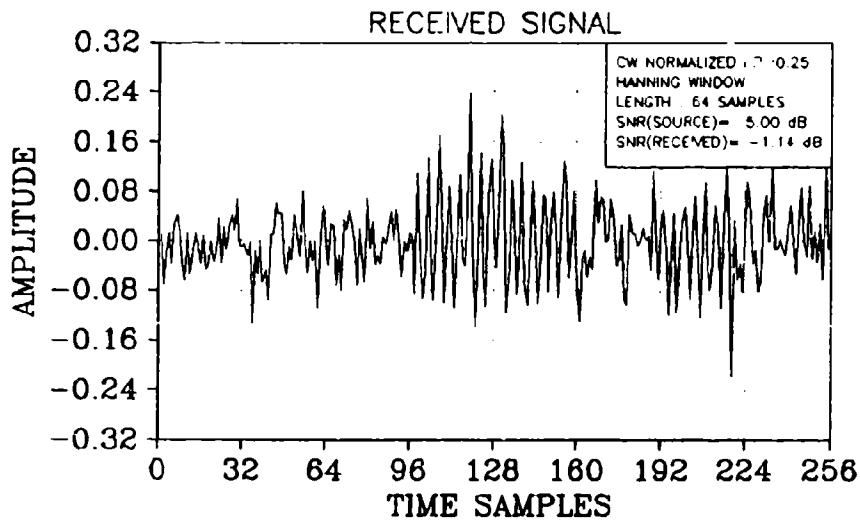


Fig. 51. Received signal (Hanning-windowed CW pulse; 3 multiples; $\tau = 80, 110, 170$; SNRR = -1 dB).

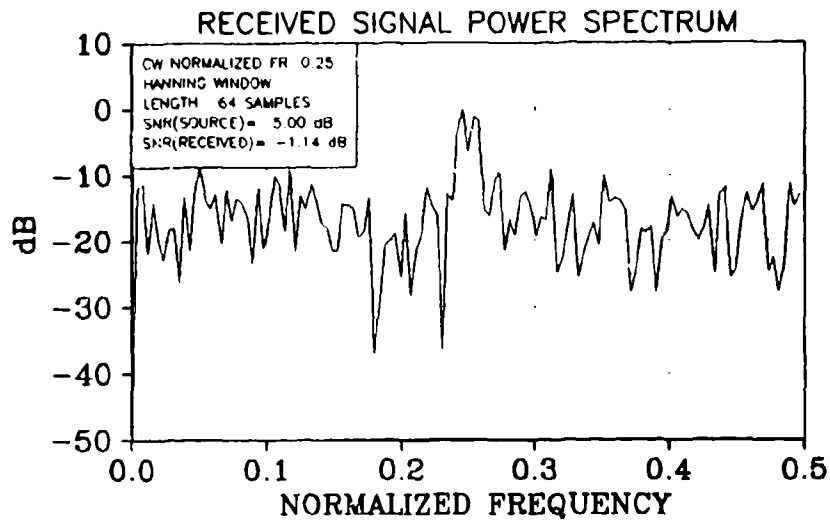


Fig. 52. Received signal power spectrum (Hanning-windowed CW pulse; 3 multiples; $\tau = 80, 110, 170$; SNRR = -1 dB).

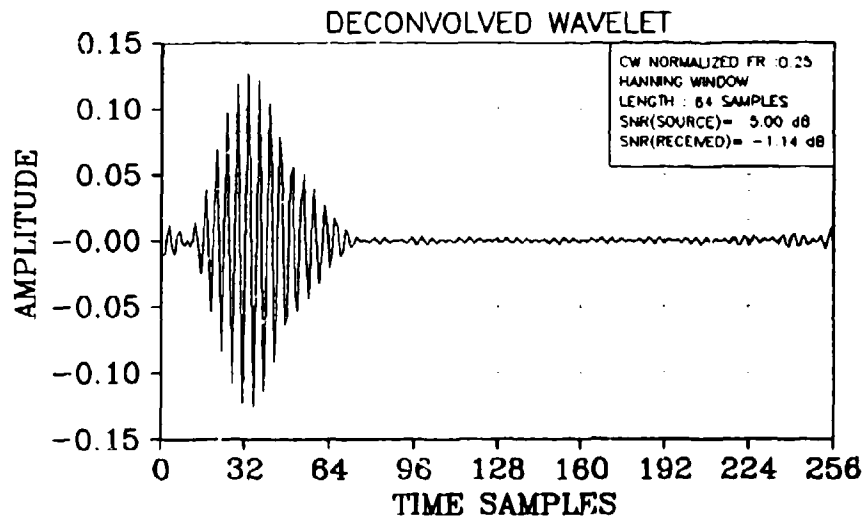


Fig. 53. Deconvolved wavelet (Hanning-windowed CW pulse; 3 multiples; $\tau = 80, 110, 170$; SNRR = -1 dB).

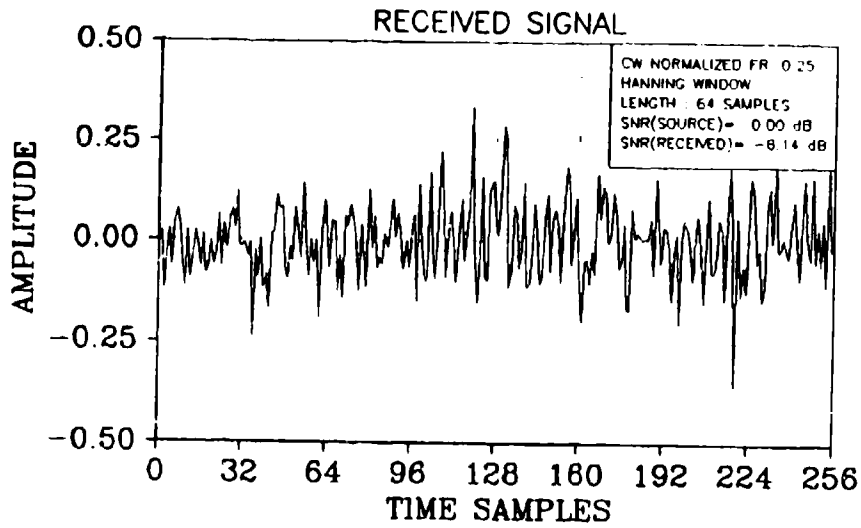


Fig. 54. Received signal (Hanning-windowed CW pulse; 3 multiples; $\tau = 80, 110, 170$; SNRR = -6 dB).

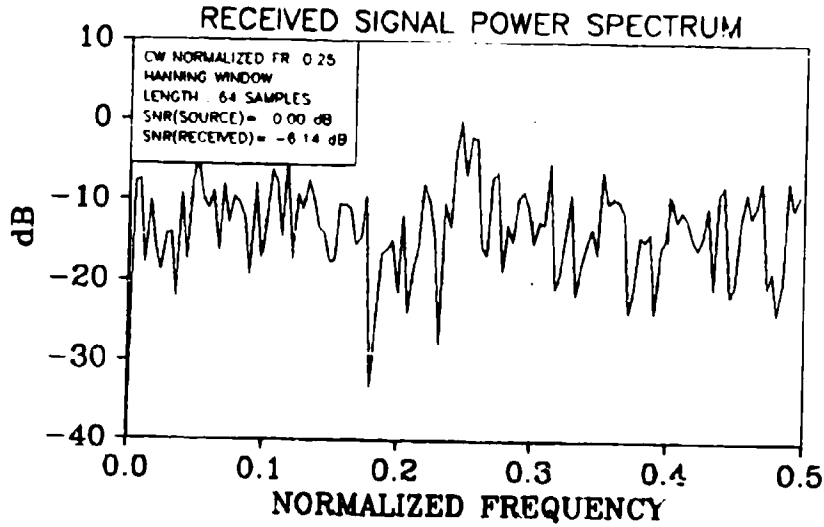


Fig. 55. Received signal power spectrum (Hanning-windowed CW pulse; 3 multiples; $\tau = 80, 110, 170$; SNRR = -6 dB).

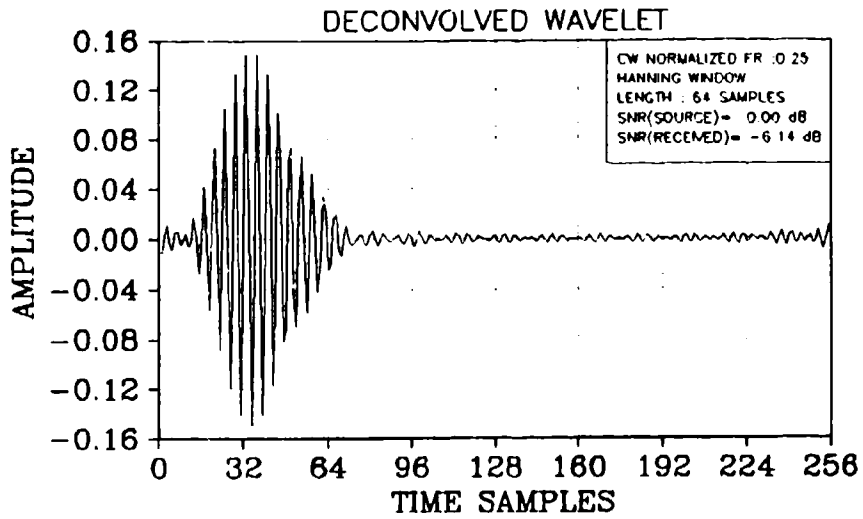


Fig. 56. Deconvolved wavelet (Hanning-windowed CW pulse; 3 multiples; $\tau = 80, 110, 170$; SNRR = -6 dB).

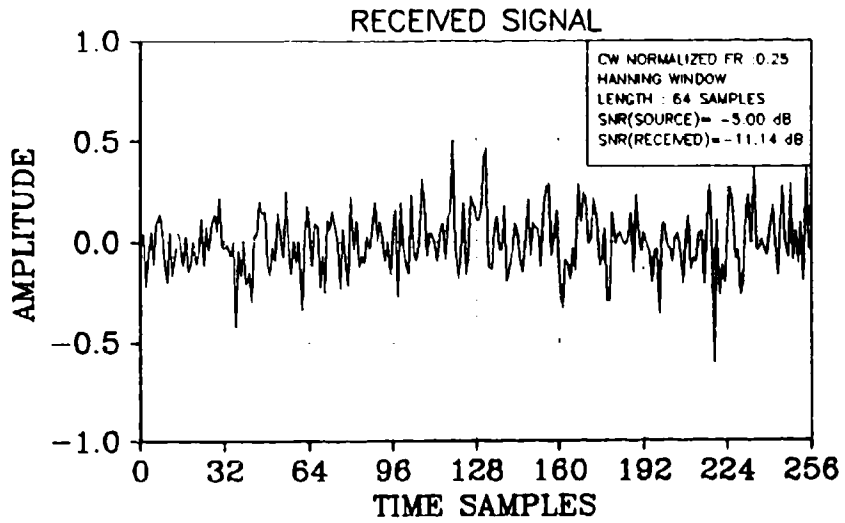


Fig. 57. Received signal (Hanning-windowed CW pulse; 3 multiples; $\tau = 80, 110, 170$; SNRR = -11 dB).

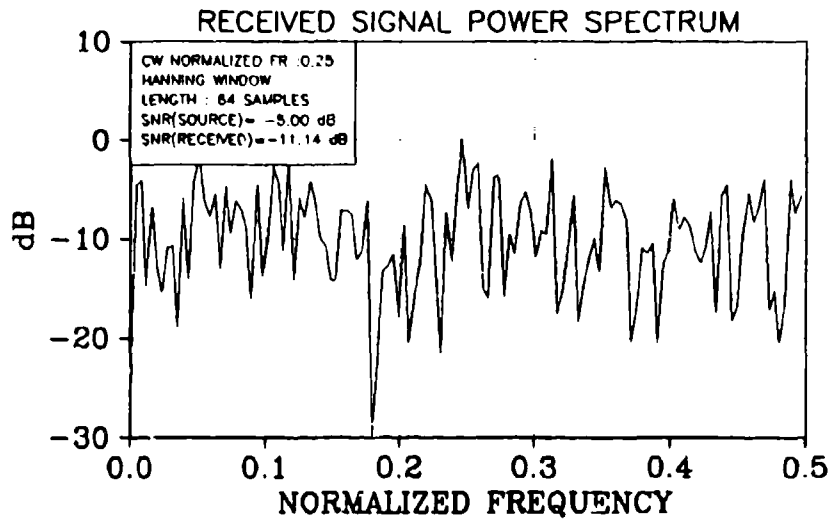


Fig. 58. Received signal power spectrum (Hanning-windowed CW pulse; 3 multiples; $\tau = 80, 110, 170$; SNRR = -11 dB).

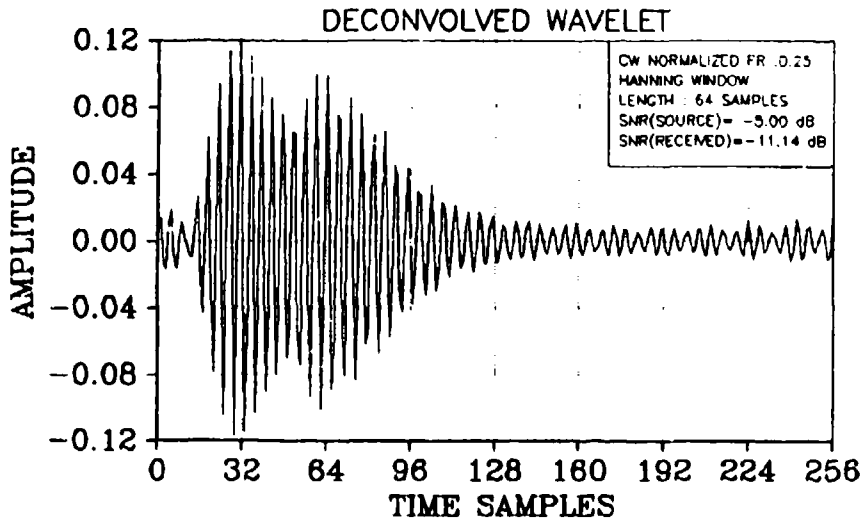


Fig. 59. Deconvolved wavelet (Hanning-windowed CW pulse; 3 multiples; $\tau = 80, 110, 170$; SNRR = -11 dB).

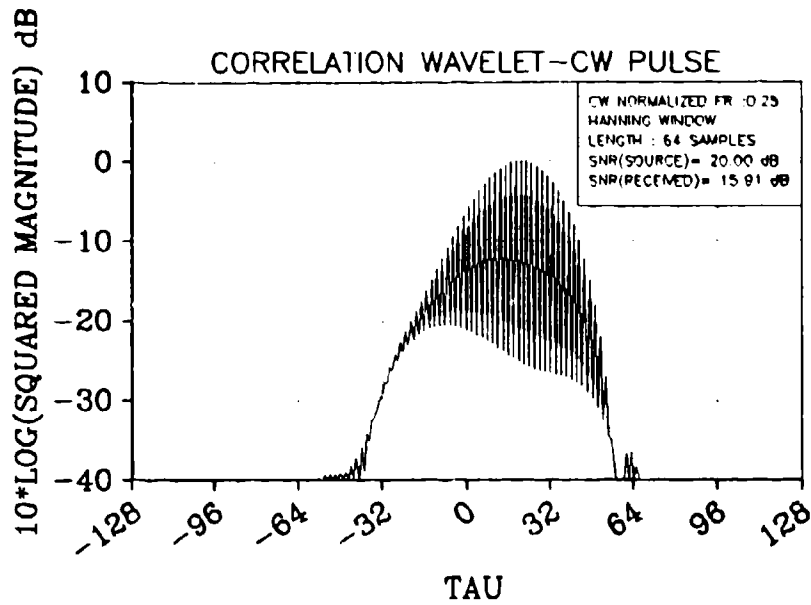


Fig. 60. Cross-correlation between the transmitted pulse and the deconvolved wavelet (Hanning-windowed CW pulse; 5 multiples; $\tau = 80, 110, 140, 170, 200$; SNRR = 16 dB).

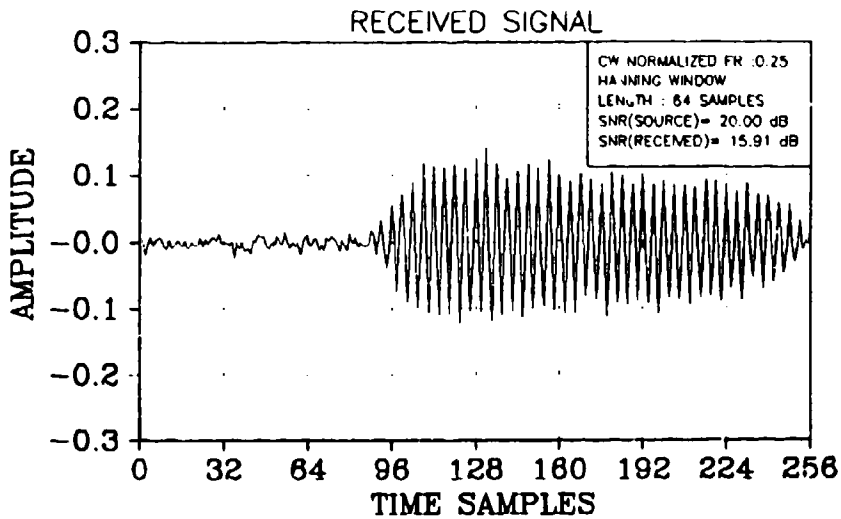


Fig. 61. Received signal (Hanning-windowed CW pulse; 5 multiples; $\tau = 80, 110, 140, 170, 200$; SNRR = 16 dB).

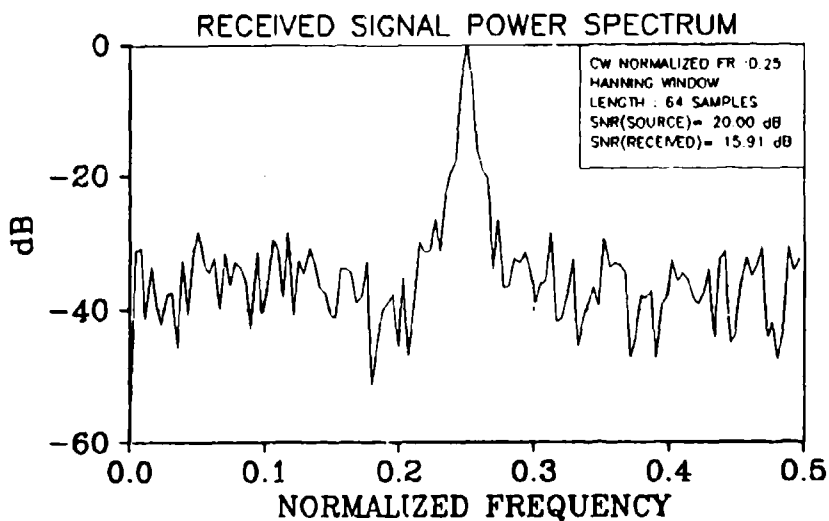


Fig. 62. Received signal power spectrum (Hanning-windowed CW pulse; 5 multiples; $\tau = 80, 110, 140, 170, 200$; SNRR = 16 dB).

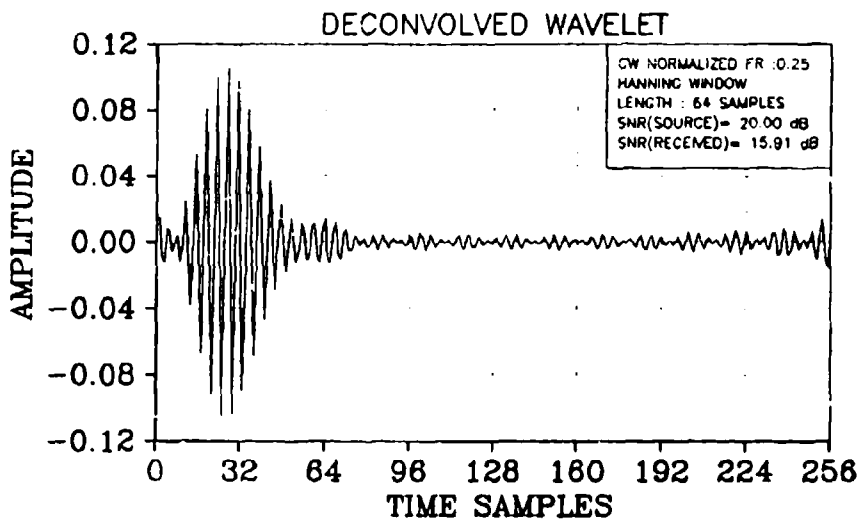


Fig. 63. Deconvolved wavelet (Hanning-windowed CW pulse; 5 multiples; $\tau = 80, 110, 140, 170, 200$; SNRR = 16 dB).

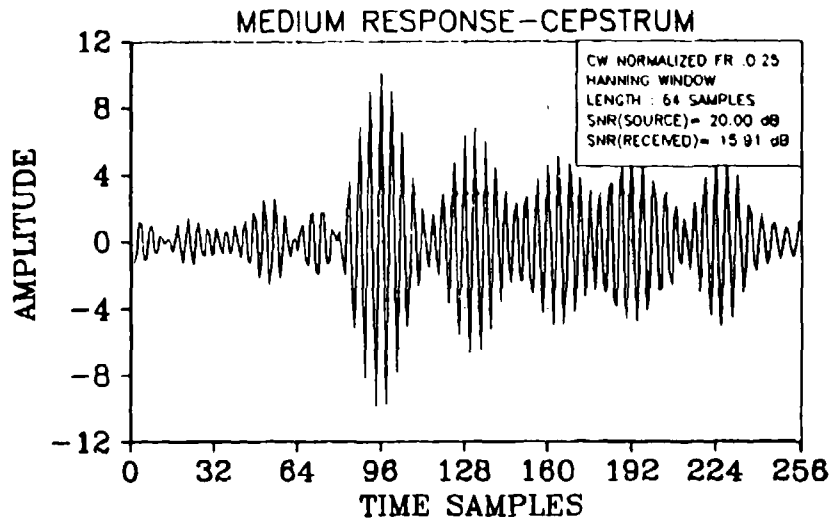


Fig. 64. Deconvolved medium response by cepstrum (Hanning-windowed CW pulse; 5 multiples; $\tau = 80, 110, 140, 170, 200$; SNRR = 16 dB).

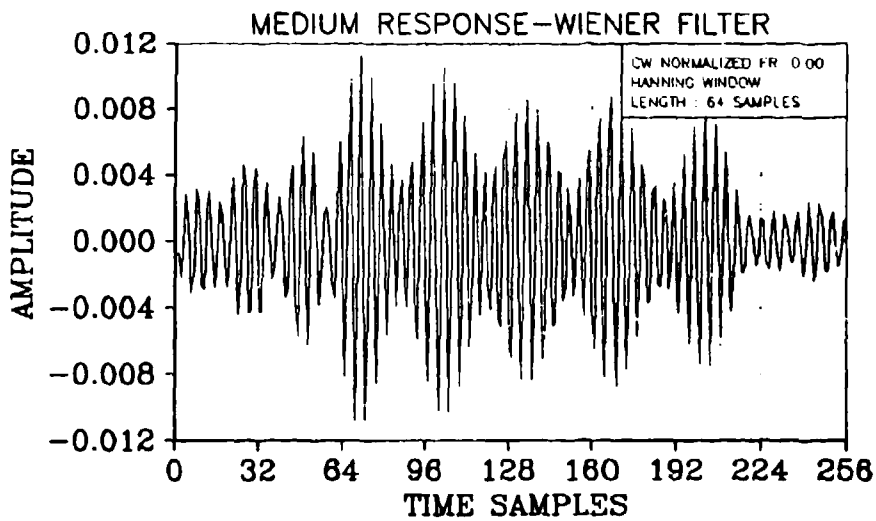


Fig. 65. Deconvolved medium response by Wiener filtering (Hanning-windowed CW pulse; 5 multiples; $\tau = 80, 110, 140, 170, 200$; SNRR = 16 dB).

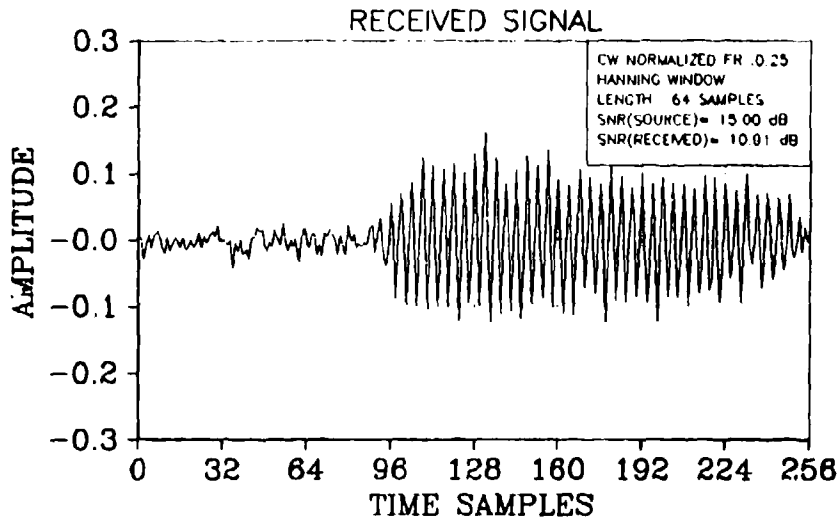


Fig. 66. Received signal (Hanning-windowed CW pulse; 5 multiples; $\tau = 80, 110, 140, 170, 200$; SNRR = 11 dB).

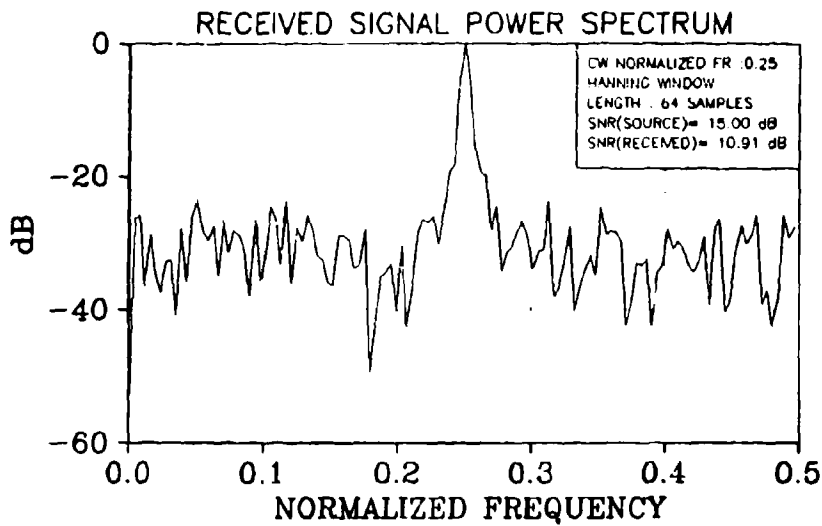


Fig. 67. Received signal power spectrum (Hanning-windowed CW pulse; 5 multiples; $\tau = 80, 110, 140, 170, 200$; SNRR = 11 dB).

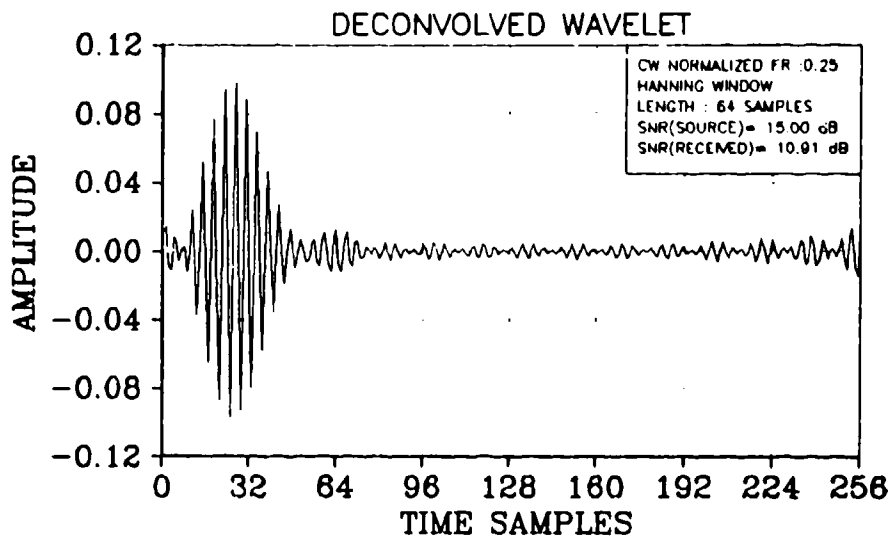


Fig. 68. Deconvolved wavelet (Hanning-windowed CW pulse; 5 multiples; $\tau = 80, 110, 140, 170, 200$; SNRR = 11 dB).

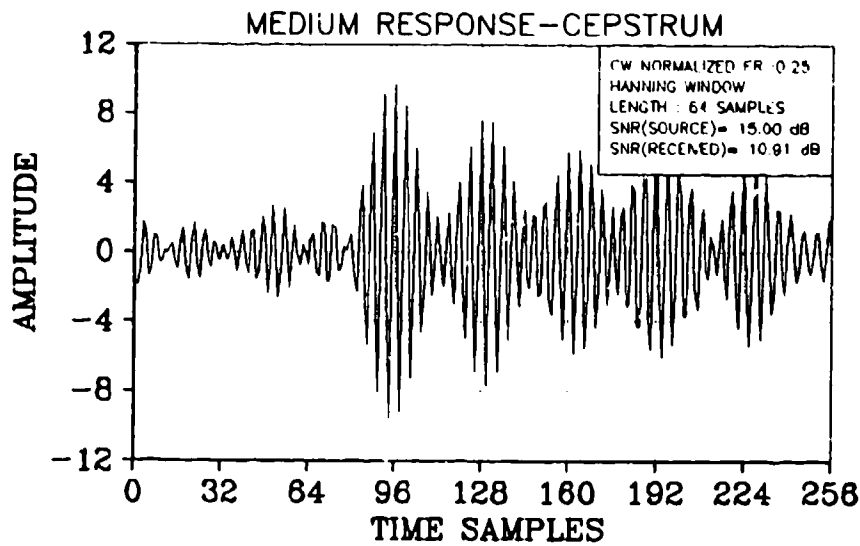


Fig. 69. Deconvolved medium response by cepstrum (Hanning-windowed CW pulse; 5 multiples; $\tau = 80, 110, 140, 170, 200$; SNRR = 11 dB).

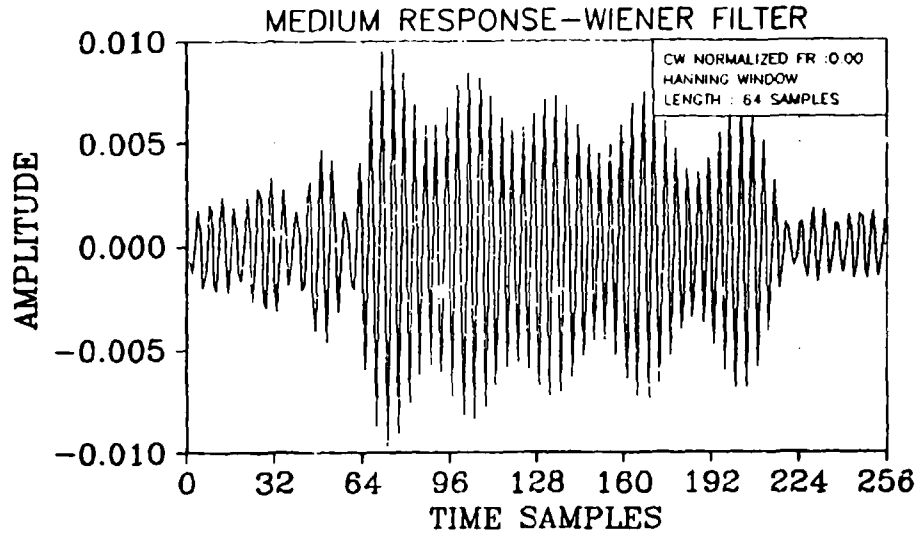


Fig. 70. Deconvolved medium response by Wiener filtering (Hanning-windowed CW pulse; 5 multiples; $\tau = 80, 110, 140, 170, 200$; SNRR = 11 dB).

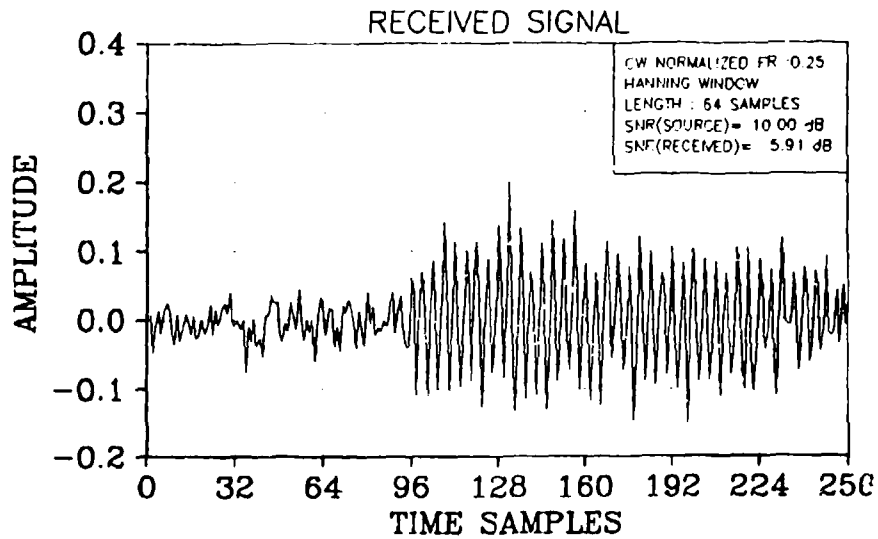


Fig. 71. Received signal (Hanning-windowed CW pulse; 5 multiples; $\tau = 80, 110, 140, 170, 200$; SNRR = 6 dB).

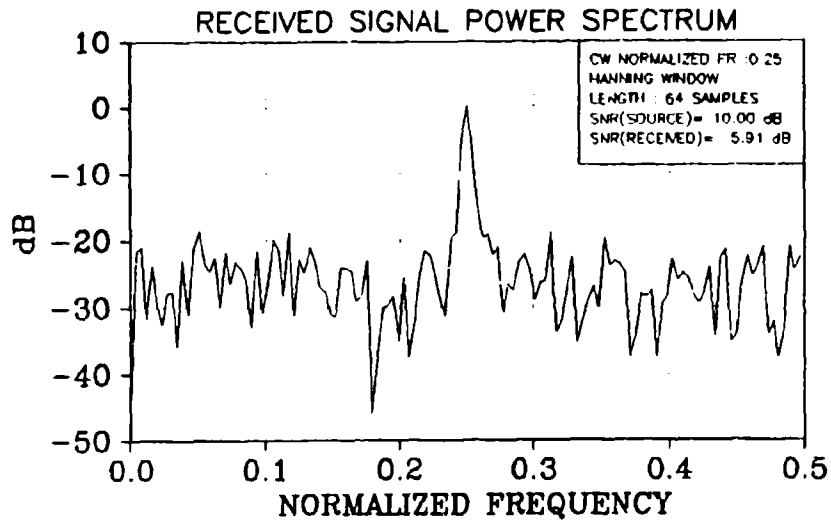


Fig. 72. Received signal power spectrum (Hanning-windowed CW pulse; 5 multiples; $\tau = 80, 110, 140, 170, 200$; SNRR = 6 dB).

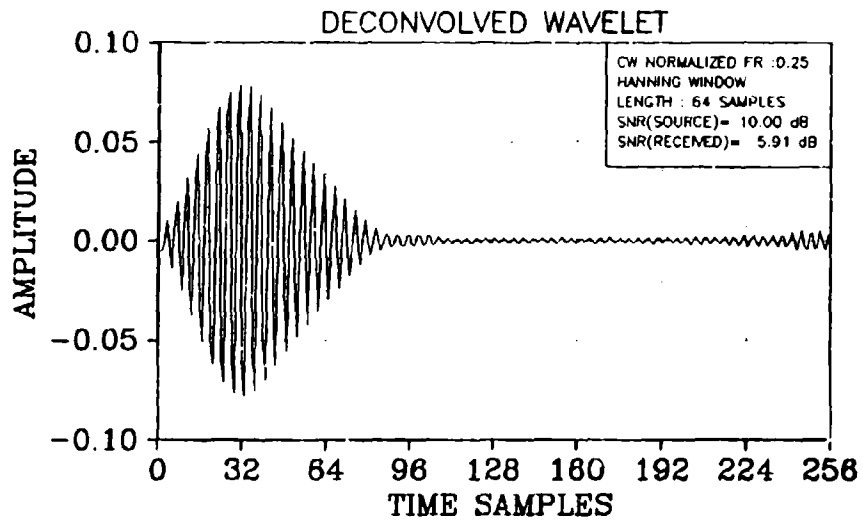


Fig. 73. Deconvolved wavelet (Hanning-windowed CW pulse; 5 multiples; $\tau = 80, 110, 140, 170, 200$; SNRR = 6 dB).

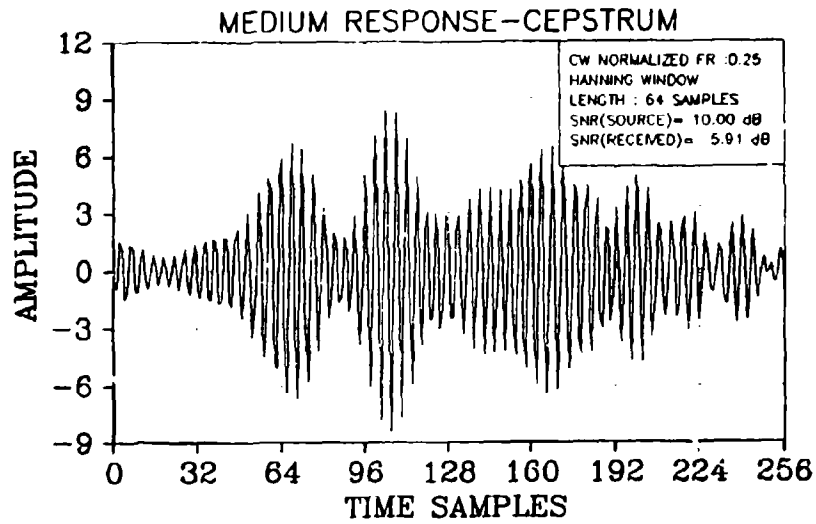


Fig. 74. Deconvolved medium response by cepstrum (Hanning-windowed CW pulse; 5 multiples; $\tau = 80, 110, 140, 170, 200$; SNRR = 6 dB).

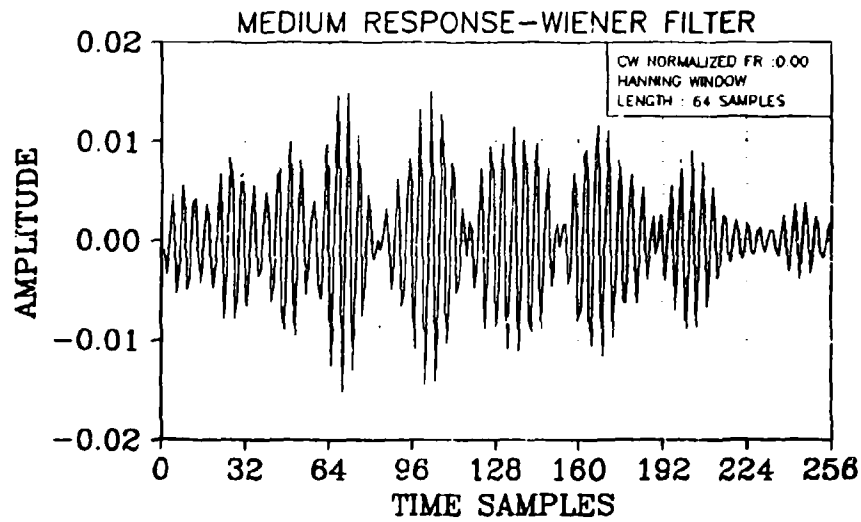


Fig. 75. Deconvolved medium response by Wiener filtering (Hanning-windowed CW pulse; 5 multiples; $\tau = 80, 110, 140, 170, 200$; SNRR = 6 dB).

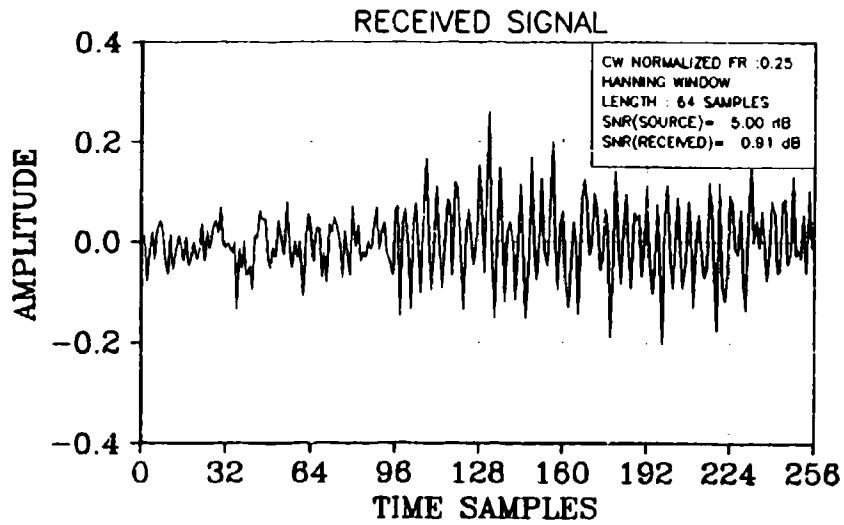


Fig. 76. Received signal (Hanning-windowed CW pulse; 5 multiples; $\tau = 80, 110, 140, 170, 200$; SNRR = 1 dB).

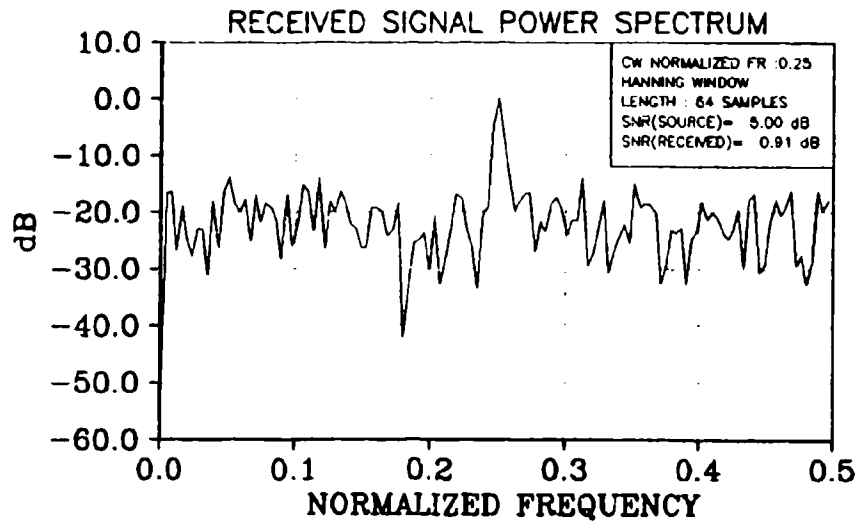


Fig. 77. Received signal power spectrum (Hanning-windowed CW pulse; 5 multiples; $\tau = 80, 110, 140, 170, 200$; SNRR = 1 dB).

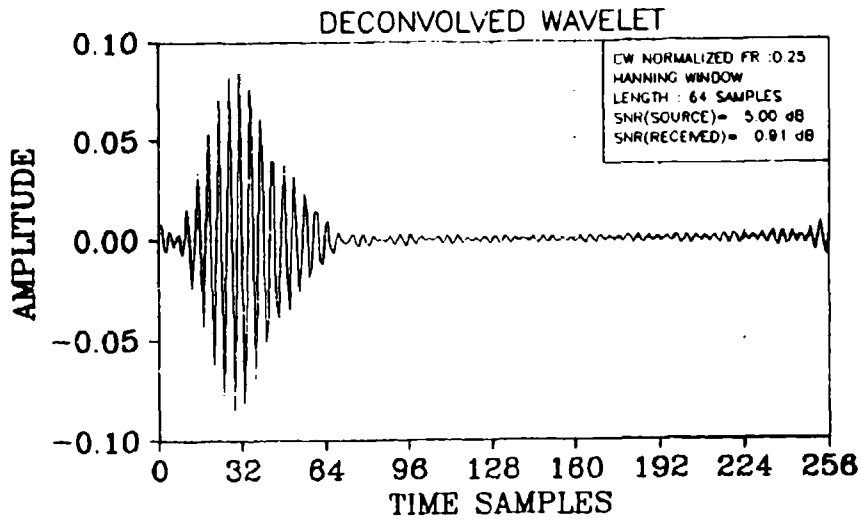


Fig. 78. Deconvolved wavelet (Hanning-windowed CW pulse; 5 multiples; $\tau = 80, 110, 140, 170, 200$; SNRR = 1 dB).

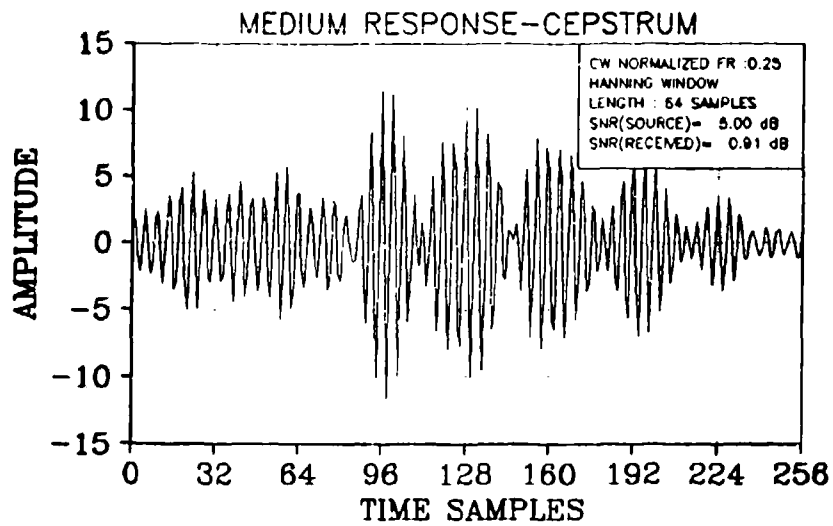


Fig. 79. Deconvolved medium response by cepstrum (Hanning-windowed CW pulse; 5 multiples; $\tau = 80, 110, 140, 170, 200$; SNRR = 1 dB).

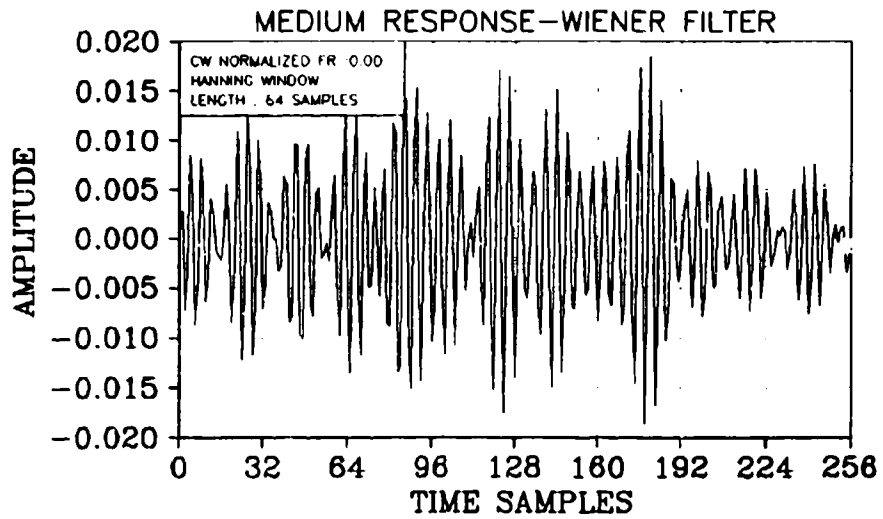


Fig. 80. Deconvolved medium response by Wiener filtering (Hanning-windowed CW pulse; 5 multiples; $\tau = 80, 110, 140, 170, 200$; SNRR = 1 dB).

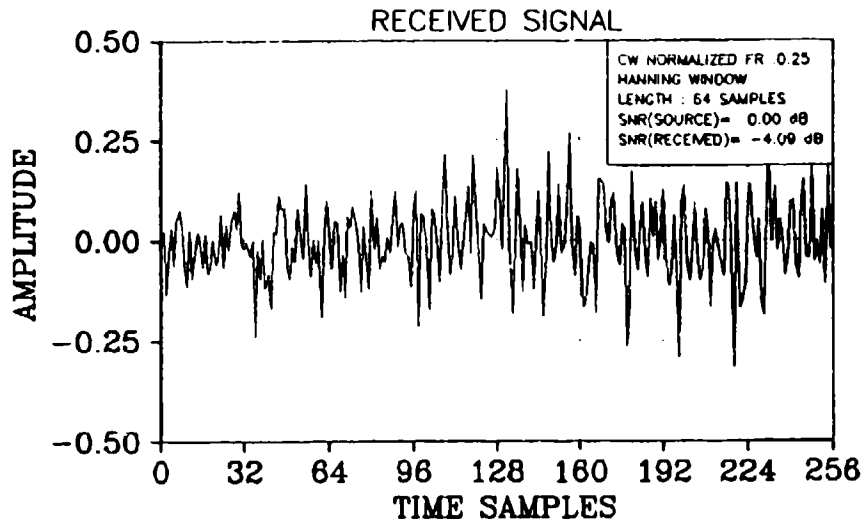


Fig. 81. Received signal (Hanning-windowed CW pulse; 5 multiples; $\tau = 80, 110, 140, 170, 200$; SNRR = -4 dB).

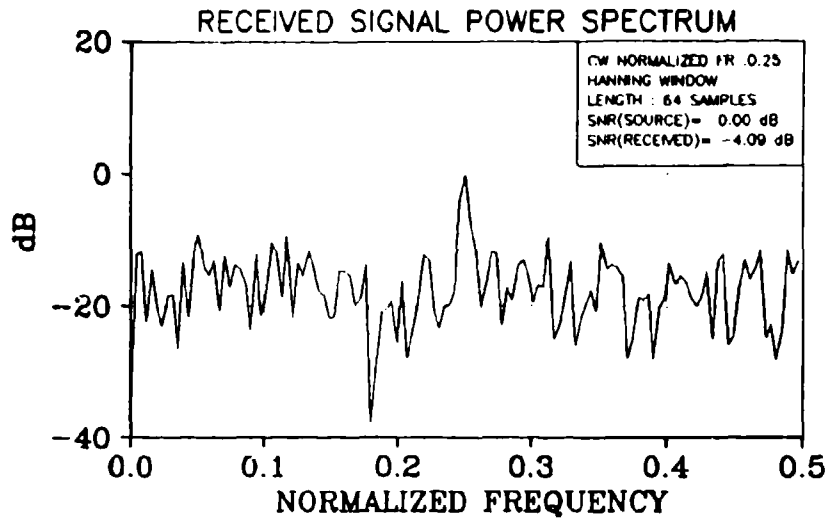


Fig. 82. Received signal power spectrum (Hanning-windowed CW pulse; 5 multiples; $\tau = 80, 110, 140, 170, 200$; SNRR = -4 dB).

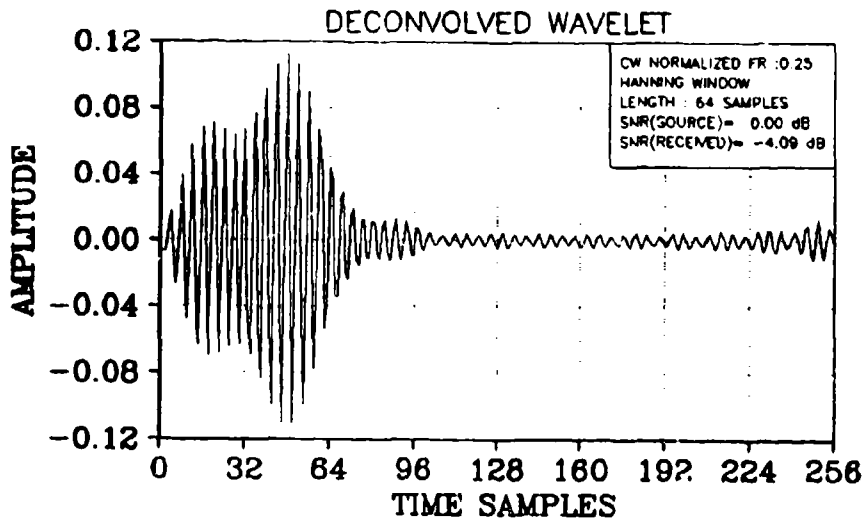


Fig. 83. Deconvolved wavelet (Hanning-windowed CW pulse; 5 multiples; $\tau = 80, 110, 140, 170, 200$; SNRR = -4 dB).

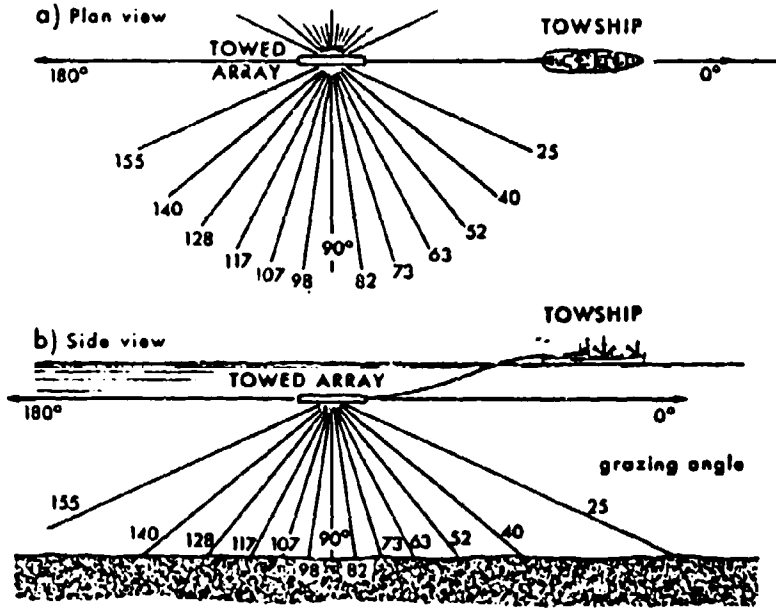


Fig. 84. Configuration of the active sonar backscattering experiment.

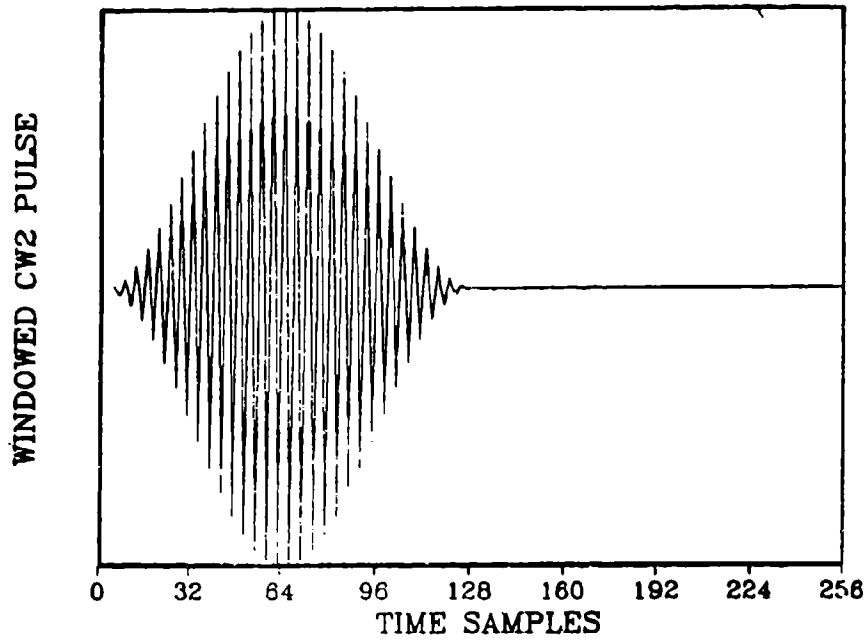


Fig. 85. Transmitted pulse: Hanning-windowed CW pulse of 2 s.

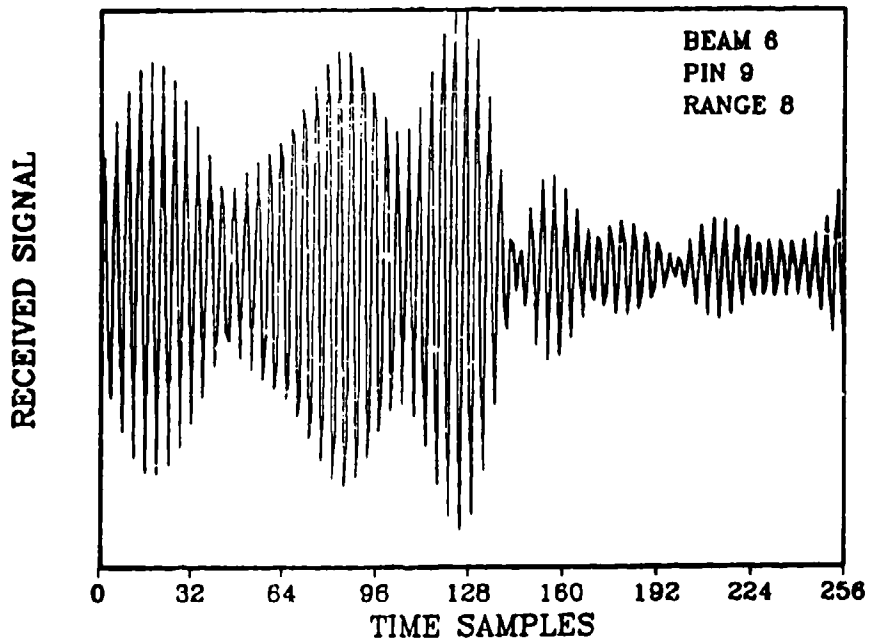


Fig. 86. Received signal (beam 6, ping 9, range 8).

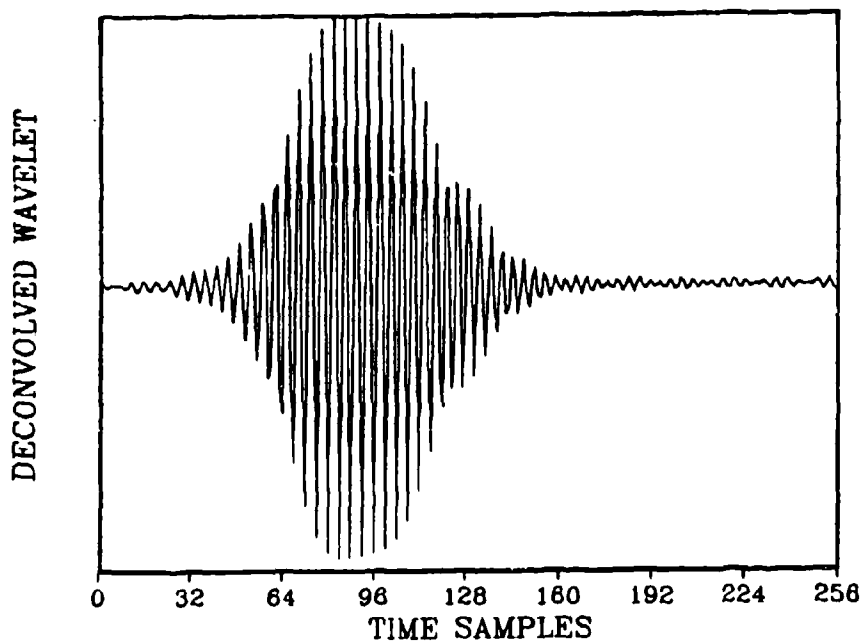


Fig. 87. Deconvolved wavelet.

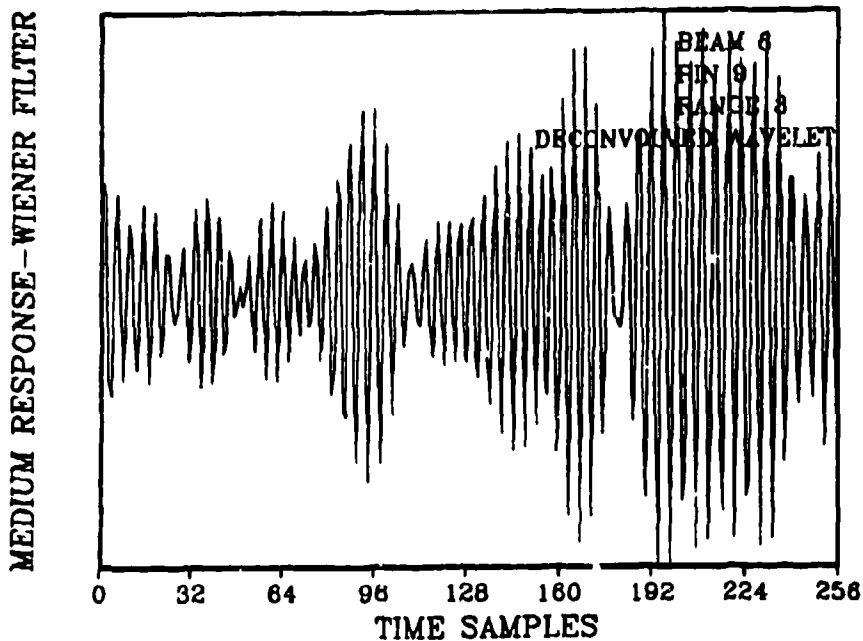


Fig. 88. Deconvolved medium response by Wiener filtering with the deconvolved wavelet as input

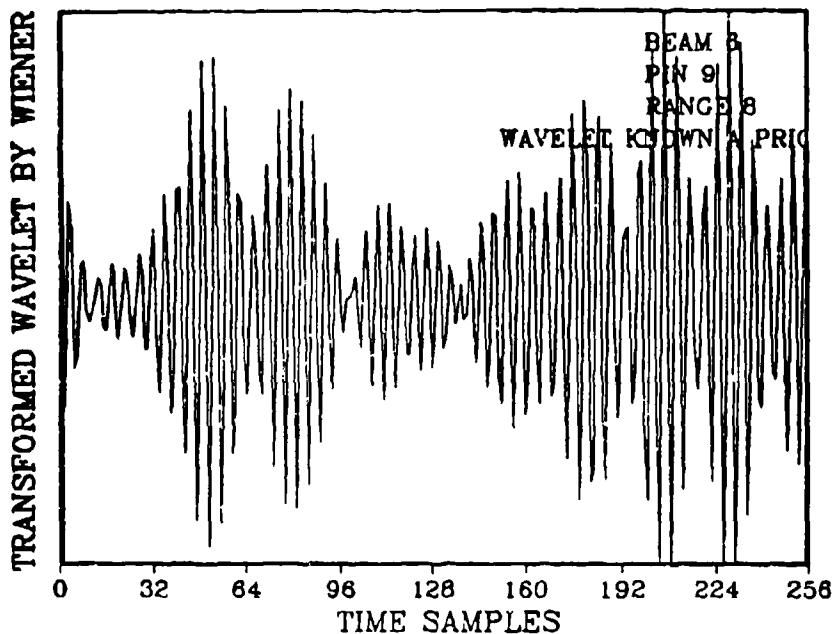


Fig. 89. Deconvolved medium response by Wiener filtering with the transmitted pulse as input.

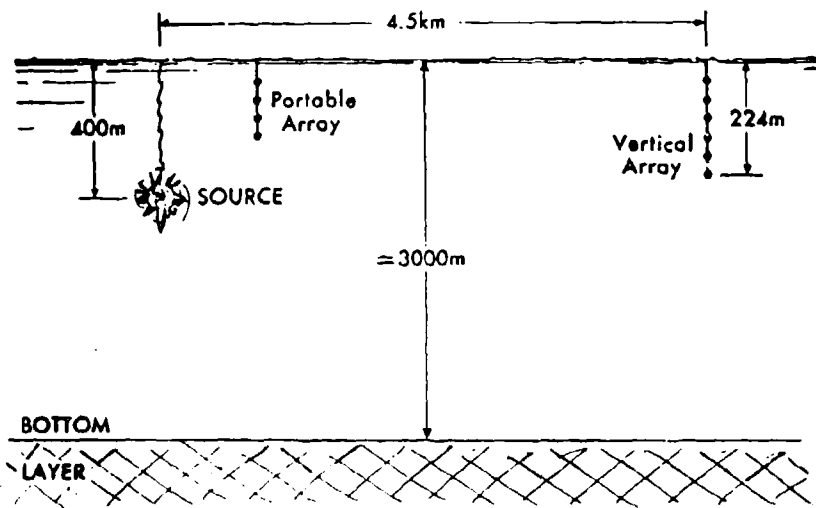


Fig. 90. Configuration of the explosive experiment.

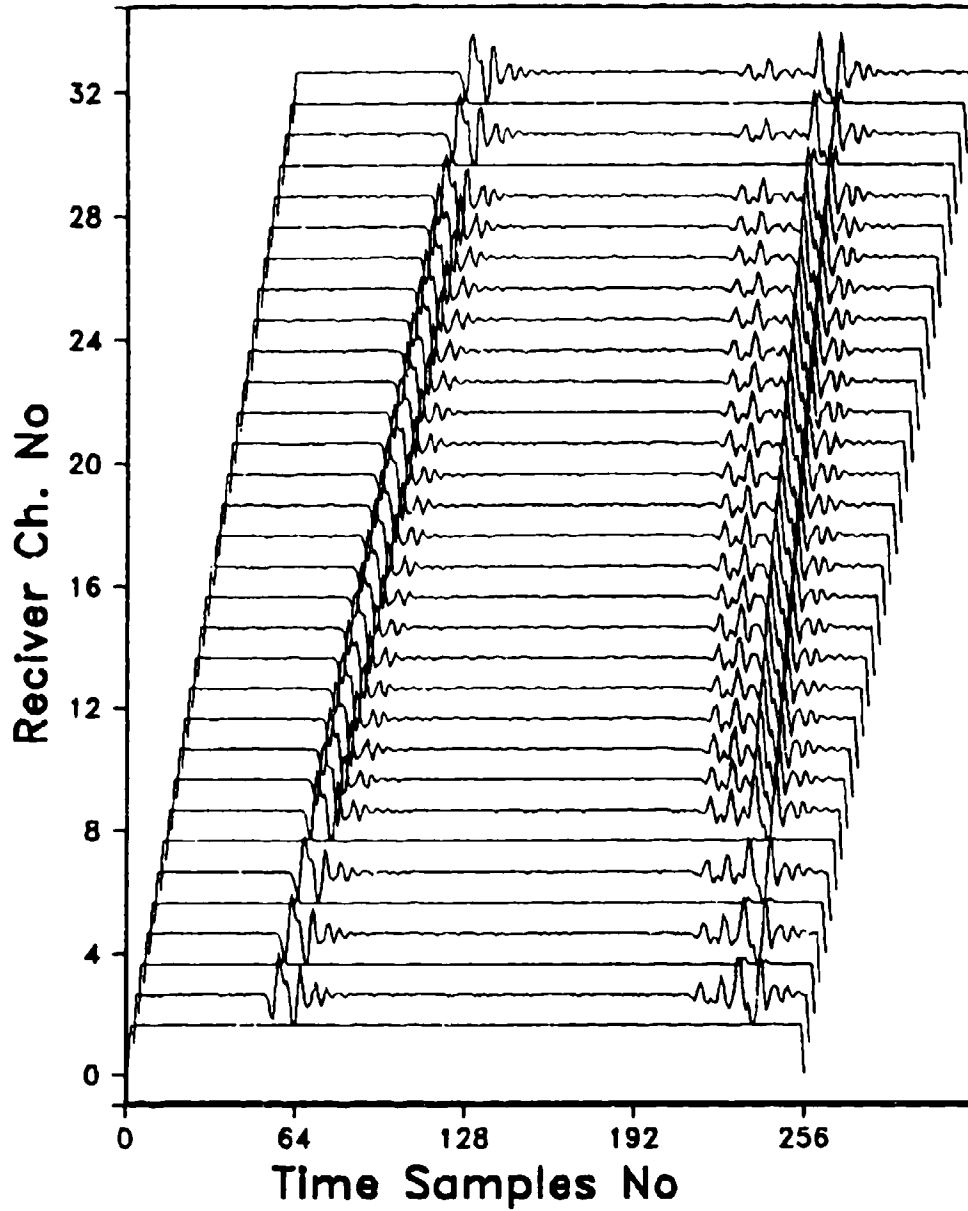


Fig. 91. Received signal on each hydrophone of the vertical array.

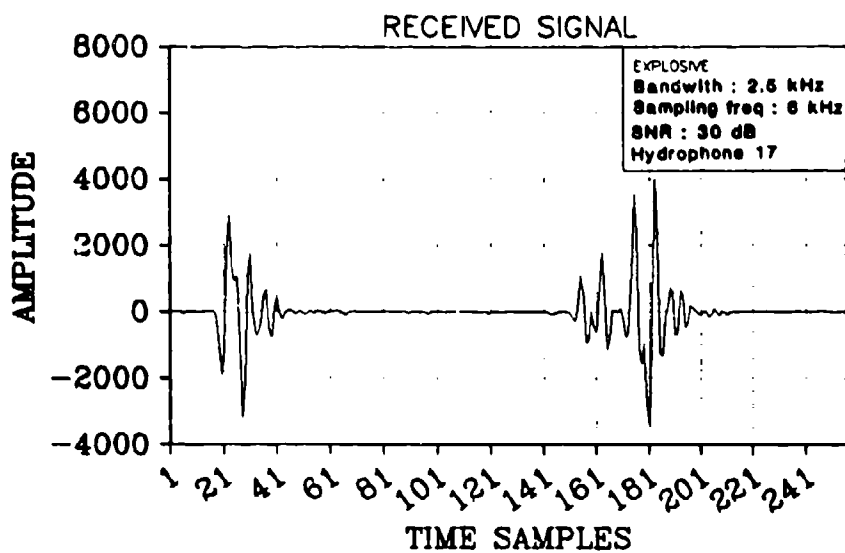


Fig. 92. Received signal on hydrophone 17.

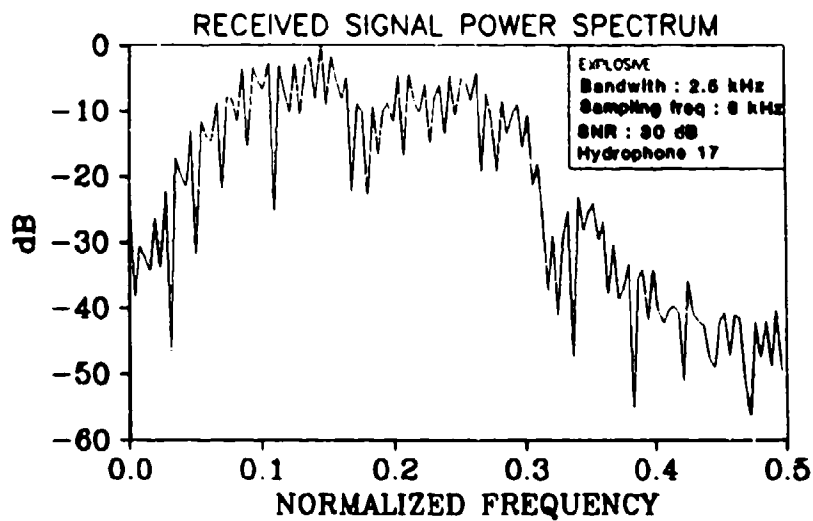


Fig. 93. Power spectrum of the received signal on hydrophone 17.

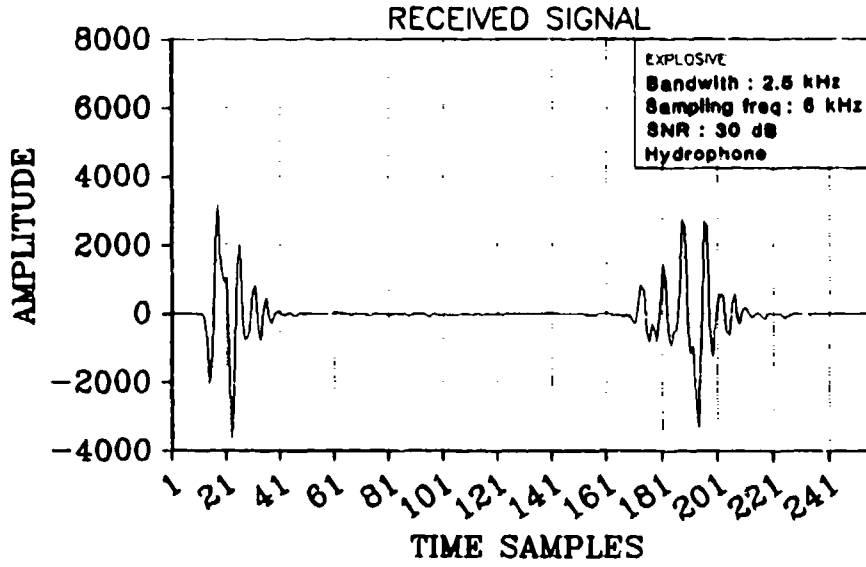


Fig. 94. Received signal on hydrophone 4.

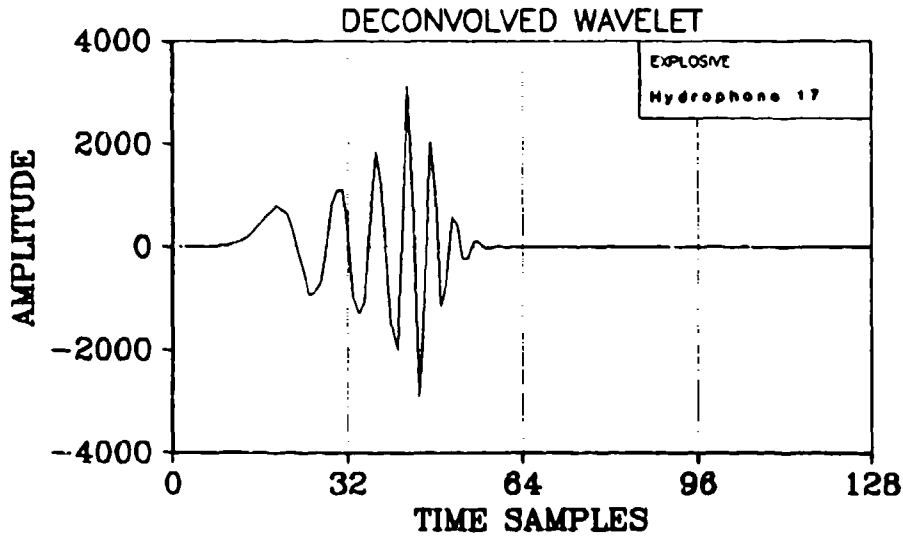


Fig. 95. Deconvolved wavelet on hydrophone 17.

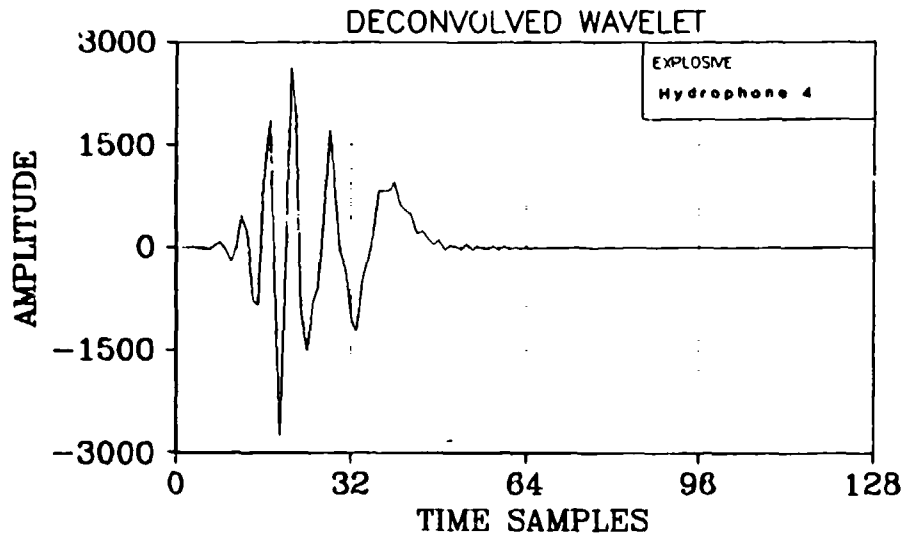


Fig. 96. Deconvolved wavelet on hydrophone 4.

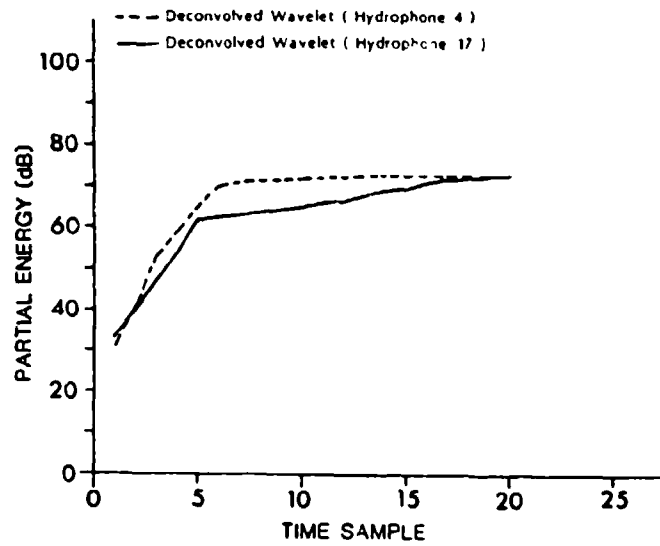


Fig. 97. Comparison of the partial energies of the deconvolved wavelet on hydrophone 17 and deconvolved wavelet on hydrophone 4.

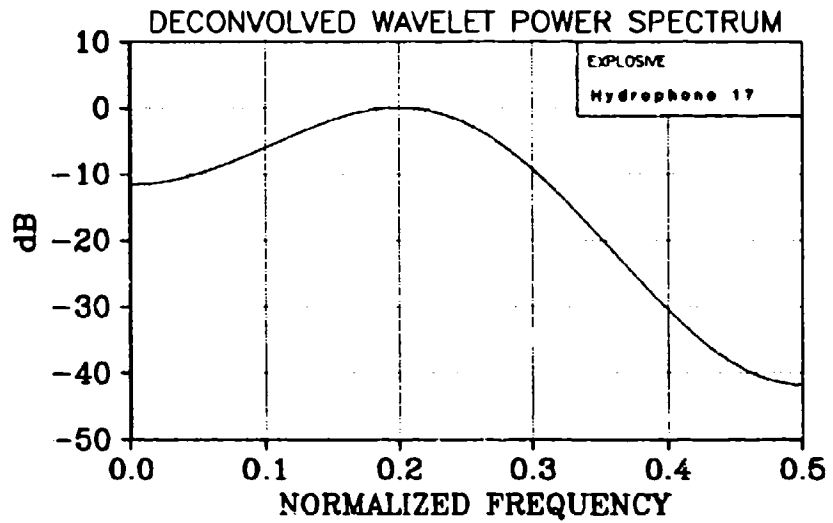


Fig. 98. Power spectrum of the deconvolved wavelet on hydrophone 17.

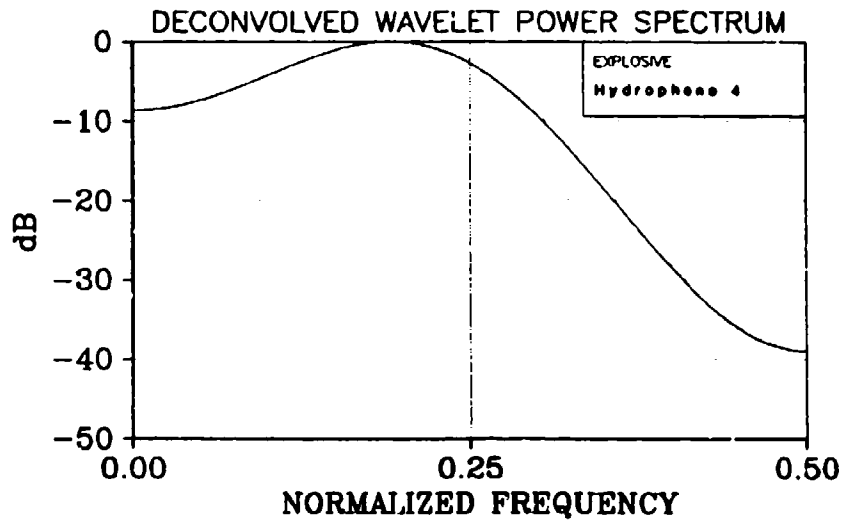


Fig. 99. Power spectrum of the deconvolved wavelet on hydrophone 4.

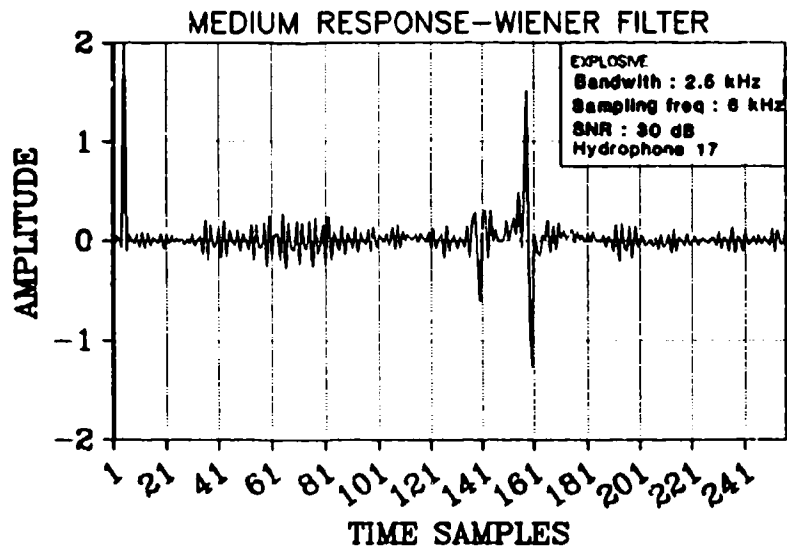


Fig. 100. Deconvolved medium response on hydrophone 17 by Wiener filtering.

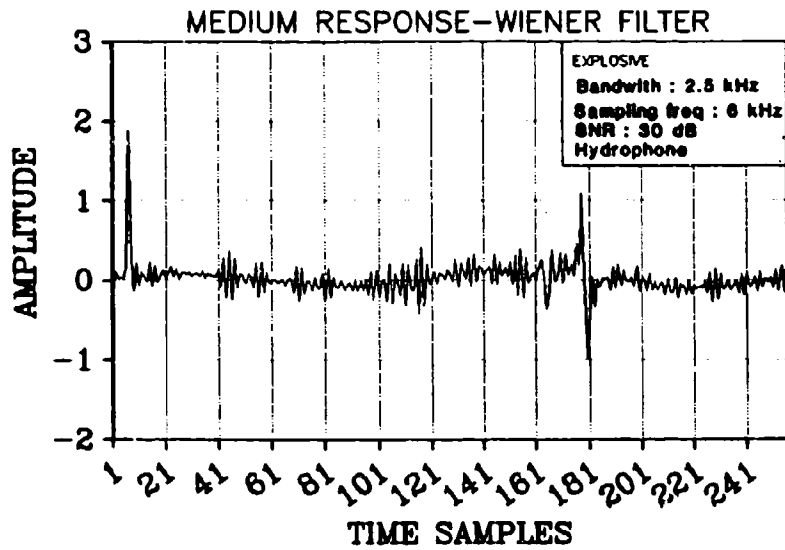


Fig. 101. Deconvolved medium response on hydrophone 4 by Wiener filtering.

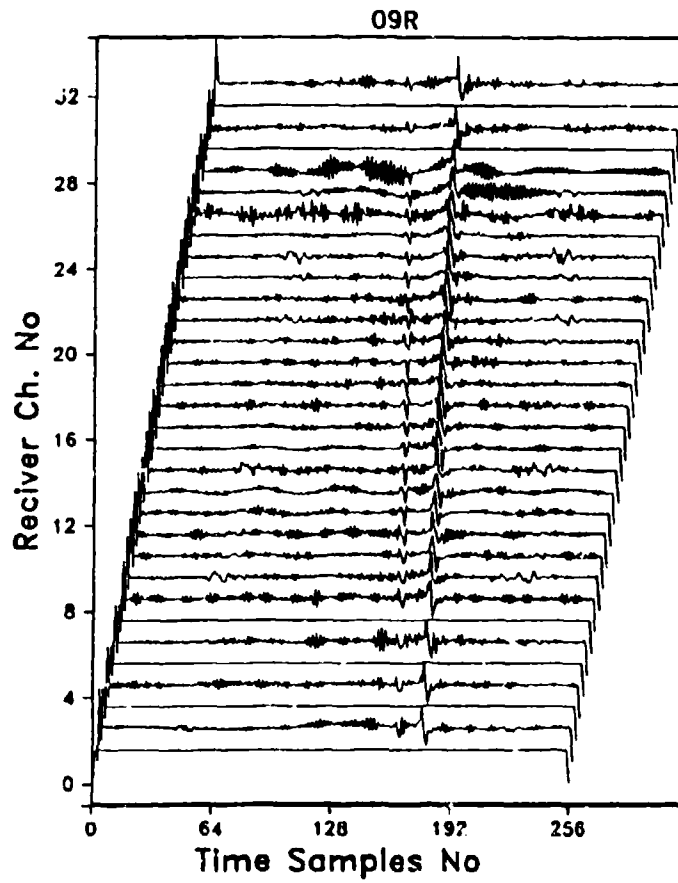


Fig. 102a. Deconvolved medium response on each hydrophone of the vertical array by Wiener filtering.

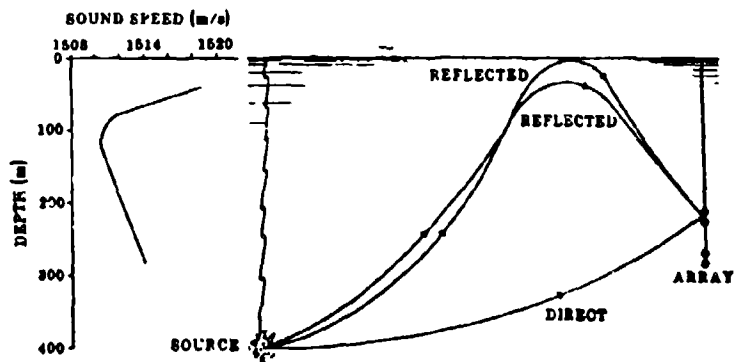


Fig. 102b. Propagation model.

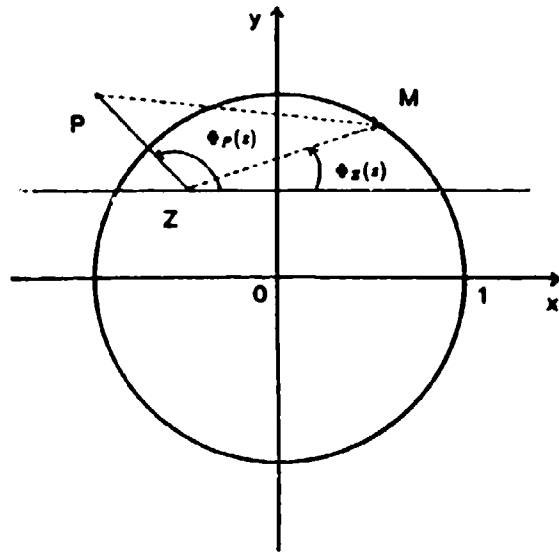


Fig. 103. Zero-pole diagram of the transfer function $G_{sp}(z)$.

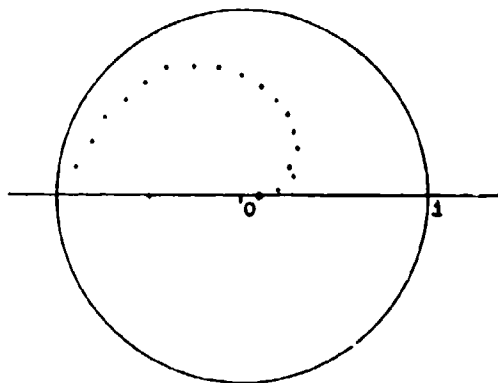


Fig. 104. Zero-pole diagram of the transfer function $X_0(z)$.

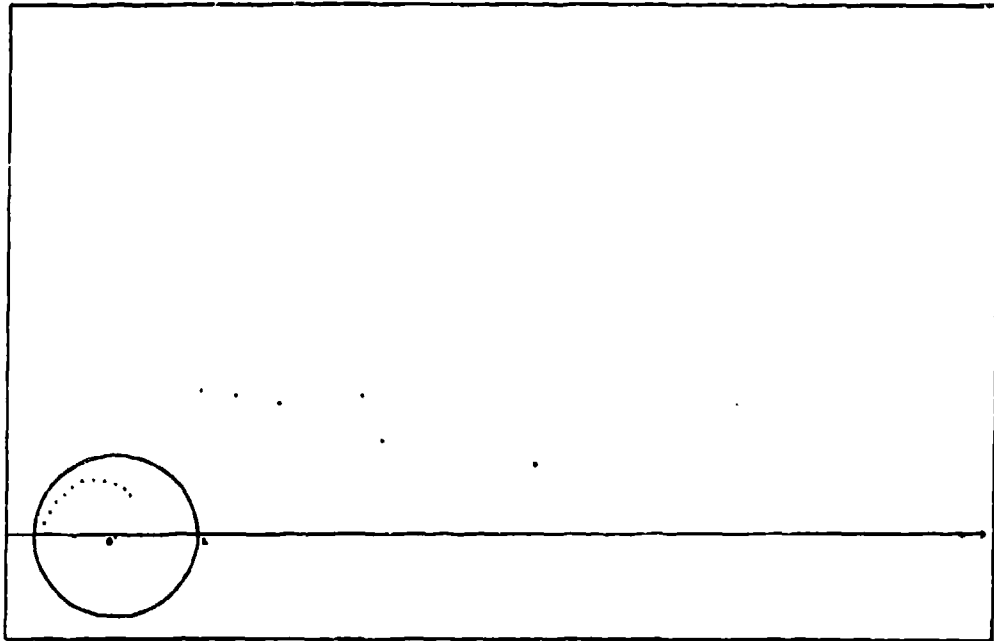


Fig. 105. Zero-pole diagram of the transfer function $X_1(z)$.

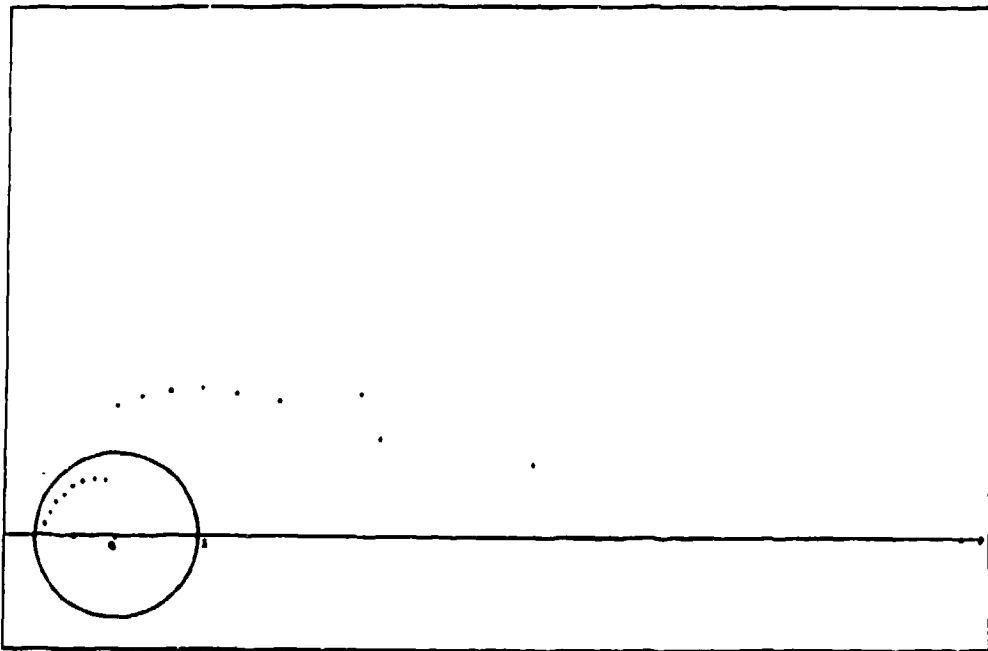


Fig. 106. Zero-pole diagram of the transfer function $X_2(z)$.

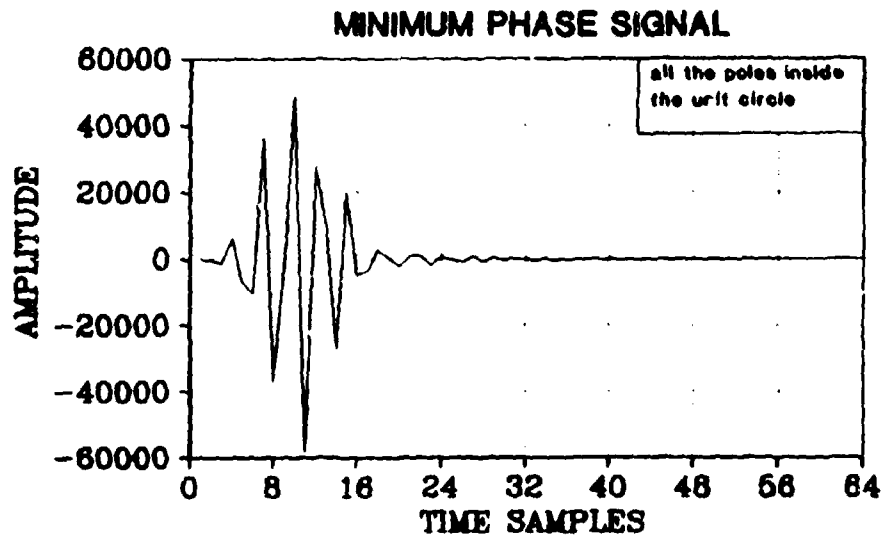


Fig. 107. Minimum phase signal $x_0(t)$.

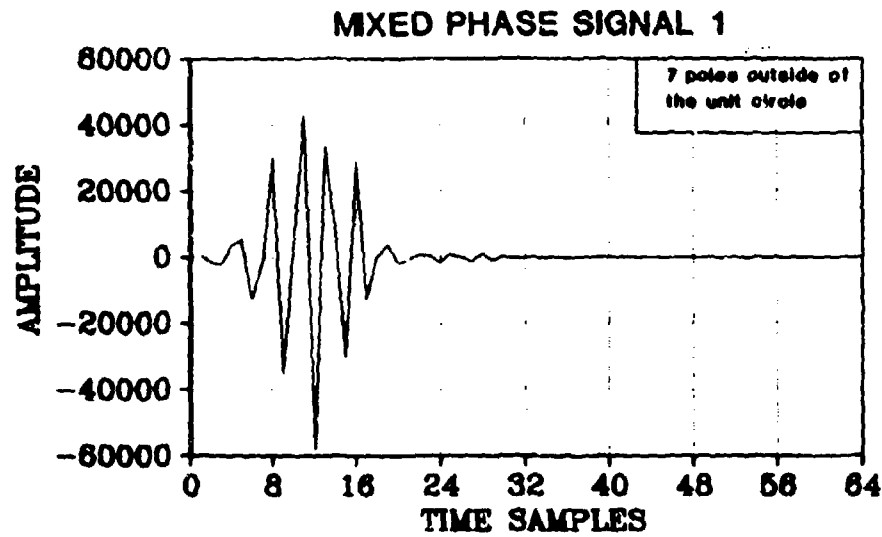


Fig. 108. Mixed phase signal $x_1(t)$.

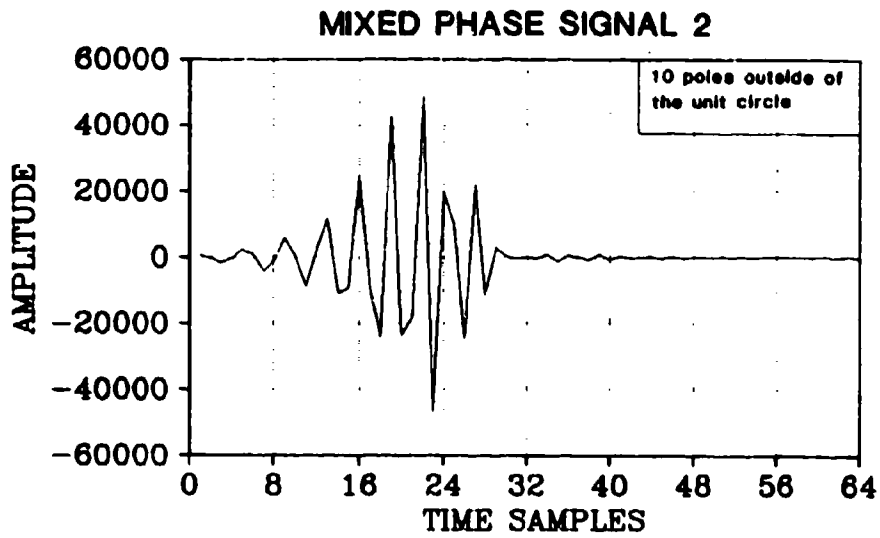


Fig. 109. Mixed phase signal $z_2(t)$.

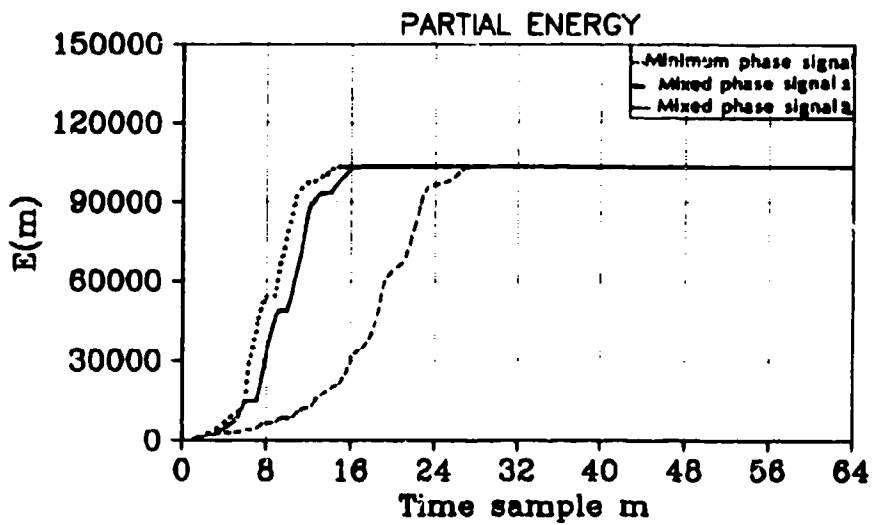


Fig. 110. Comparison of the partial energies of the signals $x_0(t)$, $x_1(t)$ and $x_2(t)$.

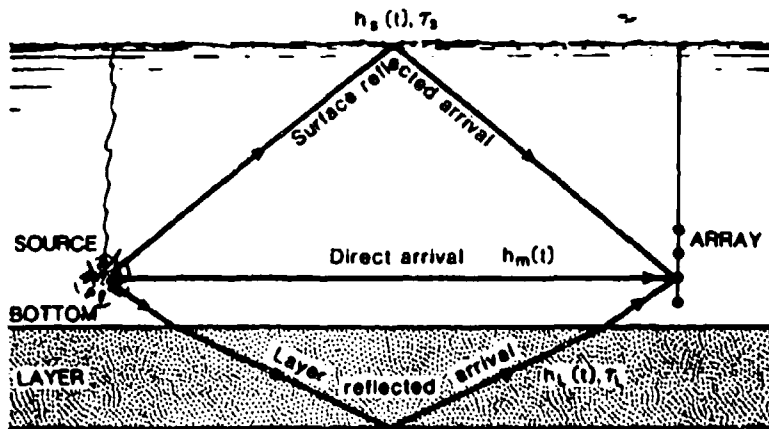


Fig. 111. Expression of the complex cepstrum.

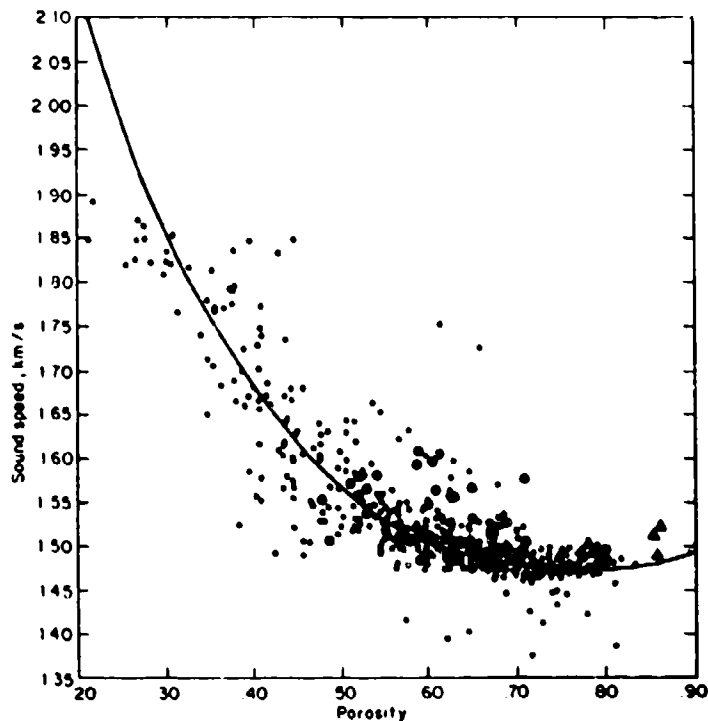


Fig. 112a. Sound speed vs porosity in underwater sediments made on core samples (from Urick [18]).

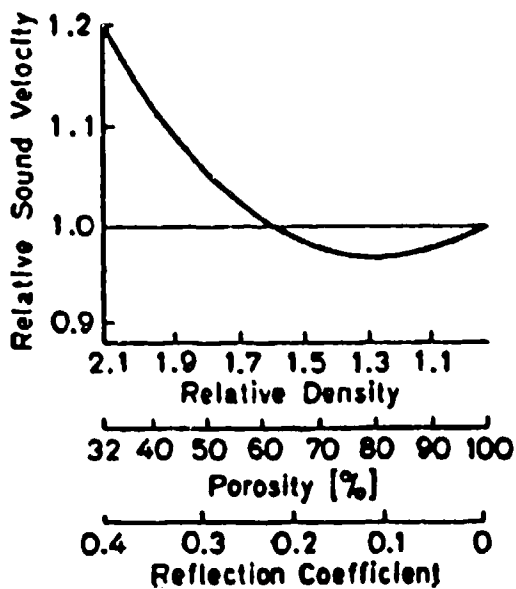


Fig. 112b. Relationship between the main characteristics of underwater sediments.

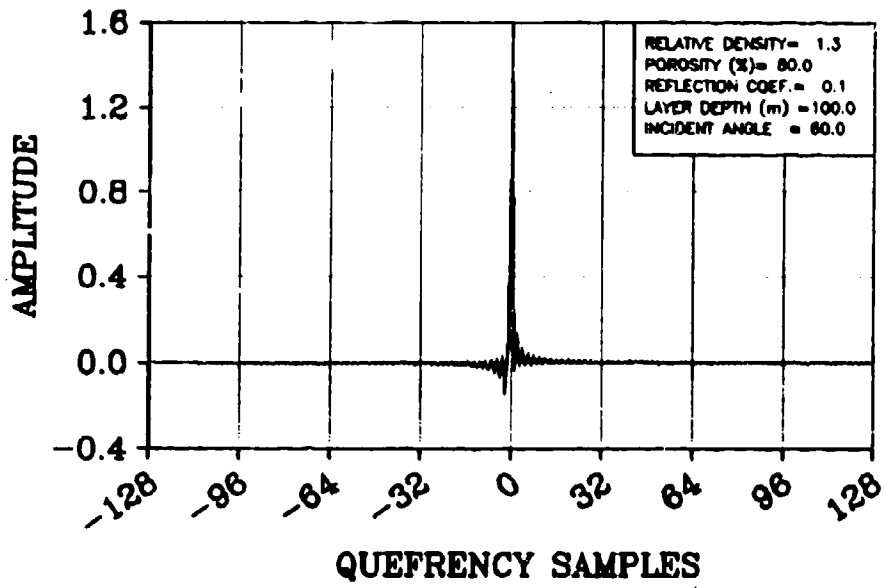
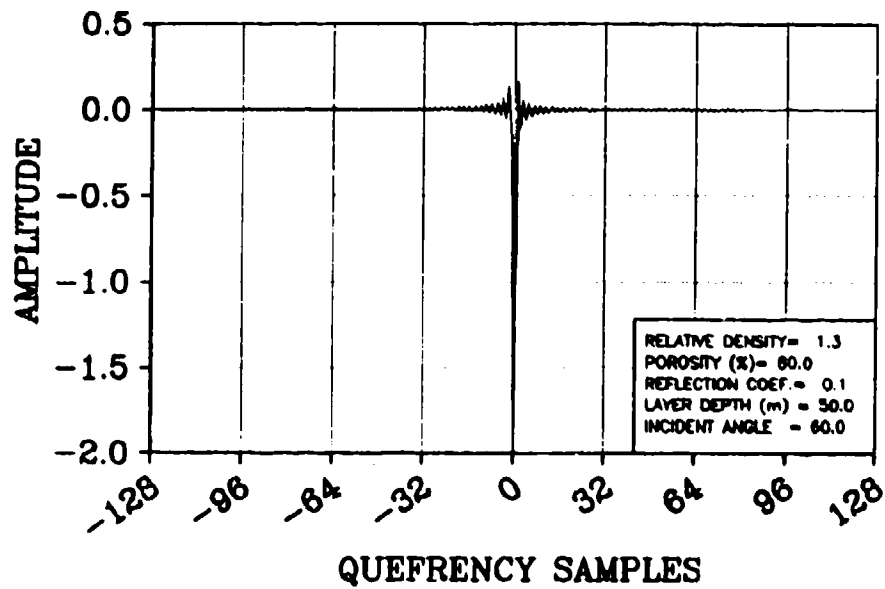


Fig. 113. Layer complex cepstrum with porosity = 80%: (a) layer depth = 50 m; (b) layer depth = 100 m.

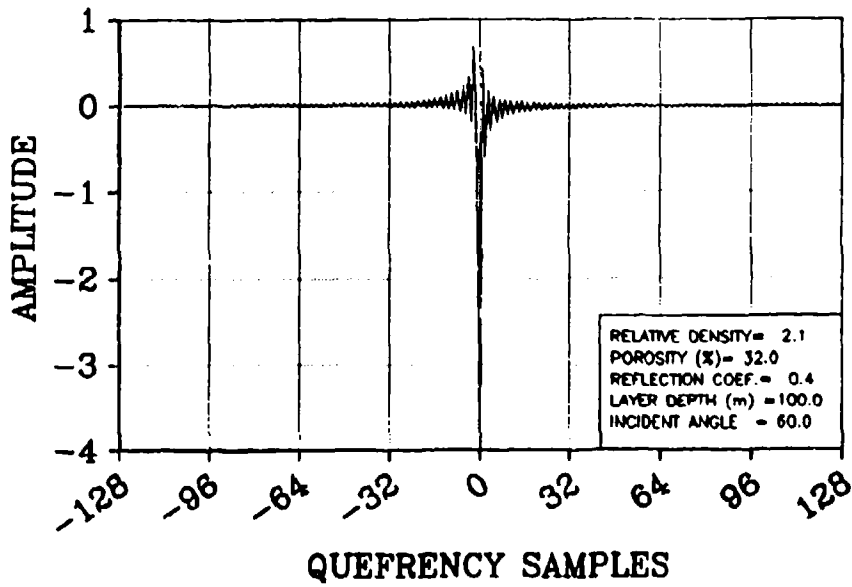
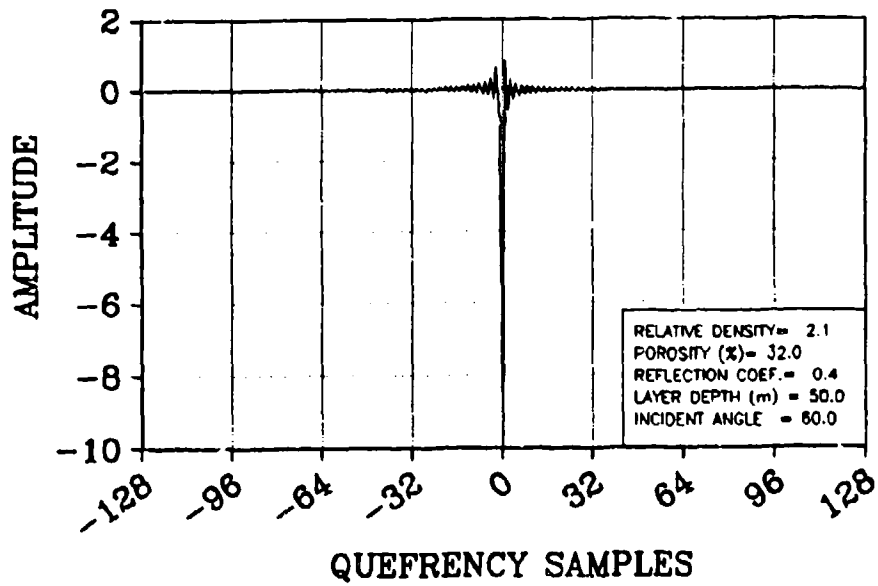


Fig. 114. Layer complex cepstrum with porosity = 32%: (a) layer depth = 50 m; (b) layer depth = 100 m.

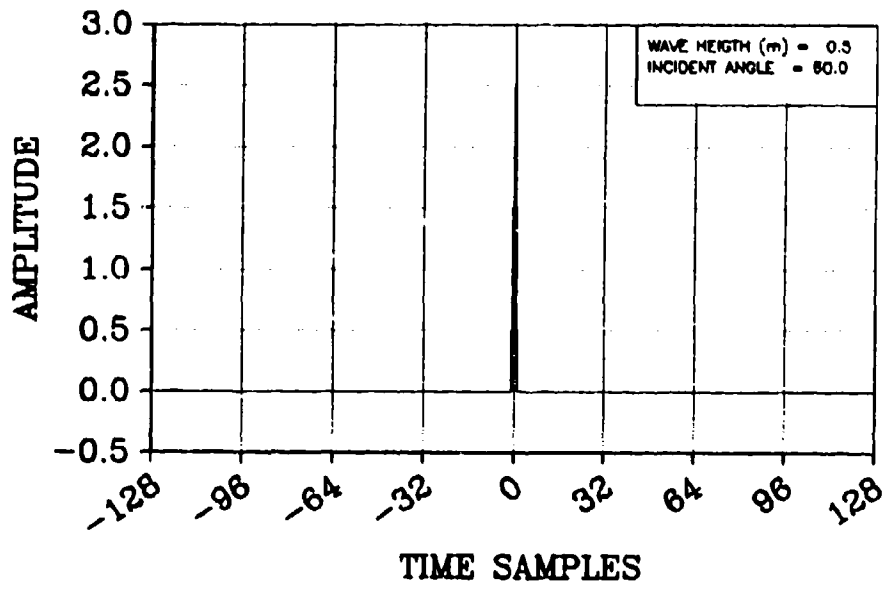


Fig. 115. Surface impulse response.

Initial Distribution for SM-203

Ministries of Defence

JSPHQ Belgium	2
DND Canada	10
CHOD Denmark	8
MOD France	8
MOD Germany	15
MOD Greece	11
MOD Italy	10
MOD Netherlands	12
CHOD Norway	10
MOD Portugal	2
MOD Spain	2
MOD Turkey	5
MOD UK	20
SECDEF US	60

NATO Authorities

Defence Planning Committee	3
NAMILCOM	2
SACLANT	3
SACLANTREPEUR	1
CINCWESTLANT/ COMOCEANLANT	1
COMSTRIKFLTANT	1
CINCIBERLANT	1
CINCEASTLANT	1
COMSUBACLANT	1
COMMAIREASTLANT	1
SACEUR	2
CINCNORTH	1
CINC SOUTH	1
COMNAVSOUTH	1
COMSTRIKFORSOUTH	1
COMEDCENT	1
COMMARARMED	1
CINCHAN	3

SCNR for SACLANTCEN

SCNR Belgium	1
SCNR Canada	1
SCNR Denmark	1

SCNR Germany	1
SCNR Greece	1
SCNR Italy	1
SCNR Netherlands	1
SCNR Norway	1
SCNR Portugal	1
SCNR Turkey	1
SCNR UK	1
SCNR US	2
SECGEN Rep. SCNR	1
NAMILCOM Rep. SCNR	1

National Liaison Officers

NLO Canada	1
NLO Denmark	1
NLO Germany	1
NLO Italy	1
NLO UK	1
NLO US	1

NLR to SACLANT

NLR Belgium	1
NLR Canada	1
NLR Denmark	1
NLR Germany	1
NLR Greece	1
NLR Italy	1
NLR Netherlands	1
NLR Norway	1
NLR Portugal	1
NLR Turkey	1
NLR UK	1

Total external distribution	233
SACLANTCEN Library	10
Stock	37
Total number of copies	280